ANL-95/42

Energy Technology Division
Energy Technology Division
Energy Technology Division
Energy Technology Division
Energy Technology Division
Energy Technology Division

Practical Superconductor Development for Electrical Power Applications

Annual Report for FY 1995

Argonne National Laboratory, Argonne, Illinois 60439
operated by The University of Chicago
for the United States Department of Energy under Contract W-31-109-Eng-38

Reproduced from the best available copy.

Available to DOE and DOE contractors from the
Office of Scientific and Technical Information
P.O. Box 62
Oak Ridge, TN 37831
Prices available from (423) 576-8401

Available to the public from the
National Technical Information Service
U.S. Department of Commerce
5285 Port Royal Road
Springfield, VA 22161

Distribution Category:
Electric Power
Applications (UC-1394)

ANL-95/42

ARGONNE NATIONAL LABORATORY
9700 South Cass Avenue
Argonne, Illinois 60439

PRACTICAL SUPERCONDUCTOR DEVELOPMENT FOR ELECTRICAL POWER APPLICATIONS

ANNUAL REPORT FOR FY 1995

U. Balachandran

Contributors:

T. R. Askew
Y. S. Cha
S. E. Dorris
J. T. Dusek
J. E. Emerson
B. L. Fisher
K. C. Goretta
K. E. Gray†
J. D. Hettinger†
J. R. Hull
R. T. Kampwirth†
D. S. Kupperman
M. T. Lanagan
J. S. Luo††
M. Marinelli
V. A. Maroni††
R. L. McDaniel
N. Merchant††
D. J. Miller†
R. C. Niemann
J. J. Picciolo
T. Pillai
J. L. Routbort
J. P. Singh
V. R. Todt†
K. L. Uherka
C. A. Youngdahl

Energy Technology Division

October 1995

Work supported by

U.S. DEPARTMENT OF ENERGY
Office of Energy Efficiency and Renewable Energy

†Materials Science Division.
††Chemical Technology Division.

Contents

Figures

Tables

PRACTICAL SUPERCONDUCTOR DEVELOPMENT FOR ELECTRICAL POWER APPLICATIONS

ANNUAL REPORT FOR FY 1995

Abstract

Development of useful high-critical-temperature (high-T_c) superconductors requires synthesis of superconducting compounds; fabrication of wires, tapes, and films from these compounds; production of composite structures that incorporate stabilizers or insulators; and design and testing of efficient components. This report describes the technical progress of research and development efforts aimed at producing superconducting components in the (Bi,Pb)-Sr-Ca-Cu, (Tl,Pb,Bi,V)- (Ba,Sr)-Ca-Cu, and Y-Ba-Cu oxide systems. The topics that are discussed are synthesis and heat treatment of high-T_c superconductors, formation of monolithic and composite conductors, characterization of structures and superconducting and mechanical properties, and fabrication and testing of prototype components. Collaboration with industry and academia is documented.

1 Introduction

The superconductor program at Argonne National Laboratory (ANL) includes development of bulk and film processing that is directed toward improving the properties of high-critical-temperature (high-T_c) superconductors, developing processing methods for the production of commercial conductors, and fabricating and testing prototype conductors. Team relationships with industrial and academic partners are an integral part of this program. The principal objective of the ANL program is to develop methods to fabricate and use structurally reliable high-T_c superconductors for the generation, transmission, and storage of electrical energy. Ceramic processing and joining techniques are being developed to provide useful conductors from one or several high–T_c superconductors. Work has focused on superconductors based on bismuth–strontium–calcium–copper oxide (Bi-2212), lead-doped bismuth-strontium-calcium-copper oxide (Bi-2223), and pure and metal–doped (M, where M is bismuth, lead, or vanadium) thallium-strontium-barium-calcium–copper oxide (Tl-1223), and yttrium-barium-copper oxide (Y-123).

Monolithic and composite conductors in the form of wires, tapes, films, or other shapes must meet several requirements. For most applications, the conductors must be capable of carrying large currents in the presence of large magnetic fields and they must be strong, flexible, and chemically and cryogenically stable. Potential applications for such conductors include transmission lines, motors, generators, transformers, magnetic energy storage devices, and electronics. The principal impediments to the use of bulk high-T_c superconductors are low critical current density (J_c) in large applied magnetic fields, relatively poor mechanical properties, and the need for very long lengths with uniform properties. Processing methods for improveing all of the characteristics of high-T_c superconductors have been and continue to be developed. The goals of ceramic fabrication include promoting high conductivity by obtaining phase-pure final materials and imparting favorable grain alignment, which will maximize flux pinning through microstructural control, and increasing flexibility and reliability by minimizing microstructural flaws and optimizing the strength and toughness of each material.

This report reviews the technical progress and status of (1) Bi- and Tl-based high-T_c superconductor wires and tapes, which constitute the main focus of the materials efforts; (2) Y-123 superconductors; (3) characterization of superconducting and electrical properties, microstructures, and mechanical properties; (4) investigation of fundamental properties; and (5) fabrication and testing of prototype superconducting devices. Interaction with industry and academia is also documented.

2 Technical Progress in 1994–1995

2.1 Bi–Pb–Sr–Ca–Cu–O Superconductors

2.1.1 Phase Development

Composition Studies

The effect of total Pb content on the microstructure and J_c of Bi-2223 tapes that were made by the two-powder process was investigated. Earlier studies suggested what seemed superficially to be contradicting trends (Balachandran et al., 1994a; Dorris et al., 1993, 1994a). One study indicated that phase purity improved and J_c increased as Pb content increased from $Pb_{0.3}$ to $Pb_{0.4}$; a second study showed that J_c decreased as the Pb content increased from $Pb_{0.3}$ to $Pb_{0.5}$ because of the appearance of a Pb/Bi-rich phase in the samples that contained more Pb. The difference was attributed to variations in composition other than Pb content (the Sr content of the first $Pb_{0.3}$ sample was relatively high and the (Bi+Pb) content was relatively low when compared with later $Pb_{0.3}$ samples). Both studies showed that an optimum Pb content exists and that deviations of $Pb_{0.1}$ from the optimum strongly influence the microstructure and properties of tapes. It was proposed that Bi-2223 formation is retarded and J_c is decreased when the Pb content is too low, because the necessary liquid phase does not form, whereas J_c decreases when the Pb content is too high because Pb/Bi-rich phases coat the grain boundaries. To confirm these ideas and to better optimize the Pb content, powder-in-tube (PIT) tapes were made from powders with Pb content between $Pb_{0.3}$ and $Pb_{0.5}$.

Pb-doped Bi-2212 powders, $Bi_{1.8}Pb_xSr_{2.0}Ca_{1.0}Cu_2O_8$, were prepared for x values of 0.20, 0.25, 0.30, 0.35, 0.40, and 0.50. Powder mixtures with appropriate amounts of Bi_2O_3, PbO, $SrCO_3$, $CaCO_3$, and CuO were first calcined at reduced total pressure of ≈3 torr O_2 (20°C/h to 750°C, followed by 6 h at 750°C) to ensure complete decomposition of the carbonates. After calcining at reduced pressure, the Bi-2212 phase was formed by further calcining for 24 h at 840°C in CO_2-free air at ambient pressure. The powders were ball milled in isopropyl alcohol for 12-16 h and calcined again for 24 h at 840°C in CO_2-free air at ambient pressure. Calcinations in ambient air were repeated with intermediate ball milling until nearly single-phase materials were obtained. The powders were then calcined at reduced total pressure to rid the powders of Ca_2PbO_4 and ensure that all Pb was contained in the Bi-2212 phase (Jeremie et al., 1993). Powders of 2223 precursor were prepared by mixing each of the Bi-2212 powders with an equimolar amount of $CaCuO_2$, then ball milling in isopropyl alcohol for 12-16 h and calcining at ≈3 torr (60°C/h to 720°C, followed by 3 h at 720°C) to eliminate C introduced by milling. PIT tapes were prepared from the Bi-2223 precursor powders by an established procedure (Dorris et al., 1993a).

Samples (≈3 cm long) were cut from the tapes and heat treated in 8% O_2 at temperatures of 820 and 827°C. Thermomechanical processing of the tapes began with a 50-h annealing at the chosen heat-treatment temperature, after which the tapes were uniaxially

cold pressed at ≈2 GPa. Following pressing, the tapes were annealed for an additional 100 h at the selected heat-treatment temperature. The process of pressing and then annealing was repeated until cumulative heat-treatment times of 350 h had been reached. The J_c of each tape was measured at 77 K in zero applied field with a 1 μV/cm criterion and the four-probe method. Each reported J_c value represents the average of measurements made on three separate samples. The degree of conversion to Bi-2223 was estimated by X-ray analysis of peeled tapes. The Bi-2223 fraction was calculated as $I_{00\text{-}10}(2223)/[I_{00\text{-}10}(2223)+I_{008}(2212)]$, where $I_{00\text{-}10}(2223)$ and $I_{008}(2212)$ are the integrated peak intensities for the (00-10) reflection of 2223 and (008) reflection of Bi-2212, respectively.

X-ray analysis showed that the Bi-2212 powders had nearly identical phase purities, containing mostly Bi-2212, no Ca_2PbO_4, and only a slight amount of Bi-2201. The carbon content of all Bi-2223 precursor powders was ≈500 ppm or less. Analysis of the Bi-2223 precursor powders by inductively coupled plasma–atomic emission spectroscopy (ICP-AES) produced the results shown in Table 1. I_c (0 T, 77 K) data for tapes that were heat treated at 827°C are shown in Fig. 1. The thickness of the tapes was typically 100-120 μm and their cross-sectional area was typically ≈2.0×10^{-3} cm^2.

Table 1. Stoichiometry of Bi-2223 precursor powders as determined by ICP-AES

Nominal Composition	Bi	Pb	Sr	Ca	Cu
$Bi_{1.8}Pb_{0.20}Sr_{2.0}Ca_{2.0}Cu_{3.0}O_{10}$	1.82	0.20	1.98	1.95	3.05
$Bi_{1.8}Pb_{0.25}Sr_{2.0}Ca_{2.0}Cu_{3.0}O_{10}$	1.81	0.25	1.97	1.97	3.06
$Bi_{1.8}Pb_{0.30}Sr_{2.0}Ca_{2.0}Cu_{3.0}O_{10}$	1.80	0.29	1.96	1.98	3.07
$Bi_{1.8}Pb_{0.35}Sr_{2.0}Ca_{2.0}Cu_{3.0}O_{10}$	1.80	0.35	1.98	1.96	3.07
$Bi_{1.8}Pb_{0.40}Sr_{2.0}Ca_{2.0}Cu_{3.0}O_{10}$	1.77	0.39	1.98	1.97	3.09
$Bi_{1.8}Pb_{0.50}Sr_{2.0}Ca_{2.0}Cu_{3.0}O_{10}$	1.79	0.49	1.97	1.96	3.09

The I_c (0 T, 77 K) data shown in Fig. 1 clearly show that the optimum Pb content is ≈$Pb_{0.3}$ for the composition studied here. Samples heated at 820°C showed the same trend with Pb content, but their I_c values were ≈10% lower. As suggested earlier, the optimum Pb content depends on the concentrations of the other constituents, so the optimum Pb content may differ for another composition. Figure 2 shows backscattered electron images of tapes (longitudinal view) after 250 h at 820°C in 8% O_2. The $Pb_{0.20}$ sample (Fig. 2a) contained primarily 2:1 alkaline earth cuprate, CuO, and Bi-2212, the phases that were initially present in the precursor mixture, suggesting that the formation of Bi-2223 was slow. The $Pb_{0.3}$ sample (Fig. 2b) contained the same second phases but in smaller concentrations. X-ray analysis of peeled tapes showed that the $Pb_{0.2}$ sample contained only ≈60% Bi-2223 after 250 h of heat treatment, whereas the $Pb_{0.3}$ sample consisted of ≈98% Bi-2223 (the small amount of Bi-2223 in the $Pb_{0.2}$ is believed to form during cooling because of back reaction). These results are consistent with idea that Bi-2223 formation is retarded when Pb content is too low, presumably because of the absence of a liquid phase.

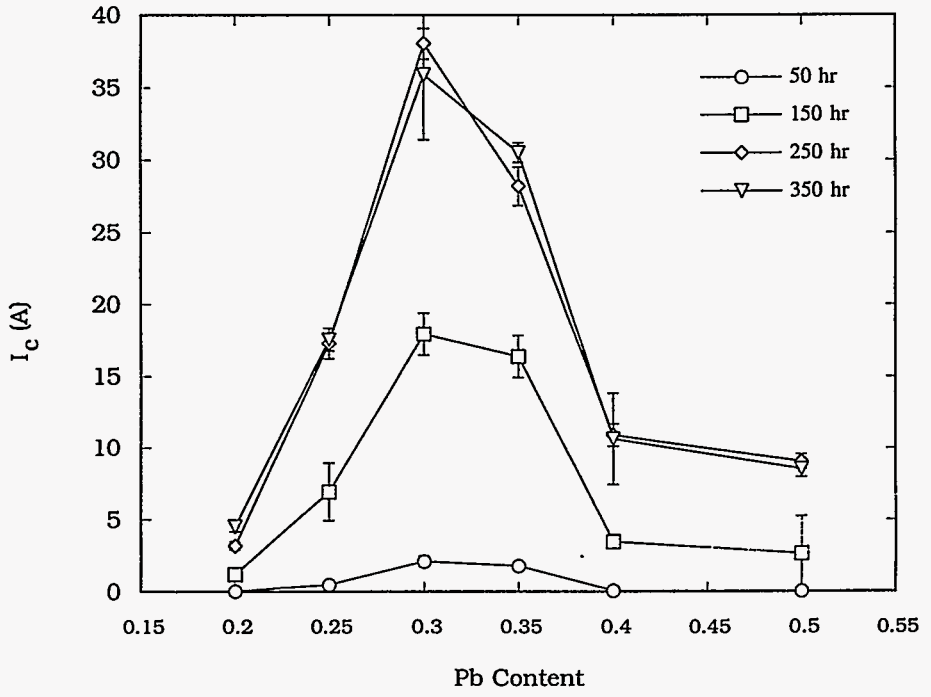

Fig. 1. Critical current (I_c) vs. Pb content for Bi-2223 tapes heat treated at 820°C in 8% O_2 for total heat-treatment times of 50, 150, 250, and 350 h with intermediate pressing.

The density of the $Pb_{0.4}$ sample (Fig. 2c) was higher than that of the $Pb_{0.3}$ sample, hinting that $Pb_{0.4}$ may have contained more liquid during the reaction. However, the concentration of alkaline-earth cuprates and CuO was approximately the same for the two samples, suggesting that the degree of Bi-2223 conversion was similar. These findings were confirmed by X-ray analysis, which showed that both samples contained 95-98% Bi-2223 after 250 h at 820°C. In addition to the alkaline earth cuprates and CuO, however, thin streaks of a Bi/Pb-rich phase were evident in the $Pb_{0.4}$ sample. These streaks can be seen in the $Pb_{0.4}$ sample only at higher magnification, but are obvious in the $Pb_{0.5}$ sample (Fig. 2d), where they are larger and more abundant. The appearance of the Bi/Pb-rich phase suggests that the Pb content of $Pb_{0.4}$ was too high. The increase in Pb content evidently increases the core density but degrades the phase purity, and, as a result causes I_c to decrease.

This study confirms Pb content as a critical variable in fabricating tapes by the two-powder process and that deviations of $Pb_{0.1}$ from the optimum strongly influence the microstructure and properties of these tapes. When the Pb content is lower than optimum, Bi-2223 formation is retarded, presumably because a liquid phase is lacking, whereas a Bi/Pb-rich phase forms when the Pb content is higher than optimum. These results indicate that the optimum Pb content depends on the content of the other Bi-2223 constituents. For example, Majewski et al. (1991) indicate that a liquid phase does not form in samples with a high alkaline-earth concentration or a low (Bi+Pb) content, so, for such samples, the optimum may be expected to shift to higher Pb content.

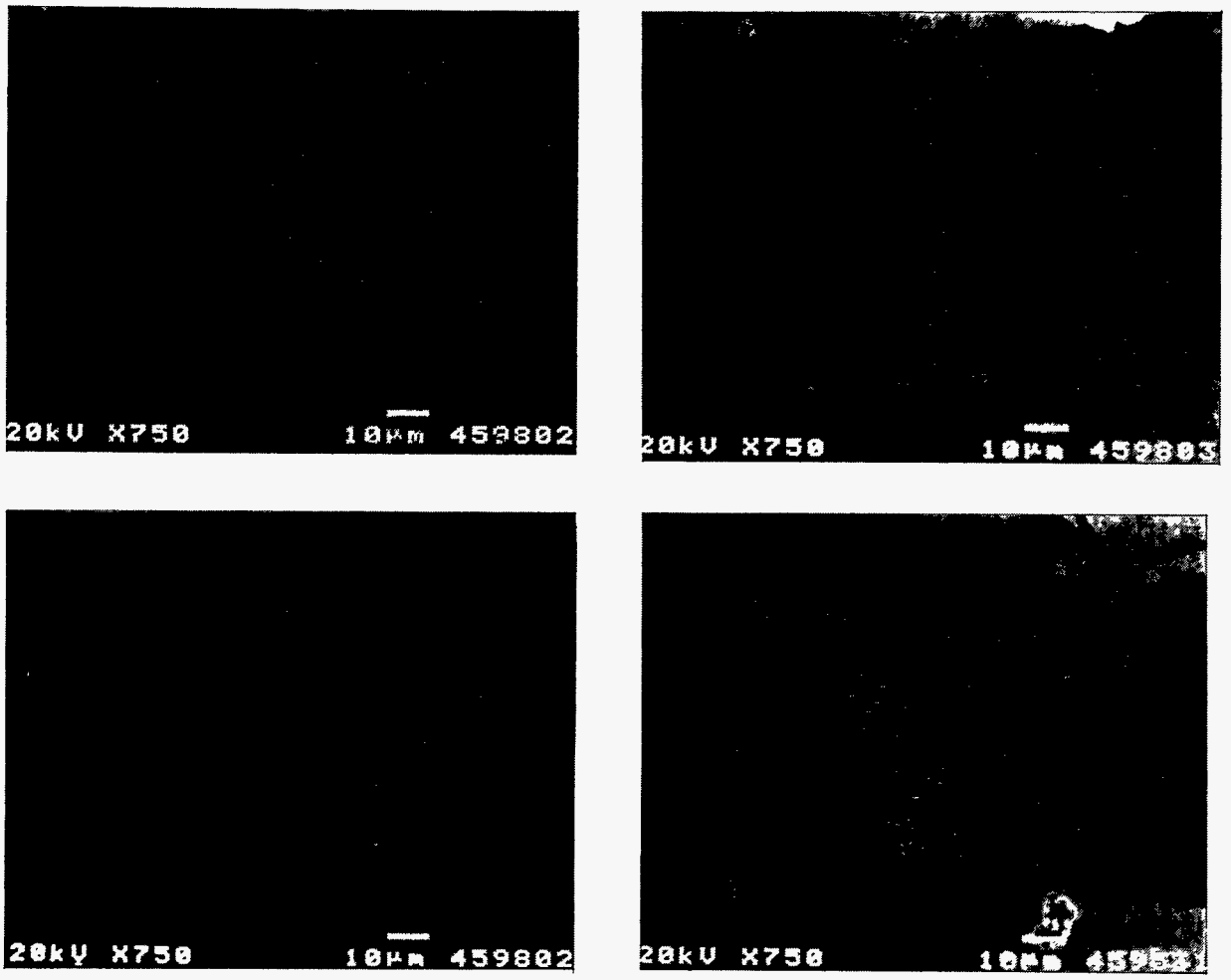

Fig. 2. Backscattered electron images of (a) $Pb_{0.20}$, (b) $Pb_{0.30}$, (c) $Pb_{0.40}$, and (d) $Pb_{0.50}$ samples (longitudinal views) after 250 h at 820°C in 8% O_2.

Microstructural Development in Ag/Bi-2223 Conductors: Role of Lead

The purpose of this ongoing project is to investigate the evaluation of Bi(Pb)-Sr-Ca-Cu-O phase with respect to microstructural development during thermomechanical processing of Ag/Bi-2223 composite conductors (De Rochemont et al., 1994). A major objective during FY 1995 has been to elucidate/characterize the role that Pb plays in the formation of Bi-2223 during heat treatment. The intention of this objective is to identify the optimum Pb stoichiometry and Pb incorporation method for maximum composite conductor performance, primarily in terms of J_c at 77 K.

In FY 1995, we conducted detailed followup work on specimens and results from the prior year's work (Dorris et al., 1994a and b; Tetenbaum et al., 1994, 1995) which showed that incorporation of most of the Pb into the Bi-2212 component of the precursor powder produced Ag/Bi-2223 composites with higher J_c values than did incorporation of the lead as Ca_2PbO_4 in the second-phase component of the precursor powder. In the course of this work, we found that Pb loss during heat treatment of Ag/Bi-2223 composite conductors blocks the progress of Bi-2223 formation; the mode of Pb incorporation is the major factor that controls the length of the induction period preceding the onset of Bi-2223 formation;

fully processed composites that are fabricated from powders with Pb in the Bi-2212 component had fewer Bi-2212 intergrowths and back-reacted grains than did composites made from powders with Pb in the Ca_2PbO_4 form; a reaction that involves Pb transportation between orthorhombic Bi(Pb)-2212 and tetragonal Bi-2212 + Ca_2PbO_4 can be manipulated by adjusting O_2 pressure and processing temperature and this reaction can be probed both chemically and spatially by imaging Raman microscopy; and the Pb stoichiometry of the precursor powder is connected in a sensitive way to the development of Bi-2223 phase, to the microstructure of the composite core, and to the J_c of the composite conductor. The key features of these results are summarized below.

Previously, we reported the results of a study designed to explore the effectiveness of the Ag sheath in limiting Pb loss during heat treatment of Ag/Bi-2223 composites (Poeppel et al., 1993). Additional measurements to quantify the Pb loss rate under the conditions of our prior study have now been completed and are reported in Fig. 3, together with the FY 1993 phase conversion results and some additional conversion data collected during the past year. In the quantification experiments, short sections (≈25 mm in length) of Ag/Bi-2223 composites were peeled open prior to heat treatment to expose the ceramic core. These opened samples were processed at 825°C in 0.075 atm O_2 for various times ranging from 10 to ≈30,000 min and then analyzed for Pb loss by ICP-AES. Fully sheathed specimens of the same composite were run in parallel with the opened specimens to provide a baseline for determining both the phase conversion kinetics and the level of containment provided by the sheath.

The results in Fig. 3 show that the closed (fully sheathed) composite specimens reached complete conversion to Bi-2223 in ≈2000 min, whereas the open specimens never achieved more than ≈40% conversion (as reported in our prior work). The Pb loss (presumably due to evaporation) is relatively small (a few percent) for the closed specimens and probably occurs by seeping out of the ends of the short samples. Lead loss from the opened specimens is continuous and nearly complete after ≈3 x 10^4 min (≈500 h). Also, after ≈1000 min, half of the Pb is lost from the opened samples and the Bi-2223 formation reaction stops. Two conclusions can be drawn from these results: (1) Pb is essential to the conversion reaction and (2) the Ag sheath plays a key role in retaining the Pb during heat treatment. The Bi-2223 that forms prior to ≈50% Pb loss does not tend to decompose as the remaining Pb vaporizes out of the sample. This latter observation suggests that Pb is more centrally involved in the conversion reaction than it is in stabilizing the Bi-2223 phase.

Figure 4 presents the results of a series of experiments designed to explore the early stages (first 1000 min) of the thermomechanical process for two-powder Ag/Bi-2223 composites. In this work, Bi-2223 precursor powders were formed by mixing $Bi_2Pb_zSr_2CaCu_2O_x$ with a $Pb_{(0.4-z)}$-Ca-Cu-O second phase. Fully processed samples with a series of z values produced the J_c values presented in the upper curve in Fig. 4. During FY 1995, as-rolled specimens from this same series of composites were heat treated for 10, 100, 300, and 1000 min, then quenched and analyzed by X-ray diffraction (XRD) for phase conversion to Bi-2223. After 10 min, there was no evidence of Bi-2223 for any of the z values; after 100 min, only the z = 0.3 sample showed the presence of Bi-2223; and after 300 min, samples from z = 0.2 to z = 0.4 had reacted to form Bi-2223. After 1000 min, all of the samples showed signs of reaction, but the samples with higher z values (i.e., with half or more of the Pb in the Bi-2212 component of the precursor) had progressed

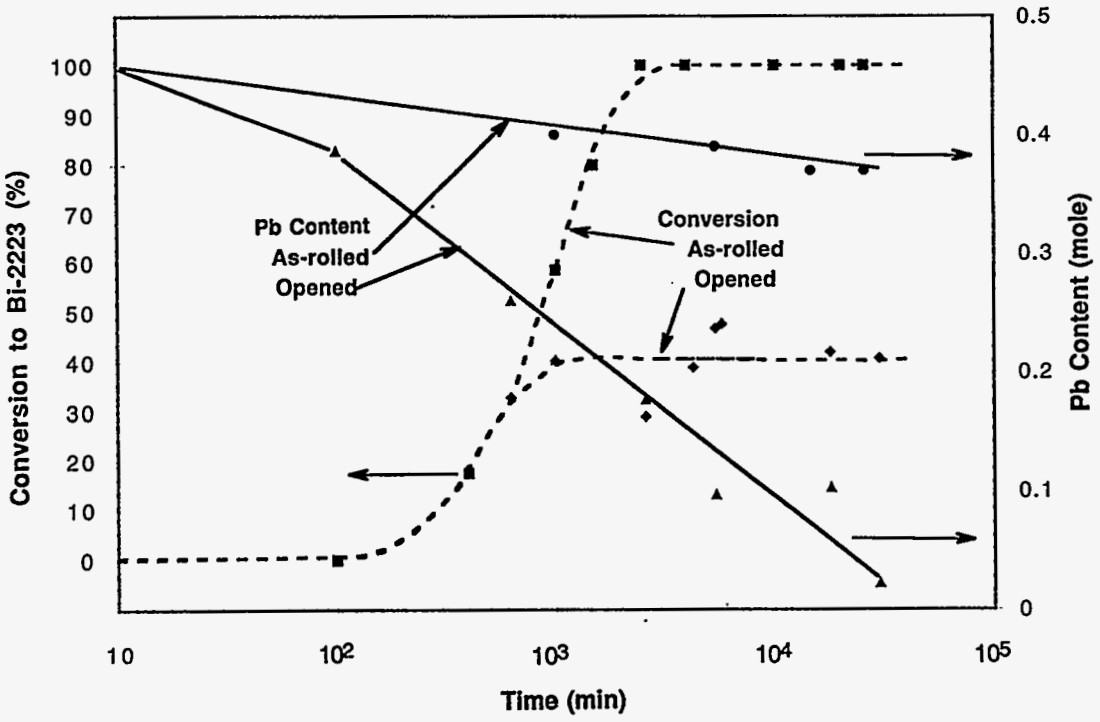

Fig. 3. Correlation of Pb loss with Bi-2223 phase formation for fully sheathed (as-rolled) and opened Ag/Bi-2223 composites heat treated at 825°C in 0.075 atm O_2.

significantly farther in terms of Bi-2223 formation. From these experiments, we find that the mode of lead deployment profoundly influencess the induction period preceding the onset of Bi-2223 formation in two-powder Ag/Bi-2223 composites.

Figure 5 contains a summary of extensive scanning electron microscopy (SEM) and energy-dispersive X-ray (EDX) examination of fully processed samples; the J_c curve for this series of composite specimens is again reproduced in this figure. SEM/EDX findings with regard to second phase (mainly alkaline-earth cuprates), Bi-2212, and Bi-2223 fractions indicate that all of the samples in the series contain 5-30% of second-phase material, including the z = 0.4 sample that produced the highest J_c. The most significant correlation with J_c is the amount of residual Bi-2212, which is lowest for the samples with the highest J_c. Furthermore, from the character of the Bi-2212 grains detected by SEM/EDX it appears that they may have formed in part as a result of Bi-2223 decomposition during the ramped cooldown period following the final heat treatment. This back reaction may be facilitated by residual liquid phase that persists (even after 250 h of heat treatment) for some z values because the Pb that causes the formation of this liquid phase is not yet fully deployed in Bi-2223 grains, i.e., the formation reaction in most of the samples was not complete at the end of the final heat treatment.

The addition of Pb to the Bi-2212 phase is known to cause a crystallographic transformation from a tetragonal (T) structure (Pb-free) to an orthorhombic (O) structure (Pb-doped). There is mounting evidence that during the Bi-2223 formation reaction, Pb first enters the Bi-2212 phase effecting this T → O transformation and then Bi-2223 grains grow by liquid phase transport of alkaline-earth cuprates to the Pb-doped Bi-2212. We have successfully utilized Raman microspectroscopy (RMS) and imaging Raman microscopy

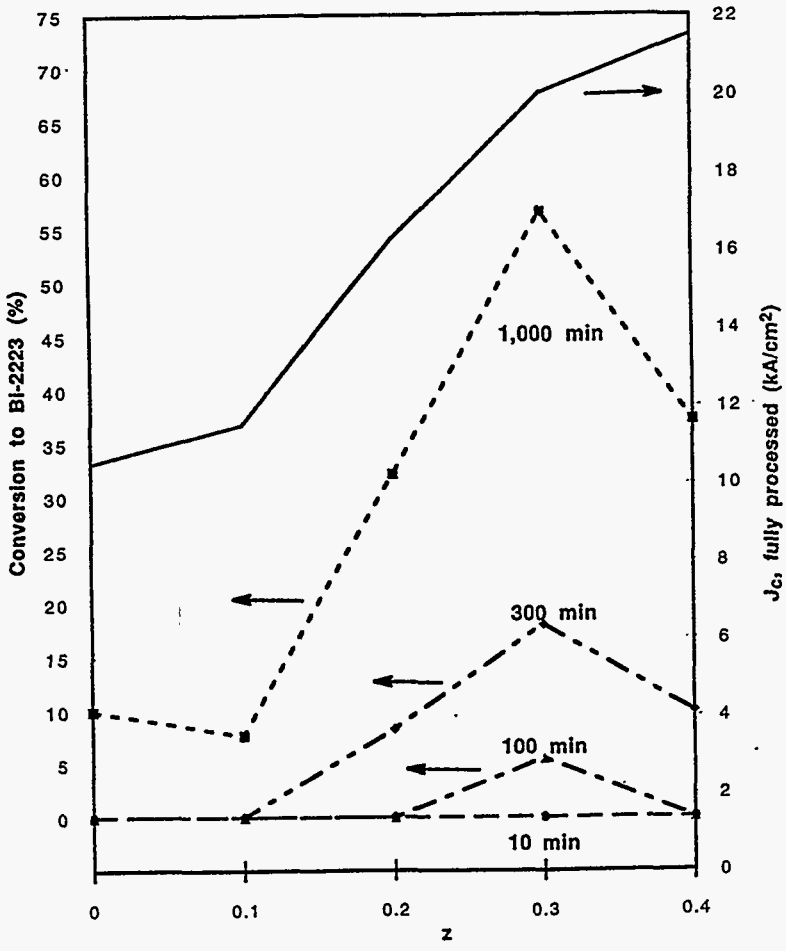

Fig. 4. Effect of Pb deployment in two-powder Ag/Bi-2223 composites on induction period preceding initiation of Bi-2223 formation reaction (10, 100, 300, and 1000 min), where z is stoichiometric Pb content of the Bi-2212 component. Solid-line curve shows J_c for fully processed conductor as reported by Dorris et al. (1993).

(IRM) to explore the T → O transition and to identify and image Pb-containing phases in Bi-2223 pellets and Ag-clad composites. Specifically, we have observed a Pb-rich phase surrounding T Bi-2212 crystals that had been formed by controlled back reaction of Pb-doped O Bi-2212.

The general procedure for applying RMS and IRM on Ag/Bi-2223 composites is depicted in Fig. 6. The defocused Raman spectrum of the circled region in the white light image contains significant features at (A) 298, (B) 543, and (C) 632 cm^{-1}. IRM images of peaks A, B, and C, ratioed against the adjacent average background (designated A/B1, B/B2, and C/B2, respectively, where B1 and B2 are the average backgrounds defined in Fig. 4) show the location of the species that generate each peak. Focused RMS scans, taken at points X, Y, and Z in the white-light image, produced the spectra labeled as Focused X, Y, and Z in Fig. 6. Comparison of these spectra with Raman spectra of standard materials leaves no doubt that Image A/B1 is that of a Cu oxide particle (which appears in the center of the white-light image), Image B/B2 shows the location of several Ca_2PbO_4 particles, and

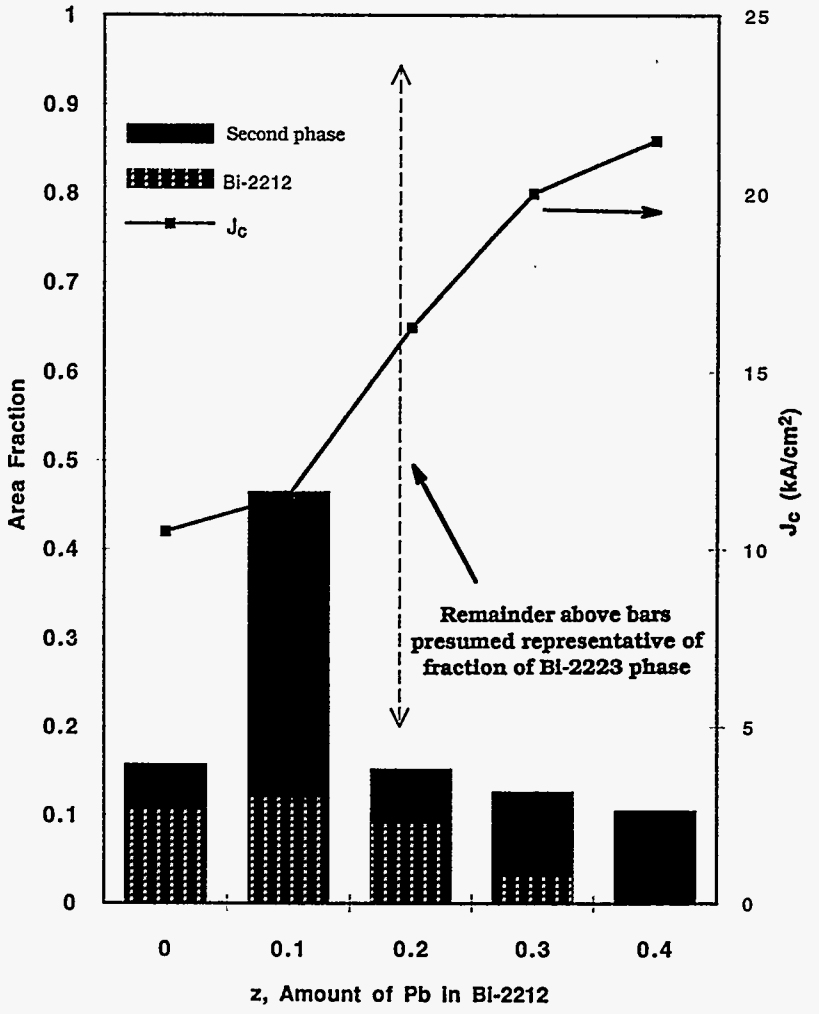

Fig. 5. Results of SEM/EDX analysis performed on samples from Dorris et al. (1993) Pb-deployment study, showing relative area fractions of second-phase material, unconverted Bi-2212, and Bi-2223.

Image C/B2 shows where Bi-2223 is located in the white-light image. RMS/IRM studies like this one are providing new insights into spatial distributions of key phases that participate in the Bi-2223 formation reaction.

In light of the growing body of evidence that Pb significantly influences phase evolution and microstructure development during thermomechanical processing of Ag/Bi-2223 composites (Luo et al., 1994a and b; Merchant et al., 1994a and b), we initiated a study to explore the effects of perturbations of metal atom stoichiometry on I_c in Ag/Bi-2223 composite conductors. In the first study of this series, we tested the effect of varying Pb stoichiometry over the range of 0.3-0.5 for two Sr values (1.9 and 2.0), using a fixed set of Bi (1.72 ± 0.05), Ca (1.97 ± 0.01), and Cu (3.10 ± 0.02) stoichiometries. The results of this test are shown in Fig. 7. An optimum was achieved for Pb = 0.3, with seemingly little sensitivity to the Sr value. Future tests in this series will include Pb values <0.3, as well as variations of Bi, Ca, and Cu stoichiometries.

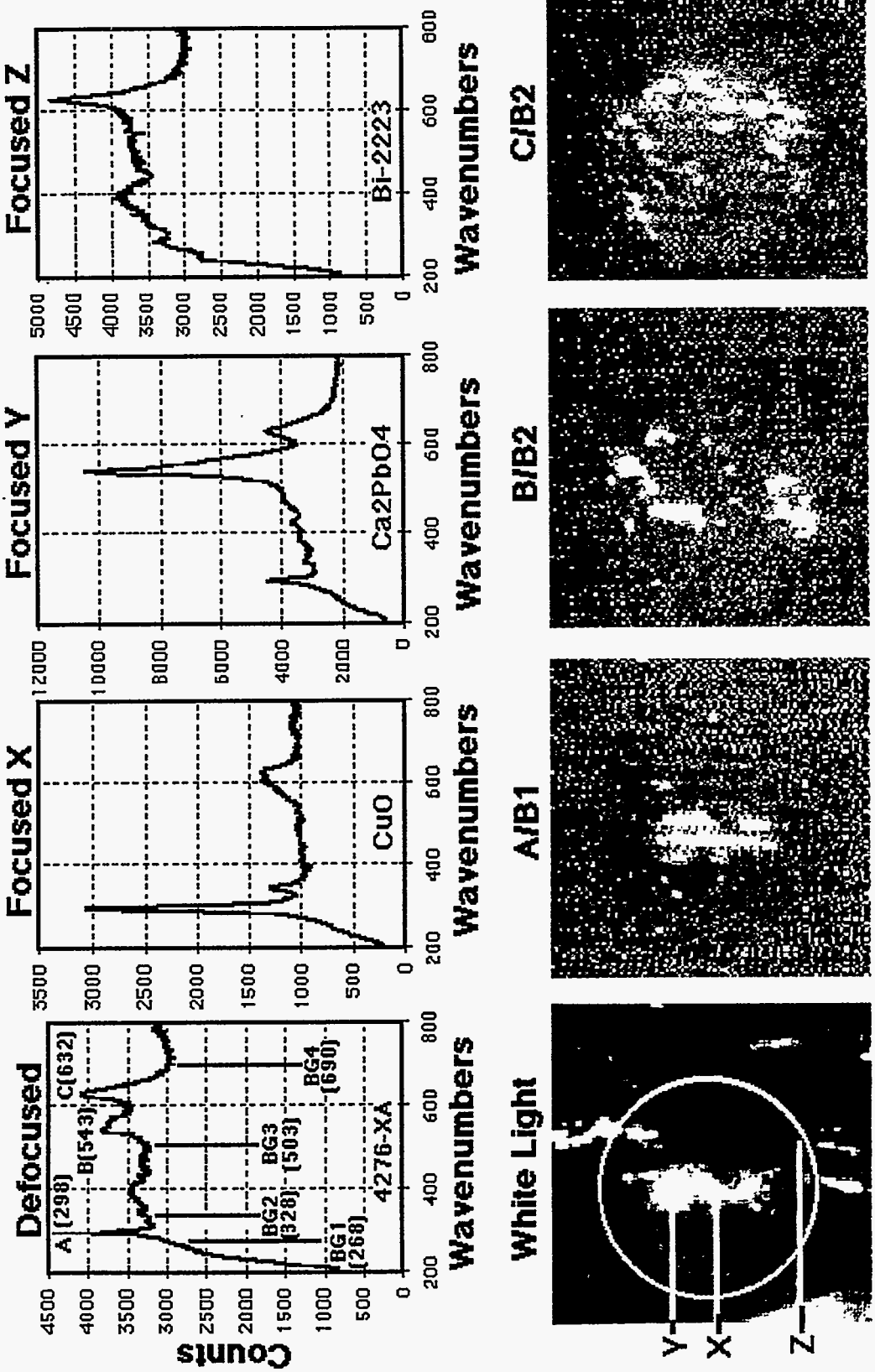

Fig. 6. Imaging Raman microscopy study of ceramic core of a fully processed Ag/Bi-2223 composite, showing spatial distribution of Cu oxide, Ca_2PbO_4, and Bi-2223 in typical core section.

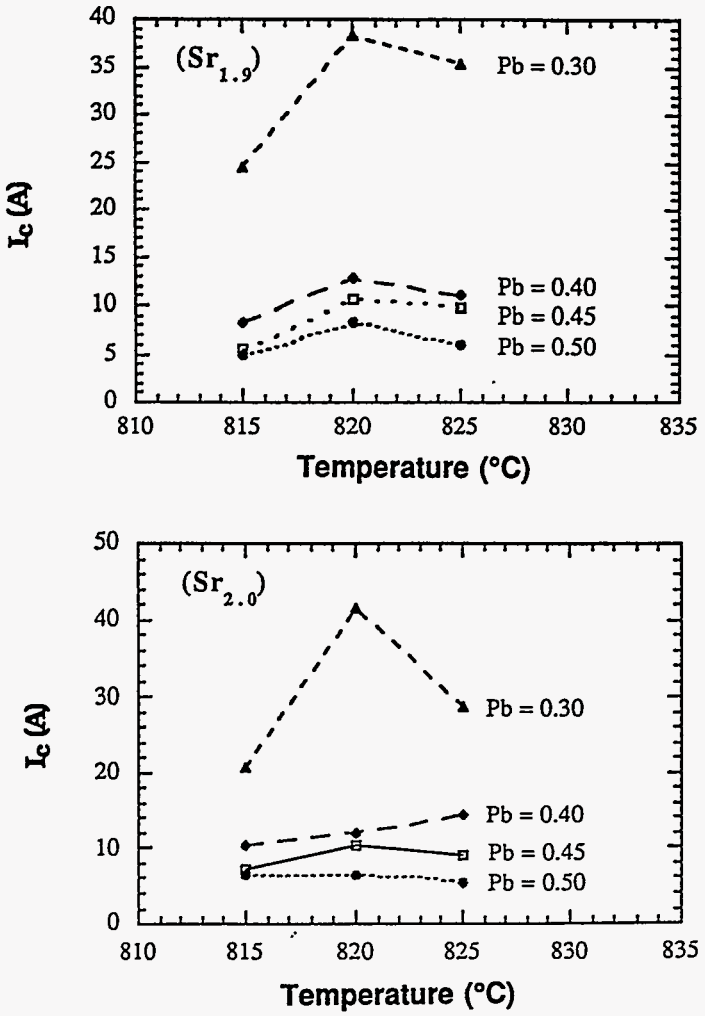

Fig. 7.
I_c values as a function of heat-treatment temperature for a series of Ag/Bi-2223 composites with varying Pb and Sr content. Fixed stoichiometries were maintained for Bi (1.72 ± 0.05), Ca (1.97 ± 0.01), and Cu (3.10 ± 0.02); processing sequence between rolls was 50/100/100 h in 0.08 atm.O_2.

Collaborative Phase-Development Work with American Superconductor Corporation

A significant portion of the work on Pb effects was conducted in collaboration with American Superconductor Corporation (ASC) and the ASC-led Wire Development Group (WDG). Although the composite conductors employed to produce the above-reported results were fabricated at ANL, several key experimental powders and pressed pellets that were examined at ANL were synthesized at ASC and at Los Alamos National Laboratory. The insights gained from this work have been shared with ASC and the other members of the WDG in connection with their in-house powder processing and composite fabrication activities and their contributions to the advances in Ag/Bi-2223 conductor performance achieved by ASC during FY 1995.

Collaboration with Ames Laboratory/Iowa State University

Despite considerable success in the development of commercial processes for preparation of Bi-2223, many details of the chemistry that occurs at high temperature are not well understood. For a standard PIT process, growth of Bi-2223 is usually carried out inside an Ag sheath and can typically be completed in a few days. The optimal properties often depend on the phases in the starting materials, the partial pressure of O_2, the proximity of Ag, and a host of other processing variables. One way to observe the phases that

form during processing is to quench at intermediate times and look for phases in the quenched material. A complementary method is to study the transformation in situ with X-rays (Polonka et al., 1993). The quench method has the advantage of reproducing the conditions of the commercial process better than the X-ray method, but it is not certain that all phases are preserved during the quench. The X-ray method has the advantage of direct observation of the process. The disadvantage is that the X-rays penetrate only ≈1 μm, so only the surface grains are observed. Hence, the two methods are complementary. Our goal is to determine the identity of the phases that form during the transformation, the kinetics of growth and decay of various phases, and the changes in kinetics with temperature.

We have used in-situ high-temperature X-ray measurements to follow the crystallographic changes that occur as Pb-doped Bi-2212 plus other phases transform into Bi-2223 in a PIT process for forming tape conductors. On the initial ramp to the reaction temperature, the Bi-2212 X-ray lines first diminish in amplitude and then begin to grow again above 700°C. Significant changes occur at 790°C. Lines associated with Ca_2PbO_4 form, but then disappear after 20–230 min at temperature. The Bi-2223 phase begins to grow at ≈810°C (Xu et al., 1995a and b).

2.1.2 Tape and Coil Development

Several programs in wire, tape, and coil development are ongoing. Much of the effort is focused on direct collaboration with industry. Each effort will be discussed individually.

Collaboration with Intermagnetics General Corporation

For the past few years, we have collaborated with Intermagnetics General Corporation (IGC) to develop high-T_c superconducting wires and tapes for possible electric power and high-field magnet applications. Potential commercial applications of the conductors include motors, generators, and transmission cables. Fabricating robust and high-quality conductors is important for the various applications envisaged for high-T_c superconductors.

The Ag-clad Bi-2223 conductors were fabricated by the PIT technique wherein partially reacted Bi-2223 powders were packed into high-purity Ag tubes, drawn through a series of dies and then rolled to a final thickness of ≈0.1 mm. Through a series of uniaxial-pressing and heat treatments, a J_c value >4 x 10^4 A/cm^2 has been obtained in short-length samples (Balachandran et al., 1994b). Because uniaxial pressing is not suitable for fabricating long-length conductors, a modified processing technique was employed for fabricating monocore and multifilament conductors (Haldar et al., 1994).

At 77 K and zero applied field, a J_c of ≈1.6 x 10^4 A/cm^2 has been achieved in a 125-m monofilament conductor. Figure 8 shows the I_c along the length of an 850-m 37-filament conductor. The I_c was 16 A, corresponding to a J_c of 1.2 x 10^4 A/cm^2. Recently, a 1250-m 37-filament conductor was fabricated with an overall J_c >1 x 10^4 A/cm^2. Consistent results have been obtained from long-length monocore and multifilament conductors, indicating that considerable progress has been made in their development. Compact and robust pancake coils have been fabricated from these conductors. The coils and test magnets have been characterized at various temperatures and applied magnetic fields. A test magnet, fabricated with eight double pancake coils, generated a field of 1 T at 4.2 K and 0.6 T at 27 K, in a background field of 20 T. Total length of the conductor in the magnet was 770 m.

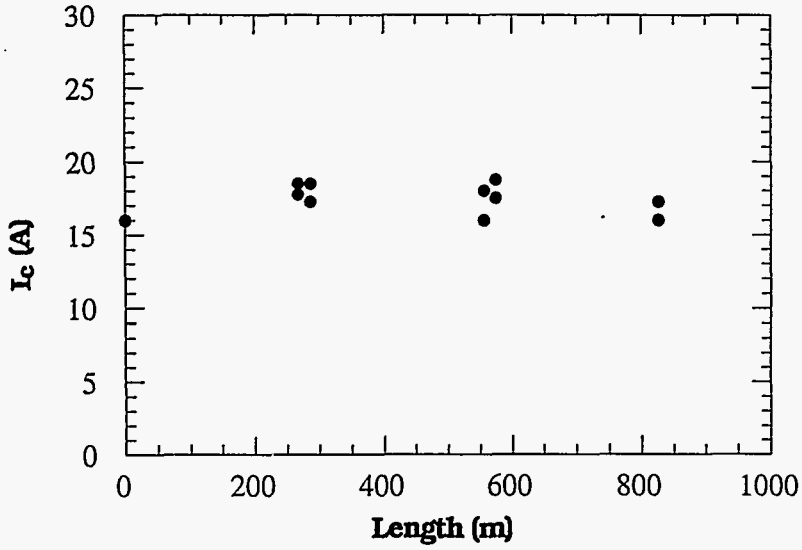

Fig. 8.
Critical current vs. length of 37-filament conductor at 77 K.

American Superconductor Corporation Collaboration

Our collaborative fabrication project with ASC, which includes ANL participation in the ASC-led WDG, has continued during FY 1995. The primary emphasis of the ANL contribution has been on phase evolution and microstructure development in Ag/Bi-2223 multifilament composite conductors. In this activity we are exploring the influence/effect of key processing parameters (i.e., temperature, O_2 pressure, and time) by applying the same methodology that was developed earlier for monofilaments. An added feature of the work on multifilament composites relates to the filament count and its possible influence on the Bi-2223 formation reaction. Figure 9 shows conversion-vs.-time data for four composites with a wide range of filament counts. (The composites designated OPIT were fabricated from oxide powder precursors, whereas the one designated MP contained a metallic precursor powder.) Within the limits of the characteristic uncertainty for these types of measurements, the filament count does not seem to discernibly influence the kinetics of Bi-2223 formation. Related studies of O_2 pressure and temperature variations indicate that Ag/Bi-2223 multifilament composites behave in a manner similar to that which was observed for Ag/Bi-2223 monofilaments in prior years.

Wire–in–Tube Processing

A coated-wire-in-tube (CWIT) process for fabricating Ag/superconductor composite conductors is being developed in collaboration with BASF Corp. This process has several potential advantages, the most important of which is that it greatly increases the Ag/superconductor interface area. This may significantly enhance superconducting properties, because abundant evidence exists (Lelovic et al., 1995a; Pashitski et al., 1995; Welp et al., 1995) that a thin, well-aligned layer at the Ag/superconductor interface carries a large fraction of the current in Ag-sheathed conductors. Also, the matrix of CWIT conductors consists of superconductor, whereas Ag forms the matrix of multifilament conductors, another type of conductor with an increased Ag/superconductor interface area. As a result, percolation through CWIT conductors may be improved relative to multifilament conductors, where small-scale disruptions, such as second-phase particles or cracks, may force transport through the Ag. In addition, the thickness of superconductor

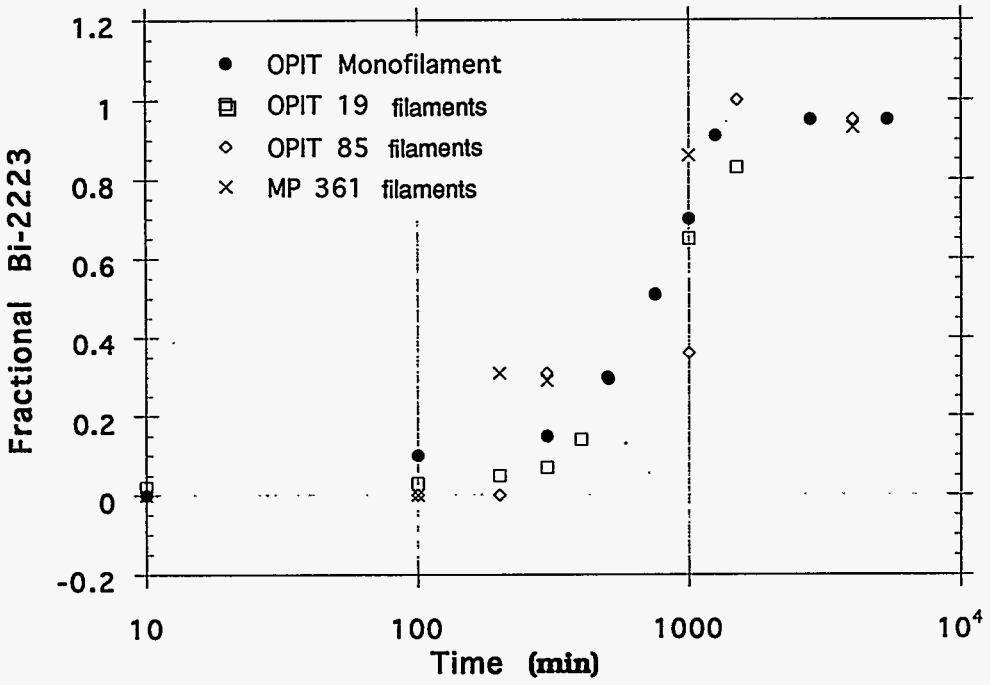

Fig. 9. Fractional conversion to Bi-2223 vs. time for Ag/Bi-2223 composites with four filament counts, processed at 825-830°C in 0.075 atm O_2. (OPIT = oxide powder precursor, MP = metallic precursor.)

layers in CWIT conductors can be reduced, and the Ag superconductor interface area increased, by decreasing the initial coating thickness, i.e., thinner superconductor layers can be made without additional mechanical deformation. By comparison, the filaments of a multifilament conductor are made finer by subjecting them to additional mechanical deformation, which can roughen the interface and cause misalignment of grains in the interface layer. Other possible benefits of the CWIT method include good strain tolerance due to the distribution of Ag on a fine scale and the ease of adapting it to the fabrication of long-length conductors, perhaps even by a continuous process.

Figure 10 is a schematic representation of the apparatus developed and used at BASF to coat Ag wire with Bi-2223 precursor that has been made by our two-powder process. At one end is a spool of Ag wire; at the other end is a winder that pulls the wire through the coating apparatus and spools up the coated wire. The wire first passes through a coating device that contains a dispersion of Bi-2223 precursor and an organic carrier in a solvent. The coating thickness can be controlled to some degree by applying slight pressure to the coating vessel. As the coated wire exits from the coating device, it passes through an air ring and/or a dryer to remove the solvent from the coating. If a thicker coating is desired, the wire can be passed through a second coating device and a subsequent air ring and dryer. Coatings made by this method adhere well to the Ag and show little or no tendency to flake off during handling. To date, coating thicknesses of 50-150 mm have been produced, and 2-3 km of coated wire have been made in less than three days, without speed as a consideration. Experience at BASF with this type of procedure indicates that the coating speed can be increased 100-500 times, so the coating process is clearly capable of efficiently manufacturing long lengths of conductor.

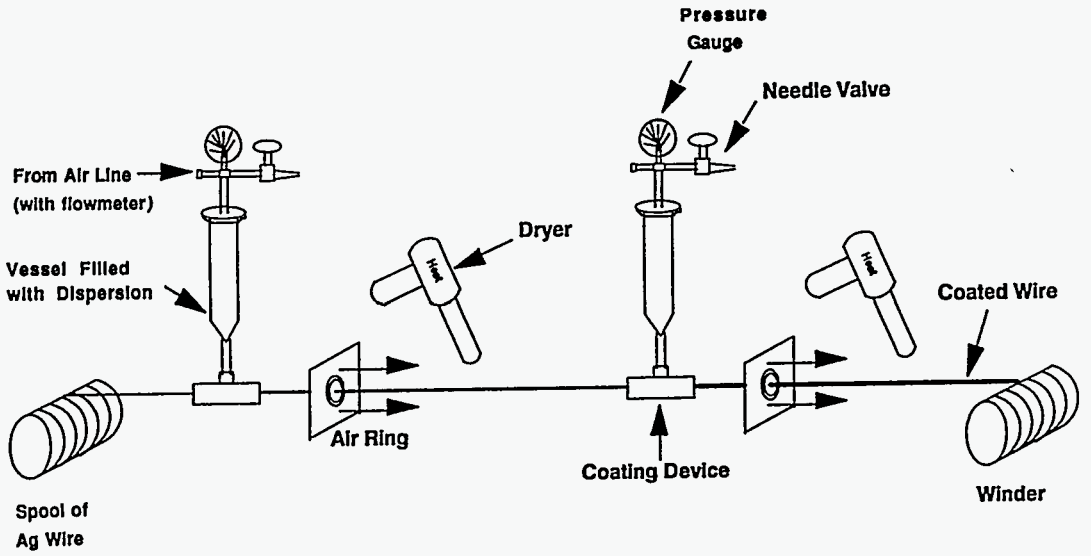

Fig. 10. Schematic representation of apparatus used to coat Ag wire with Bi-2223 precursor powder for use in CWIT process.

A bundle of 100-300 coated wires is made and loaded into a Ag tube (Fig. 11). The tube, open on both ends and filled with coated wires, is then heated to remove organics. The removal of organics is performed very slowly (5°C/h up to 720°C, then held for 24 h) under a partial vacuum (2-3 torr of flowing O_2) to facilitate removal of gaseous products and prevent decomposition of the superconductor during the process. After heat treatment, the tube is swaged at both ends, so that the coated wires are gripped during subsequent deformation steps. From this point on, the process is identical to the PIT process for producing monofilaments. The final tape is ≈250 μm thick and 4 mm wide. To vary the thickness of the superconductor layers in the final conductor, the initial coating thickness on the wire is varied. Regardless of the target layer thickness, however, the mechanical deformation sequence is the same, so the Ag/superconductor interface should be just as smooth for a 3-μm-thick layer as for a 20-μm-thick layer. This is important, because a smooth interface yields better grain alignment.

Several issues have been identified as critical to the development of the CWIT process, and these are currently being investigated. First, what is the most efficient and effective way to remove organics from the coated wires? The C concentration must be minimized, because C adversely affects the properties of PIT tapes. Because the coating is tougher and better withstands handling when it contains organics, it is most convenient to remove the organics from the wires after they have been loaded into a Ag tube, but it may be difficult to completely remove the C from such an enclosed environment. Next, do the wires deform uniformly and reproducibly so that the final structure can be predicted, or do they break apart at various points in the process, leaving an uncontrolled, wide range of Ag shapes and sizes? Similarly, how are the Ag wires distributed spatially in the core? The Ag/superconductor interface area is not increased as effectively if the Ag wires and superconductor tend to segregate. Finally, does the well-aligned, high-J_c interface layer form on the surface of the Ag wires? If so, is it continuous, and how thick is it? If the layer is formed, how well does it perform?

Coated Wire-in-Tube Processing

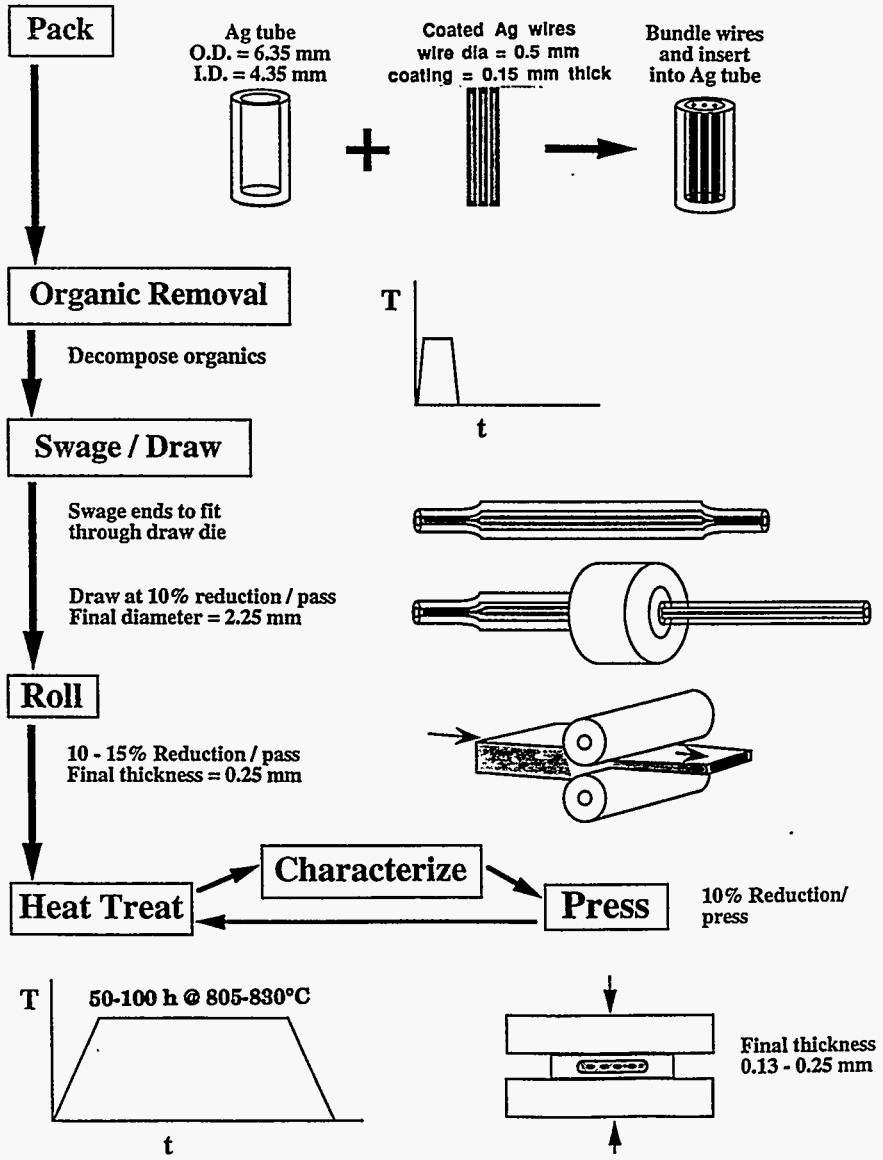

Fig. 11. Flow chart for CWIT process.

As an initial investigation of organic removal, Bi-2212 fibers made with the same organics that were used in the CWIT process were loaded into a Ag tube and heated very slowly (5°C/h to 720°C) in a partial vacuum (2-3 torr O_2) to remove the organics. After heating, the tube was cut into three sections, and the superconductor powder from each section was collected. The C content of the three powders ranged from 700 to 900 ppm and XRD of the powders showed no sign of decomposition. The C content was somewhat higher than the typical value (<400 ppm), but it was not unusually high and was in a range where adverse effects of C have not been confirmed. This suggested that the organics can be removed from within the Ag tube if moderate C concentrations can be tolerated.

To determine the effect of moderate C content on CWIT conductors, one conductor (CWIT #1) was made from wires that were first loaded into a Ag tube and then subjected to removal of organics, whereas another conductor (CWIT #2) was made from wires that had first undergone organic removal in an open tray and then were loaded into a Ag tube. The coated wire for the two samples originated from the same spool, and the organics were removed at the same time, i.e., the tube packed with coated wires (CWIT #1) was heated alongside the exposed coated wires (CWIT #2). The organics were removed by heating at 5°C/h up to 720°C, holding for 24 h at 720°C, then cooling at ≈60°C/h, all in flowing O_2 at a total pressure of 2-3 torr. The exposed coated wires were badly deformed during organic removal, nevertheless, the superconductor powder adhered to the Ag wire, and the wires were loaded into a Ag tube. CWIT #1 and #2 were then processed by the same mechanical deformation sequence that was used to produce monofilament PIT conductors. Along with the two CWIT conductors, a monofilament was made from the same powder that was used to coat the Ag wires for CWIT #1 and #2. Because the powder for the monofilament contained no organics, it did not undergo the slow organic removal heat treatment described above. Rather, it was heated at 60°C/h to 720°C, held for 3 h at 720°C, then cooled at ≈60°C/h at a pressure of 2-3 torr of flowing O_2.

After mechanical deformation, each of the three tapes (monofilament and two CWIT conductors) were ≈250 μm thick. Short samples of the tapes (≈3.0 cm) were heated for 36 h at 815°C in 8% O_2, then cooled and uniaxially pressed, heated for another 100 h under the same conditions, cooled and uniaxially pressed, then heated for a final 100 h. I_c was measured after total heat treatment times of 36, 136, and 236 h, with a 1 μV/cm criterion. J_c for the three tapes is plotted as a function of total heat treatment time in Fig. 12, where each data point represents the average of J_c measurements made on three separate samples. CWIT #1 reached a J_c of 14 kA/cm^2 after 236 h, whereas CWIT #2 exhibited a J_c of <5 kA/cm^2. This finding suggests that the wire configuration was a more important factor than organic removal, because organic removal from CWIT #2 was certainly superior to that from CWIT #1, but its wires were badly twisted during organic removal. It cannot be concluded, however, that removal of organics from within the tube is adequate or does not present problems, because the standard monofilament outperformed both CWIT samples, reaching a J_c close to 20 kA/cm^2.

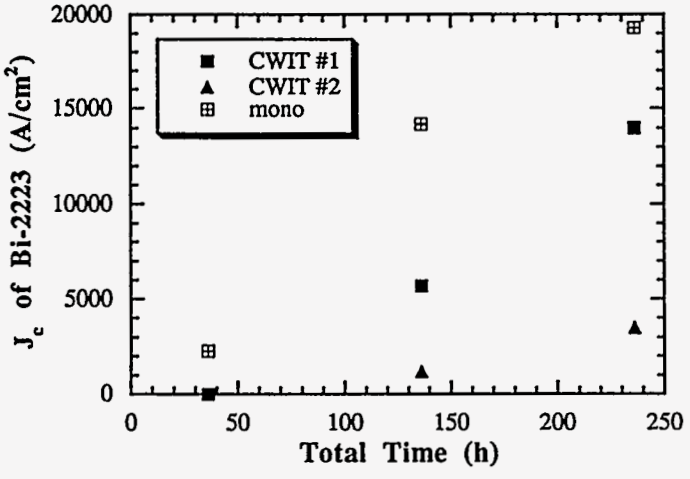

Fig. 12.
Average critical current density J_c as a function of total heat-treatment time at 815°C in 8% O_2. CWIT #1 and CWIT #2, CWIT conductors; CWIT #1, wires loaded into an Ag tube before removal of organics. CWIT #2, wires loaded into an Ag tube after removal of organics. Monofilament was made from same powder used to make CWIT #1 and CWIT #2.

Figure 13 shows a transverse view of CWIT #1 rolled to an overall tape thickness of 1000 μm. The light-colored material around the outside is the Ag sheath; the light-colored oblong shapes are Ag wires (144 in total). The darker material between the Ag wires is Bi-2223. Deformation of the wires appears to be fairly uniform in that the wires are all approximately the same size and the number of wires at the end of the process is the same as the number of wires put into the tube, within several wires. At a tape thickness of 1000 μm, the Ag wires appear to be distributed uniformly throughout the core. Examination of thinner tapes, however, shows a less uniform distribution of Ag wires in the core, suggesting that rolling may cause segregation of the wires. The effect of mechanical deformation on the Ag wire distribution will be explored in greater detail in the future.

Shown in Fig. 14 are longitudinal views of CWIT #1 rolled to 250 μm. The light streaks are Ag wires, and the dark material between the wires is superconductor. These views show that the Ag/superconductor interface is fairly smooth and that the superconductor thickness (varying between 2 and 10 μm) is uniform along its length. At higher magnification (Fig. 14b), the dense interface layer is evident, but is very thin (only 2-3 μm) and not completely continuous. It is not clear whether the interface layer must be perfectly continuous to be beneficial, but good continuity is certainly preferred. To improve the continuity of the interface layer, and perhaps increase its thickness, Ag wires that contained up to several wt.% Pb will be used as the wire inserts. Lead plays a crucial role in the formation of Bi-2223, so its presence in the wires may promote formation of Bi-2223 on their surfaces. In CWIT #2, whose wires were badly deformed during organic removal, the spatial distribution of Ag wires was less uniform and the superconductor thickness was less uniform in the longitudinal direction, with the Ag wires "pinching off" the superconductor in some places. These results suggest that the initial wire configuration can strongly affect the final microstructure.

Another experiment relating to the removal of organics consisted of five samples. The first sample (CWIT #3) was made from wires that contained organics when they were loaded into a Ag tube, i.e., the sample was like CWIT #1 except the wires were loaded in a straight and parallel configuration by means of a special rack. Sample 2 was a monofilament prepared by our standard PIT procedure with the same powder as in CWIT #3, but the powder contained no organics. Sample 3 was a monofilament also made from the powder used for CWIT #3, but the powder was put through the organic removal heat treatment, even though it contained no organics, to see the effect of the heat treatment itself. Powder for samples 4 and 5 came from the superconductor dispersion used to coat the wires in CWIT #3, so it contained organics.

Sample 4 was prepared by removing the organics from large chunks of the dispersion (≈15-25 μm in diameter) in an open tray, then processing the powder by the normal PIT procedure. Sample 5 was prepared by removing the organics from small chunks of the dispersion (≈2-3 μm in diam) placed inside a Ag tube, then processing by the normal PIT procedure. Samples 3, 4, and 5 were positioned side-by-side during the removal of organics, which was accomplished by heating in 2-3 torr of flowing O_2 at 5°C/h up to 720°C, holding for 24 h at 720°C, then cooling at ≈60°C/h.

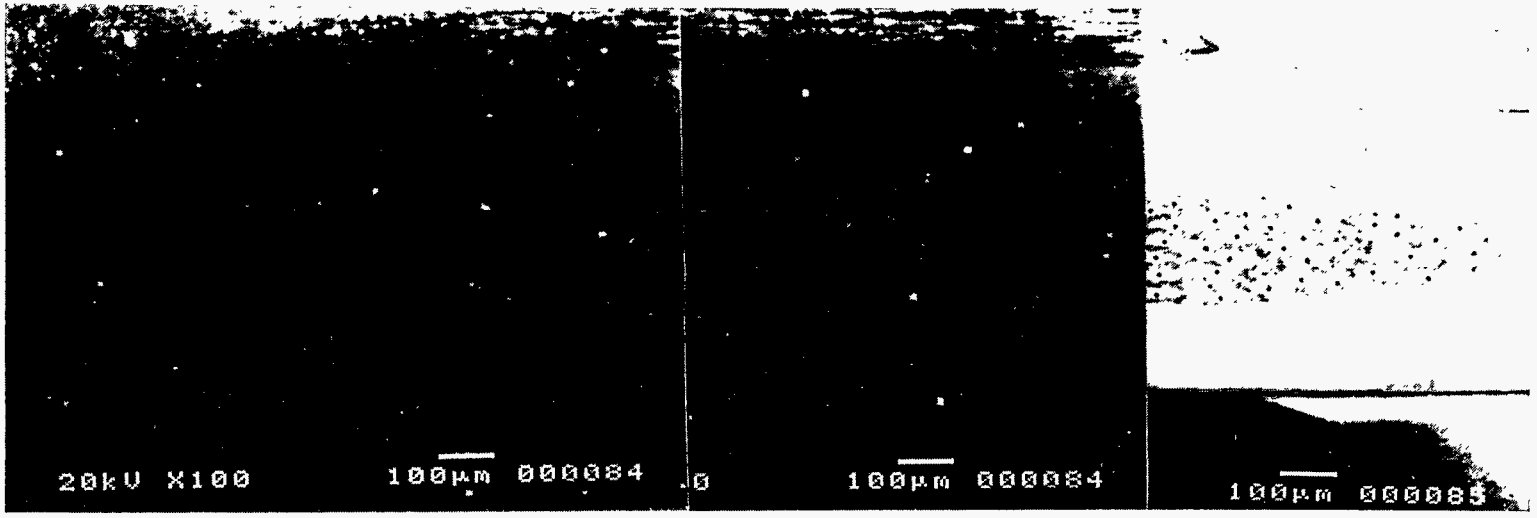

Fig. 13. Transverse secondary electron image of CWIT #1, a coated-wire-in-tube sample heated for 50 h at 815°C in 8% O_2.

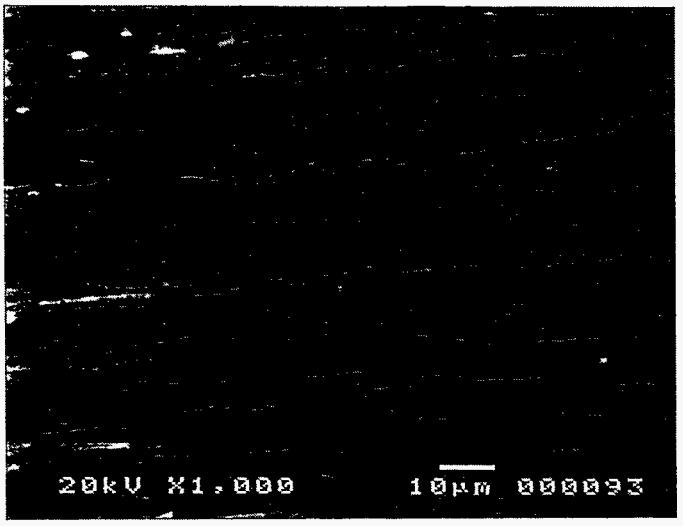

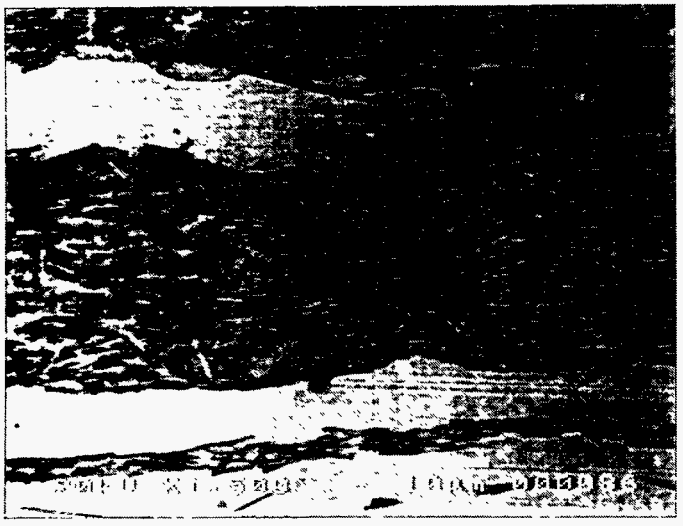

Fig. 14.
Longitudinal secondary electron images of CWIT #1, a coated-wire-in-tube sample heated for 50 h at 815°C in 8% O_2, at magnification of (a) 1000x and (b) 1500x.

After mechanical deformation, 3.0-cm-long samples were cut from the five tapes, heat treated for 50 h at 815°C in 8% O_2, then cooled and uniaxially pressed, heated for an additional 100 h under the same conditions, and so on until they had been heated for a total of 350 h. Figure 15 shows the average J_c (average of three independent samples) as a function of total heat treatment time.

CWIT #3 exhibited the highest J_c, reaching an average value of 12 kA/cm^2, with a high value of 15 kA/cm^2. The monofilament results (Samples 2-5) are lower than the typical value of 15-20 kA/cm^2, possibly because the cores were extremely thick, >200 µm, due to problems encountered during mechanical deformation. Because of the difference in core thickness, comparing CWIT #3 to the monofilament samples is not conclusive; however, the results for the monofilament samples can be compared with one another, because the core thickness of all of these samples was approximately the same. First, comparing Samples 2 and 3, it is evident that the J_c of the powder subjected to heat treatment for removal of organics (Sample 3) was lower than the J_c of the sample that did not undergo

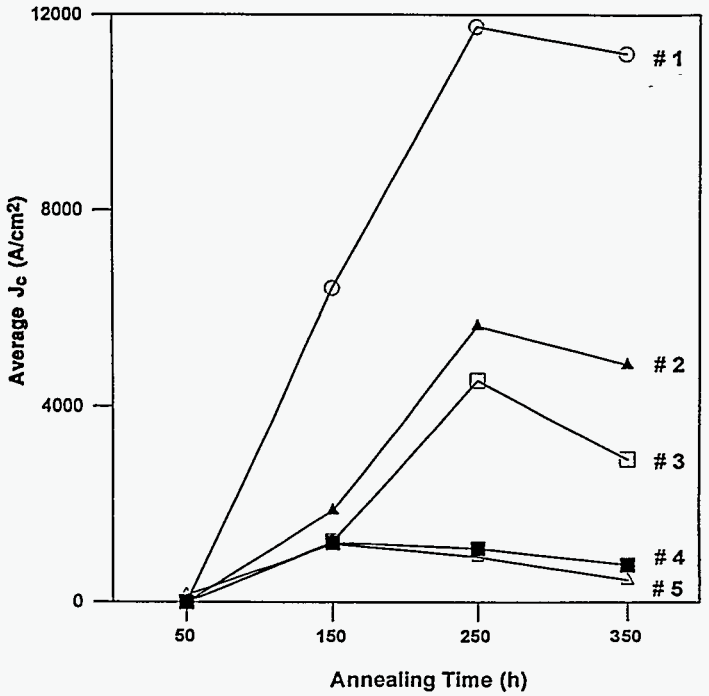

Fig. 15.
Average critical current density J_c as a function of total heat-treatment time at 815°C in 8% O_2 at 77 K and zero applied field. CWIT #3, a coated-wire-in-tube conductor from wires that were loaded into an Ag tube before removal of organics; Samples 2 and 3, monofilaments from the powder used in CWIT #3; Samples 4 and 5, monofilaments made from the superconductor dispersion used in CWIT #3.

the heat treatment (Sample 2), suggesting that the heat treatment itself damages the superconductor. The difference in J_c is not large and should be confirmed, but the difference is believable, considering that significant phase changes have been shown to occur in Bi-2223 (Grivel et al., 1993) even at the relatively low temperatures that are used to remove organics.

Samples 4 and 5 were monofilaments made from the dispersion used to make CWIT #3. Their J_c values were nearly identical to one another and were significantly lower than the J_c of the monofilaments made without organics (Samples 2 and 3), clearly indicating that organic removal can strongly influence the final properties of CWIT conductors. The similarity in J_c suggests that the removal of organics was problematic for both samples, from Sample 4 because large chunks of dispersion were used and from Sample 5 because the removal was done inside a Ag tube. Both the large size of the dispersion chunks and containment by the Ag tube could leave residual carbon and cause decomposition of the superconductor during organic removal, possibly accounting for the extremely poor J_c of these samples. Considering how poorly Samples 4 and 5 performed, presumably due to poor organic removal, the performance of CWIT #3 is startling, possibly indicating that the effect of Ag wires is beneficial enough to overcome the deleterious impact of organic removal.

The removal of organics is clearly an important issue, and will be an area of primary focus in the future. A CWIT sample whose organics are removed while inside a tube will be compared with one whose organics are removed outside the tube. This will be similar to the first experiment described above but will be done with a rack to prevent distortion of the wires during organic removal. Electrophoretic deposition will be tested as an alternative method for coating wires, because it produces superconductor coatings that contain essentially no organics. Faster organic removal treatments will be explored as a way to avoid disturbing the initial two-powder phase assemblage.

The CWIT microstructure will be better characterized and factors affecting the microstructure will be investigated. The roughness of the Ag/superconductor interface will be quantitatively characterized and compared with multifilament conductors. CWIT samples seem to possess fairly smooth Ag/superconductor interfaces, which may be an important advantage, because grain alignment is more favorable at a smooth interface. A uniform distribution of Ag wires maximizes the effect of Ag, so the distribution of wires will be monitored during mechanical deformation to determine the source of nonuniformity. Preliminary evidence suggests that rolling may be a source of nonuniformity, so factors such as tape thickness and conductor geometry (round vs. flat) will be varied to gauge their effect on the wire distribution. The crux of the CWIT method is the interface layer and how it performs. To improve continuity and perhaps the thickness of the interface layer, CWIT samples will be processed with Pb in the wires. To address the performance of the interface layer, CWIT samples will be studied by magneto-optical imaging. Finally, to test the expectation that these samples should exhibit strain tolerance comparable to that of multifilament samples, strain tolerance of CWIT samples will be measured.

Strain Tolerance of Tapes

It is important that we study the mechanical integrity of the conductors because during fabrication and in service, the tapes are subjected to tensile, bending, and electromagnetic hoop stresses. Axial strain tolerance of monocore and multifilament conductors was studied by subjecting the tapes to in-situ tensile tests. Retention of I_c as a function of applied strain was measured at 77 K and in applied fields of 0 and 0.5 T. Figure 16 shows normalized I_c as a function of applied strain, in an applied field of 0.5 T, for monocore and multifilament conductors. As seen in Fig. 16, multifilament conductors appear to have better strain tolerances than do monofilament conductors, retaining more than 90% of their initial I_c at ≥1% strain. In contrast, e_{irr} (irreversible strain) for the monofilament conductor was 0.2%.

In-situ bending characteristics of the conductors were obtained with a custom-designed test fixture. The tests were conducted on both mono- and 61-filament conductors at 77 K and zero applied field. The effect of superconductor/Ag ratio (fill factor) on the bending characteristics of monofilament conductors was also studied;

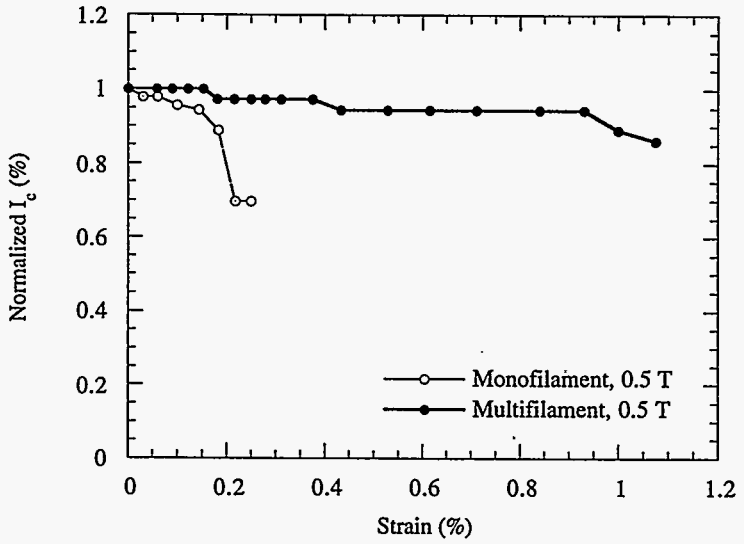

Fig. 16.
Normalized I_c vs. strain of mono- and multifilament conductors at 77 K and 0.5 T applied magnetic field.

monofilament conductors with fill factors of 23, 30, and 38% were used. Figure 17 shows the normalized I_c of monofilament and 61-filament conductors as a function of bending radius. As observed by several other research groups, the drop in I_c with decreasing bending radius is more profound in monofilament conductors than in multifilament conductors. Figure 18 shows preliminary results of the effect of superconductor/Ag ratio on the bending characteristics of the monofilament conductor. The plot shows that the e_{irr} for the monofilament conductor increases as the superconductor fill factor decreases. The results we obtained are encouraging because they show that further improvement in mechanical properties can be achieved without compromising current transport properties. At present, effort is underway to further study the effect of superconductor/Ag ratio, Ag doping, and initial packing density on the strain tolerance of Bi-2223 tapes.

Effect of Cracks on J_c of Ag/Bi-2223 Composites

A major concern in the application of PIT tapes is the effect of strain on J_c. Cracks in the superconductor core, induced during wire fabrication and coil winding, degrade J_c; however, significant shunting of current transport through the Ag sheath can occur. The electric field associated with current that shunts through the Ag sheath could be below the criterion for defining J_c.

Mechanical properties of the tape are often represented by strain tolerance from tensile or bending tests. The inherent strain tolerance of bulk Bi-2212 and Bi-2223, without an Ag sheath, can be determined from fracture strength and elastic modulus (Martin et al., 1993; Fanggao et al., 1993). The highest mechanical strength reported for bulk Bi-2223 is ≈140 MPa, which implies a strain of ≈0.1% before fracture. To increase J_c and flexibility, a fine multifilament tape is often considered. Typical strain tolerance values have been improved from 0.2–0.4% for monofilament tapes to 0.6–1.5% for multifilament tapes (Ekin et al., 1992; Dou et al., 1993; Otto et al., 1993; Yau and Savvides, 1994; Miller et al., 1991). Cracks in the core have been observed by electron microscopy after tensile/bending tests. An understanding of the effects of cracks on J_c can provide important information for tape design and fabrication.

Our previous model for current flow (Cha et al., 1994a) has been extended to Ag/Bi-2223 composites with cracks and is based on current shunting in the Ag and on interfacial resistance between the Ag and Bi-2223. Calculations from the model are compared with experimental results for Ag/Bi-2223 bars. The results provide guidance for relative placement of current and voltage leads and insight into the influence of cracks on J_c of PIT tapes.

Producing controlled defects in PIT tapes is difficult because of the small core size. In addition, part of the Ag sheath must be removed to produce cracks of known dimensions. The sinter-forge technique for bars had several advantages over the PIT process for validating a voltage-distribution model. High-quality bulk specimens with high J_c (1000–8000 A/cm^2 at 77 K) have been fabricated by sinter forging (Chen et al., 1993). Large bars with good mechanical integrity can be easily cut to produce controlled defects. Another advantage is that the Ag/Bi-2223 bond can be fabricated separately, allowing variation of contact resistance in a separate heat-treatment step.

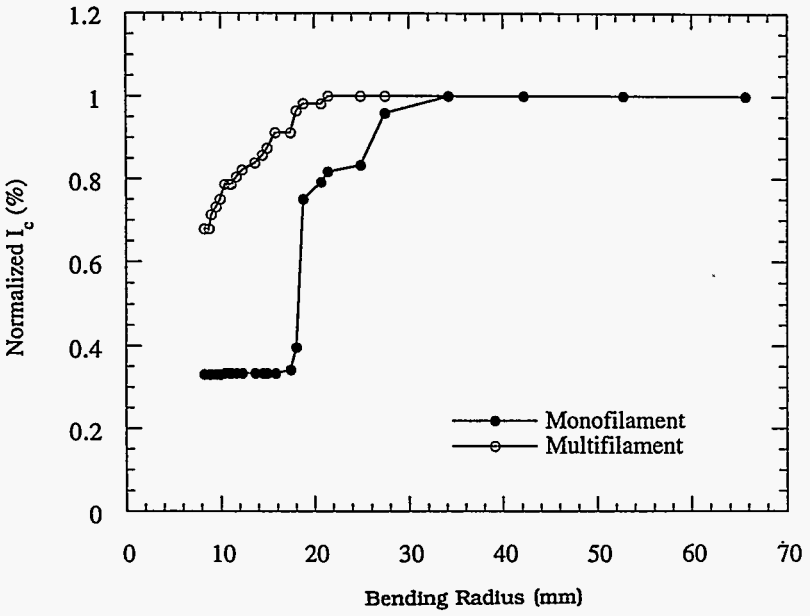

Fig. 17. Normalized I_c of mono- and multifilament conductor as a function of bending radius.

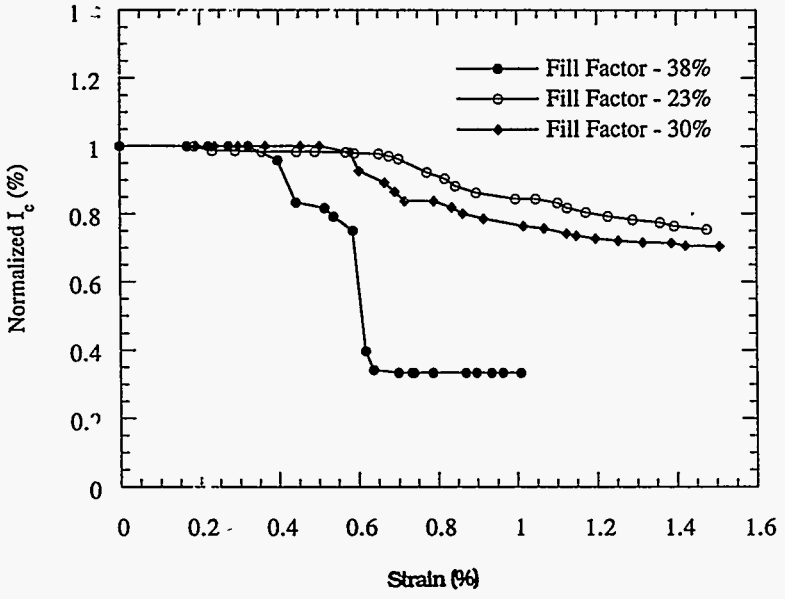

Fig. 18. Normalized I_c vs. bending strain of monofilament conductors with three superconductor fill factors.

A Bi-2223 bar (50–70 mm) was bonded to an Ag sheet by forging at 400–845°C for 1 h at 5–10 MPa (Goretta et al., 1994). Contact resistivity of this Ag/Bi-2223 composite was altered by varying the forging temperature and pressure; it can be estimated from Fang et al. (1995) under the same sinter-forged conditions. Voltages were measured at 77 K (Fig. 19) by placing voltage leads on both sides of the Ag and Bi-2223. The excellent agreement between the measured voltage profiles and calculated data confirms the crack-shunting model (Fig. 20).

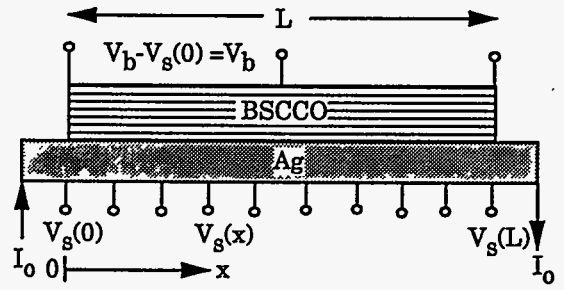

Fig. 19.
Voltage lead placement in Ag/Bi-2223 specimen.

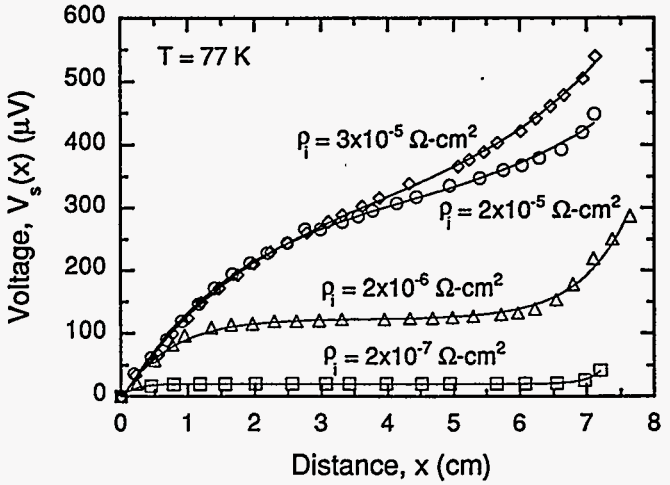

Fig. 20.
Line fit of voltage drop along Ag for sinter-forged Ag/Bi-2223, determined from model; experimental data are individual data points.

When a complete crack is present in the Bi-2223 core, all of the current is forced to shunt into the Ag via the interface. The voltage associated with current shunting is low and is manifested as a linear rise in the V-I curve at current densities below the core J_c. Such behavior has been observed for V-I curves; however, high electric field sensitivity, i.e., ≈1 nV/cm, is required (Suenaga et al., 1995).

Voltage drop in the J_c measurement is the sum of the voltage across the Ag/BSCCO interface ($2V_b$) and the voltage of the Ag in the crack zone. The voltage can be rewritten in terms of the current density ($J = I_o/wd_b$) for the tape

$$V_b = \frac{Jd_b}{2}\sqrt{\frac{\rho_s\rho_i}{d_s}}, \qquad (1)$$

as long as $\lambda L > 10$. If J_c degradation is caused by the cracks in the core, use of $2V_b = V_c$ and $J = J_e$ can yield the equivalent current density J_e in a tape with multiple cracks, i.e.,

$$J_e = \frac{E_c}{d_b N}\sqrt{\frac{d_s}{\rho_s\rho_i}}, \qquad (2)$$

where E_c (1 μV/cm) is the critical field and N is crack density (number of cracks per cm). This suggests that J_e is proportional to the square root of d_s and inversely proportional to N and d_b. J_e in Eq. 2 cannot be exceeded by the core J_c.

Figure 21 shows calculated equivalent current density J_e as a function of crack density, based on Eq. 2 for $\rho_i = 10^{-9}$–10^{-11} Ω-cm^2 at 77 and 4.2 K, with d_s = 75 μm and d_b = 50 μm. The maximum values of J_e in Fig. 21 are the critical current densities J_{co} of the Bi-2223 core. These densities are a series of horizontal lines that depend on J_c. The intersection points of J_{co} and J_e define where cracks would first be detected by electrical measurement. This implies that the tape with a lower J_c value has a better e_{irr}. For example, a tape with a J_c of 10^4 A/cm^2 allows only N = 0.1 cm^{-1}, whereas a tape with a J_c of 10^3 A/cm can have one crack per centimeter before degradation occurs if $\rho_i = 10^{-9}$ Ω-cm^2. The present model is based on complete cracks; however, a more realistic model would include partial cracks. Future work will include the effects of partial cracking on J_c value.

Joining of Tapes

A novel etching technique has been developed to produce superconducting butt joints between Ag-clad conductors. The Ag sheath from one side of the tape was selectively etched to expose the underlying superconductor core. Joints were formed by bringing the two tapes together and subjecting them to heat treatment. Detailed microstructural analysis and current transport measurements of the joints have been performed. I_c as a function of heat-treatment time for the butt joint is shown in Fig. 22. Typical I_c through the joint was 23 A, which is ≈70% of that carried by a normal tape. The butt joint shows a uniform and well-textured grain structure when examined by SEM (Fig. 23). At present, the effects of various joint configurations, processing techniques, and strain on the current transport properties of the joints are being studied.

Heat Treatment of Ag-Sheathed Bi-2223 Tapes

As reported previously (Balachandran et al., 1994a), cooling rate had a pronounced effect on the J_c of Ag-sheathed Bi-2223 tapes at 825°C. Tapes sintered at 815°C show very little change in J_c when the cooling rate is decreased from 100 to 10°C/h, whereas a significant increase in J_c was observed for tapes sintered at 825°C.

A detailed study was carried out to evaluate the changes in microstructure and Bi-2223 content and the resulting effects of these changes on J_c as a function of cooling rate. Tapes were sintered at 825°C and cooled at 100, 50, 25, or 10°C/h to 400°C. Subsequently, these tapes were cooled to room temperature at 120°C/h. J_c was then measured and the microstructure was studied by SEM/EDX. In addition, XRD was conducted on the tapes to estimate the Bi-2223 fraction.

Figure 24 shows the dependence of Bi-2223 content on the cooling rate of tapes sintered at 825°C for 50 or 150 h. After the first 50 h of sintering at 825°C, tapes that were cooled quickly (50 and 100°C/h) exhibited considerably less conversion to the Bi-2223 phase that did tapes that were cooled slowly. The time required to cool a tape from 825 to 400°C at the rate of 10°C/h is 42.5 h, whereas, when the tape is cooled at 100°C/h the time required is 4.25 h. As a consequence, the J_c values of the fast-cooled tapes are lower than their slowly cooled counterparts, as shown in Fig. 25. Following another sintering cycle for 100 h, the fraction of Bi-2223 phase increased to ≈0.95 in all but the tapes cooled at 10°C/h (Fig. 24). The lower Bi-2223 content in the tapes cooled at 10°C/h could be a result of Bi-2223 decomposition that takes place at long exposure times during slow cooling.

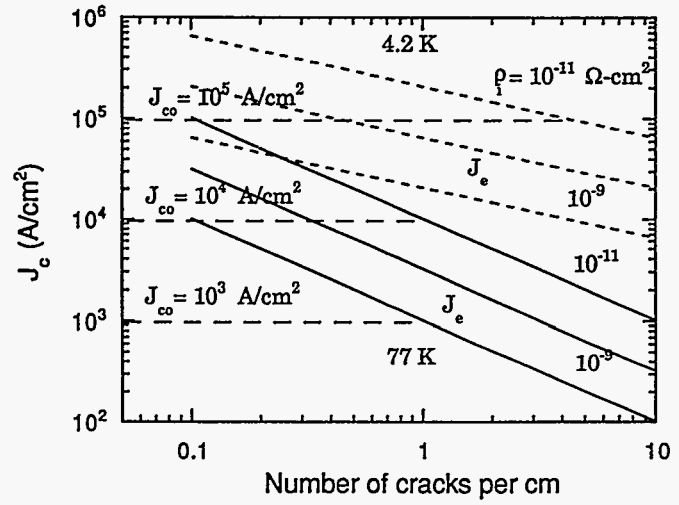

Fig. 21.
Calculated degradation of J_c varying with crack density in Bi-2223 for tape at 77 K (solid lines) and 4.2 K (dashed lines).

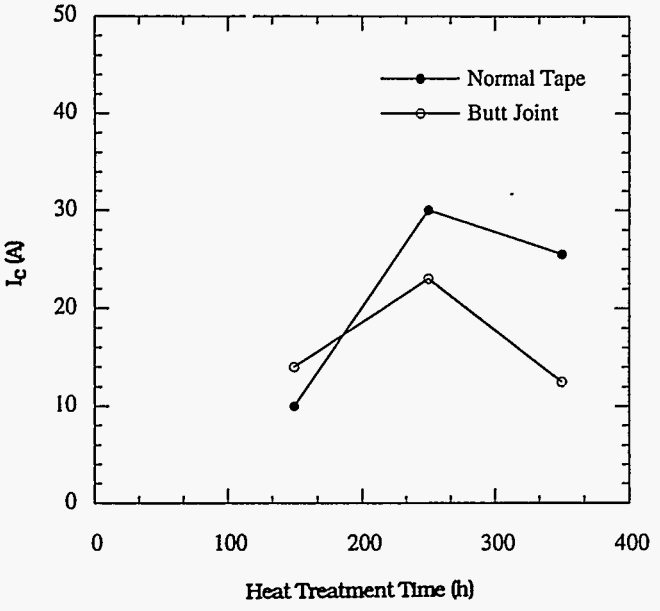

Fig. 22.
I_c as function of heat-treatment time for butt joint and normal tape.

Microstructural studies on these tapes etched in 1% butoxy ethanol in perchloric acid show a clear trend in core evolution. Increases in volume fraction of the interconnected Bi-2223 grains were observed with decreasing cooling rate (Fig. 26). Increase in grain connectivity provides an uninterrupted current path and, hence, high J_c. The optimum combination of phase purity and core density was attained in the tapes cooled at 25°C/h. These tapes yielded the highest average J_c (≈25,500 A/cm^2 at 77 K), which is ≈40% higher than the J_c values obtained for the tapes cooled at 100°C/h.

Based on the above results, a cooling schedule that employs two or more steps was implemented. The objective of the new schedule was to benefit from the slow cooling rate (10°C/h) during the initial stages of cooling (825 to 800°C) and to use a faster cooling rate below 800°C (25°C/h) to minimize dissociation of the Bi-2223 phase to Bi-2212 and secondary phases. Such a schedule promotes formation of dense, phase-pure cores. Figure 27 shows the Bi-2223 content obtained with various cooling schedules for tapes sintered at

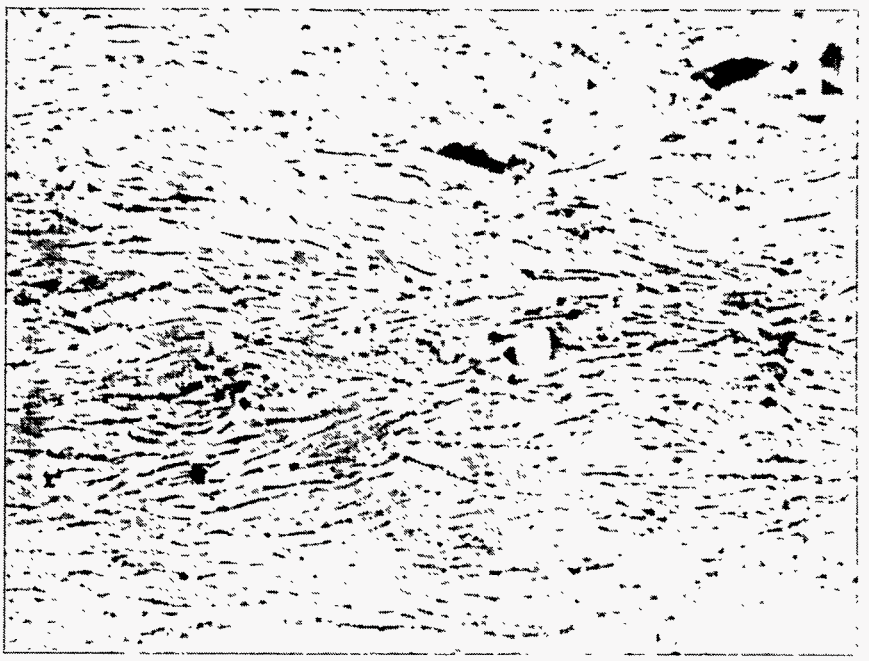

Fig. 23. SEM photomicrograph of butt joint after 250 h of heat treatment.

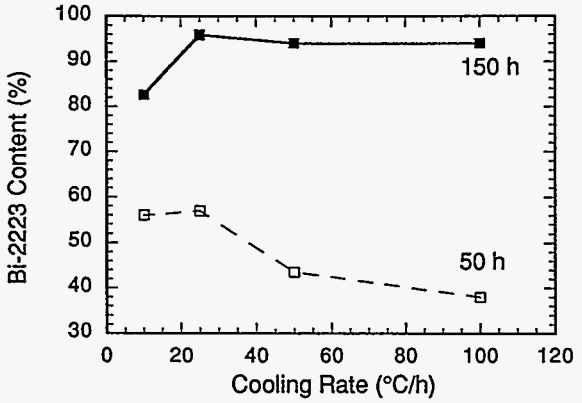

Fig. 24. Dependence of Bi-2223 content on cooling rate of tapes sintered at 825°C for 50 and 150 h.

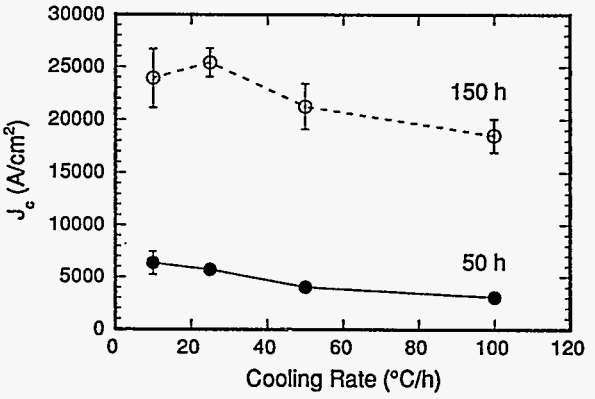

Fig. 25. Dependence of J_c on cooling rate of tapes sintered at 825°C for 50 and 150 h.

825°C. Figure 28 is an SEM photomicrograph of the microstructure obtained with the new schedule. The microstructure is extremely dense and comparable to that of the microstructure obtained in tapes cooled at 10°C from the 825 to 400°C. Also, the tapes sintered under the improved schedule showed excellent phase purity (>97% Bi-2223), as detected by XRD. Figures 27 and 28 clearly show a simultaneous improvement in phase purity and microstructure, confirming the potential of tailored cooling schedules to yield high J_c.

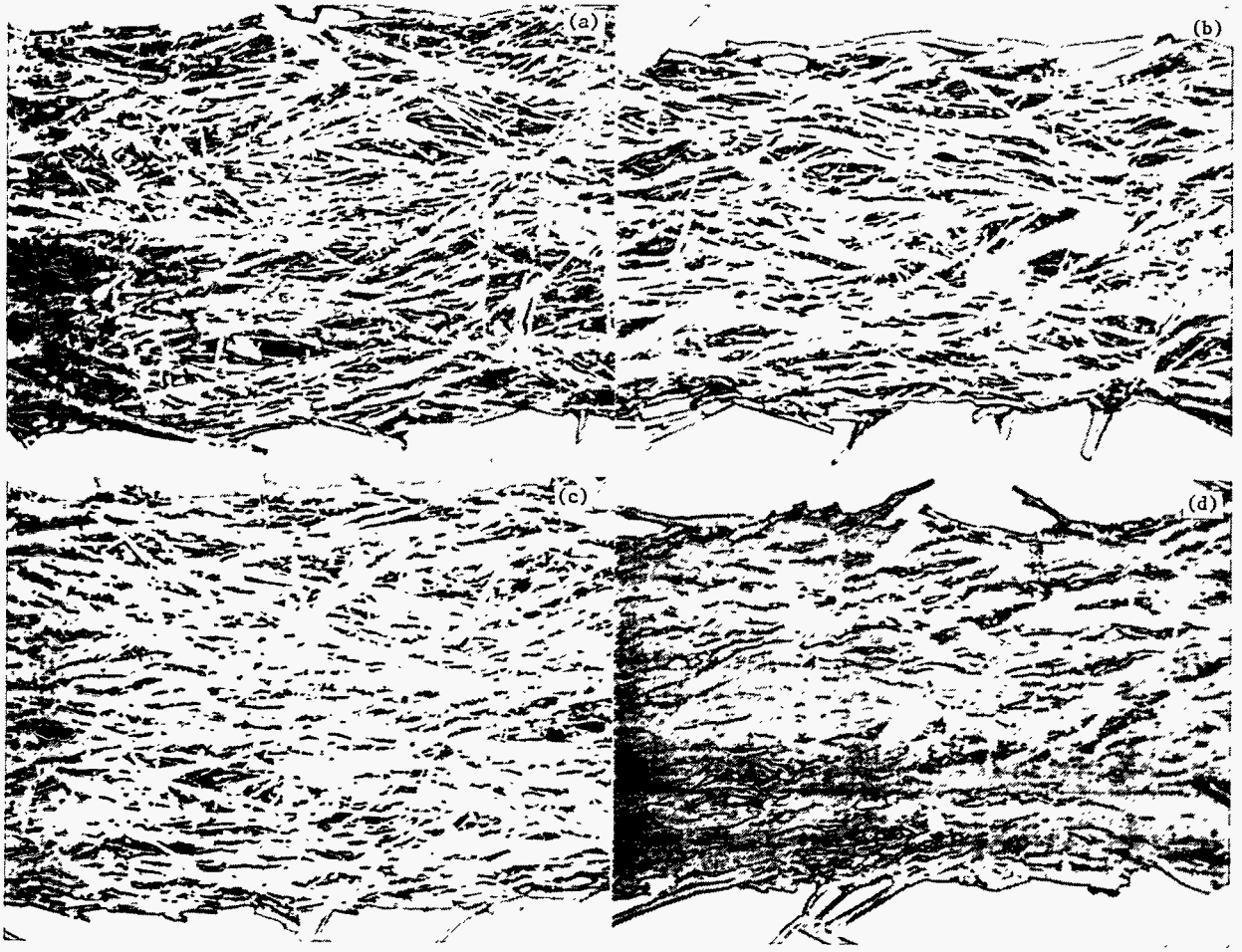

Fig. 26. SEM photomicrographs of Ag-sheathed Bi-2223 tapes sintered at 825°C and cooled at (a) 100 (b) 50 (c) 25 and (d) 10°C/h.

In addition to the microstructure and phase conversion effects, cooling rate can also influence the O_2 content of the BSCCO core. In a postannealing study, Nomura et al. (1993) observed that the J_c values of tapes increase with an increase in O_2 content. Preliminary measurements of the O_2 coefficients (referring to the value of d in $Bi_{1.8}Pb_{0.4}Sr_2Ca_2Cu_3O_d$) by iodometric titration in the above-mentioned tapes revealed that the O_2 coefficient increases with a decrease in cooling rate. Very slow cooling rates would increase O_2 content at the expense of undesirable Bi-2223 phase decomposition. In conclusion, it has been proved that cooling rate plays an important role in determining the phase purity and final microstructure, which in turn influence transport properties. A significant improvement (30% increase) in J_c was obtained by proper optimization of the cooling rate.

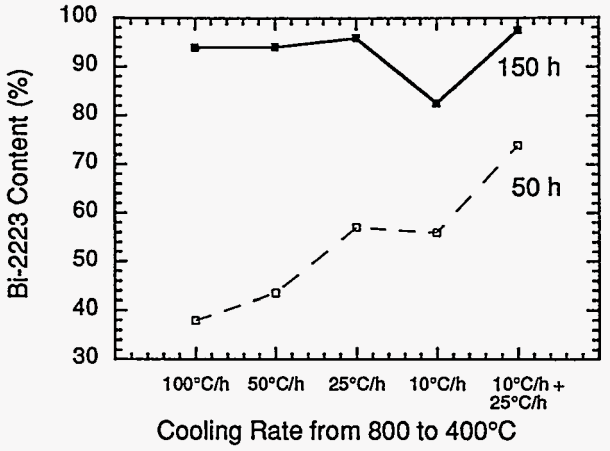

Fig. 27.
Improvement in phase purity with application of new heat-treatment schedule (10°C/h from 825 to 800°C, followed by 25°C/h to 400°C.

Fig. 28.
Back-scattered SEM photomicrograph of longitudinal cross section of Bi-2223 tape sintered according to improved schedule.

Processes for Continuous Tape Production

The objective of work performed over the past few years in collaboration with the Superconducting Products Company (SPC) and Andrew Corporation has been to develop a continuous process for manufacturing clad high-T_c wire. Both projects have been terminated. However, a process based on shaped rolling of Ag ingots or foil was developed with SPC. The approach is to use near-net-shape forming, with only a few rolling steps required once the superconductor powder is loaded into the core. A patent application on joint work with SPC was filed early in FY 1995 (Poeppel et al., 1994).

Collaboration with University of Pittsburgh

J_c values of Bi-2223 tapes made by the PIT process depend on the microstructure of the superconducting core. Conventional ceramic synthesis techniques generally lead to a multiphase microstructure with large second-phase particles and poor grain alignment. To overcome the limitations of conventional processing, a cryoprocessing technique, freeze-drying, was employed.

Aqueous solutions with the composition Bi:Pb:Sr:Ca:Cu = 1.8:0.4:2:1:2 and Ca:Cu = 1:1 were made from the respective metal nitrates. The individual nitrates were analyzed by thermogravimetry to ensure that accurate stoichiometric ratios were used. Lead was added as PbO and its dissolution was effected by adding HNO_3. The two solutions were frozen separately at 77 K by a splat-freezing step that ensured freezing rates on the order

of 10^5 K/s. The frozen solutions were then mixed in liquid N_2 with a high-shear homogenizing tool. The resultant frozen sample was then dried according to the procedure described by Krishnaraj et al. (1993). The dried and mixed precursors were denitrated by flash heating at 780-820°C for 1-2 h. The resultant powder was packed into Ag tubes and processed into tapes. The evolution of the Bi-2223 phase was studied by XRD and the microstructure was studied by SEM coupled with EDX.

X-ray diffraction data for freeze-dried Pb-2212 samples that were heat treated for various times in 100% O_2 at 820°C are shown in Fig. 29. The high reactivity of the powders is seen from the short times required for the formation of Bi-2212. After 4 h, the primary phase is Bi-2212, and after 8 h, the sample is seen to be single-phase Bi-2212, within the limits of detection by XRD. The tapes were then heat treated in 7% O_2 at 815°C, the onset temperature of the reaction to form the Bi-2223 phase, as seen from the DTAX data of Fig. 30. Bi-2223 is the primary phase after 24 h; after 50 h the tapes appear to be almost single-phase Bi-2223. This, once again, establishes the high reactivity of the powder. The freeze-drying process yielded a homogeneous precursor, with high mass throughput, allowing easy scale-up of the process for synthesis of large quantities of precursors for the manufacture of long lengths of superconducting tapes.

The thin superconducting region next to the Ag sheath appears to be the region of maximum J_c (>100,000 A/cm^2 at 77 K) in Bi-2223 tapes (Larbalestier et al., 1994; Lelovic et al., 1995a and b). Transport measurements on Bi-2223 tape at 77 K in low magnetic field applied parallel to the tape thickness indicate an exponential field dependence for transport currents. Magnetic hysteresis was measured in a 10-μm-thick layer of superconductor near the Ag sheath as a function of temperature, intensity, and orientation of applied field with respect to the tape. The characteristic field for full penetration depth for a superconducting slab was found to have a power-law dependence on temperature. Magnetization currents as a function of temperature and applied field oriented parallel to the tape thickness were determined from the width of the magnetization loop with a Bean-model expression adapted for an orthorhombic sample. The critical-state model, adjusted for scaling and magnetic relaxation, correlates well with the magnetization current of the thin layer at 77 K (Lelovic et al., 1995b).

If the interfacial length of contact between the Ag sheath and core with respect to the transverse cross section of the tape is increased, the current-carrying capacity of the tapes should improve. The length of interface between the superconducting core and the Ag sheath is defined here as the interface perimeter length (IPL) (Fig. 31), and increasing it should result in a measured increase in critical current. To compare tapes of different IPL with each other, they must have the same cross-sectional area; this can be attained by varying the mechanical-working procedures. Thus, the performance of a tape may be improved by changing its geometry.

To obtain wires with various IPL values but identical cross-sectional area, the mechanical-working schedule was altered. Three Ag tubes with powders were prepared for drawing and rolling operations. Of the three tubes, the first was drawn to a diameter of 4,064 μm, the second to 3,048 μm, and the third to 2,032 μm. After drawing, they were rolled to thicknesses at which their cross-sectional areas were identical. The first was rolled to a thickness of 254 μm, the second to 383 μm, and the third to 508 μm. Figure 32 shows the relative shapes and dimensions of the finished composite tapes. The IPL of the first is twice that of the third and 1.5 times that of the second. A wider range of IPLs

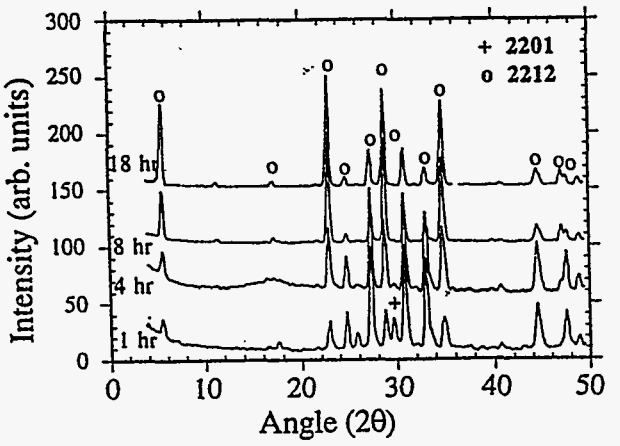

Fig. 29.
XRD data showing the evolution of Pb-2212 from freeze-dried precursors.

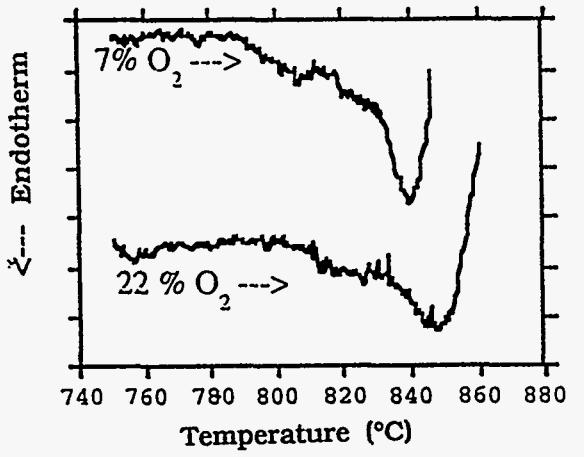

Fig. 30.
DTA of tapes under various O_2 partial pressures. Temperature for onset of reaction to form Bi-2223 phase was 815°C in 7% O_2, as seen from the endotherm.

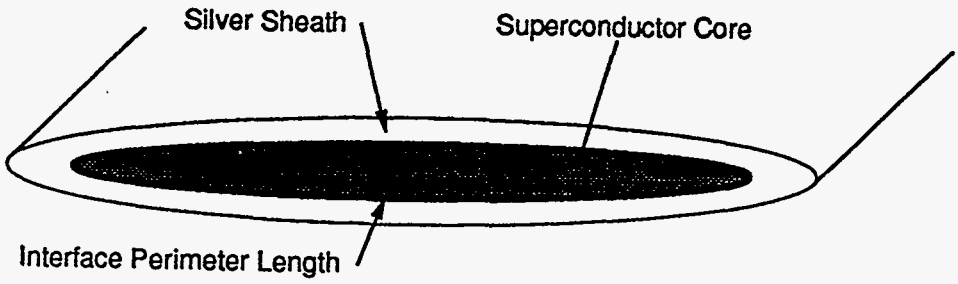

Fig. 31. Schematic representation of transverse cross section of an Ag-sheathed superconductor composite tape. The IPL is the black line that defines length of contact between Ag sheath and superconductor core.

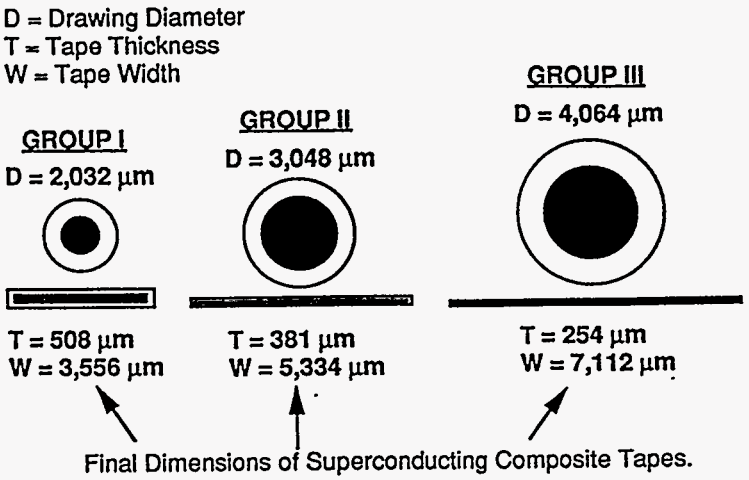

Fig. 32.
Schematic representation of mechanical working of wires to produce different IPLs with identical cross-sectional area.

was then obtained by uniaxially cold pressing the samples. Samples were heat treated in 8% O_2 at 815°C. Treatment time was 50 h. Critical current values of the composite tapes are plotted vs. IPL in Fig. 33. The plot indicates that increases in IPL result in increases in critical current.

Hot Rolling of Tapes

Hot-rolling studies were completed this past year. To improve the effectiveness of hot rolling, efforts have been undertaken to minimize sheath/core irregularities (Guo et al., 1995b). The final attempt centered on softening the core of an Al-clad Bi-2212 tape (Guo et al., 1995a). To accomplish this, Bi-deficient Bi-2212 was synthesized. It was phase pure by XRD. The Bi deficiency was then eliminated by adding either Bi metal or Bi_2O_3. Both act as lubricants during rolling, especially at high temperatures.

During hot rolling, the metallic Bi reacted with the Ag sheath, but the Bi_2O_3 did not. The Bi_2O_3-containing tapes could be rolled to a thinner core while maintaining a smooth Ag/Bi-2212 interface than could the tapes without Bi_2O_3 additions. Transport J_c values reflected the improved core structure; however, the maximum J_c obtained at 4.2 K has been only $\approx 1.5 \times 10^4$ A/cm^2. Cold rolling produces better properties.

Sinter-Forged Bi-2223 Bars

Two assemblies of Bi-2223 superconductor bars were produced for use in AC connections between utility system lines at room temperature and a fault-current limiter operating at 4 K. Each assembly, consisting of four parallel bars, arranged within a 100-mm-diam boundary, delivered 1500 A (peak), 50-60 Hz AC, through a 77-4 K temperature gradient while dissipating <0.3 W.

Bi-2223 was selected for fabrication of the AC downlinks. The Bi-2223 was synthesized by the two-powder process (Dorris et al., 1993, 1994a and b). Several processes to form the superconductor rods or bars were tested: uniaxial cold pressing or cold isostatic pressing (CIP), followed by sintering in air at 855-865°C; multiple CIP with intermediate and final sintering; and cold pressing followed by sinter forging. In sinter forging, the sample is compressed at a controlled rate during heat treatment. Results of electrical

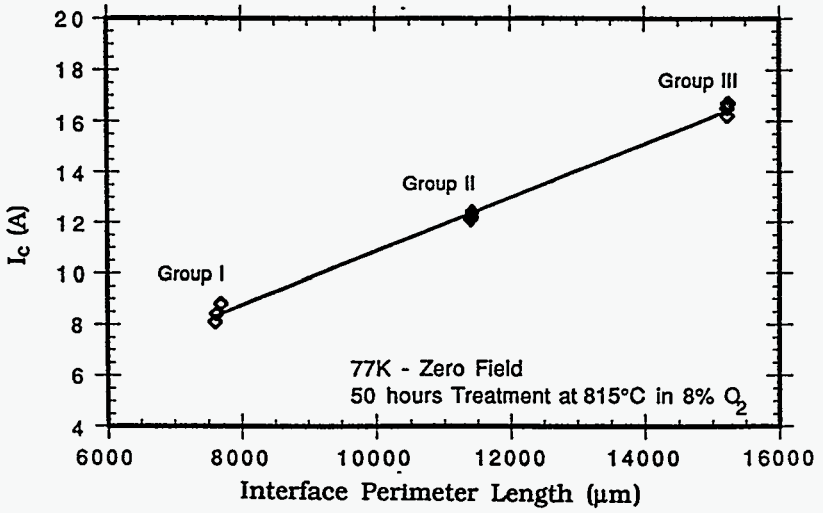

Fig. 33. Critical current vs. IPL for unpressed tapes. Each group represents composite tapes of different geometry but identical cross-sectional area.

tests of products obtained by the various processes showed that sinter-forged Bi-2223 was superior at 77 K. This material was also mechanically superior (Martin et al., 1993; Goretta et al., 1994).

The sinter-forged bars displayed DC J_c values of 950–1300 A/cm^2 at 77 K and >5000 A/cm^2 at 4 K; magnetic field sensitivity was relatively low. Although thermal conductivity tests showed values much higher than those found in the literature for polycrystalline Bi-2223 made by other processes, this undesirable result was counterbalanced by the relatively high J_c, which made passible the use of bars with smaller cross-sectional areas. Typical 50-Hz power losses at 77 K in each bar (cross-sectional area of 0.54 cm^2) were 1 mW/cm at 310 A and 1.75 mW/cm at 375 A. Losses were much lower at 4 K. Bars were 25 cm long, including Ag contacts that were sinter forged to the ends, with a 21-cm Ag-free length in the thermal gradient between the fixed-temperature terminals.

Specification of the number of bars and their cross-sectional areas and lengths depended on several considerations. Computations indicated that four parallel bars might satisfy the electrical and thermal criteria. Certain design constraints were imposed by a desired compatibility between the assemblies and a He boiloff test facility constructed to support the development of fault-current limiters that will operate in liquid He. Mixed cooling was used by conduction to liquid He and convection of He gas. Heat from the AC power loss in the superconductor was almost entirely removed by convecting He, and little heat flowed from the bulk ceramic to the liquid. The total heat delivered to the liquid by the two downlink assemblies, their contacts at the 4.2 K terminal, and the low-temperature superconductor linkage between the assemblies was 517 mW while carrying 1500 A at 50 Hz (Balachandran et al., 1995a). Power loss at contacts appeared to account for most of the heat dissipation in the liquid and was evidently greater with AC than with DC.

2.2 Tl–M–Sr–Ba–Ca–Cu–O Superconductors

The goal of this part of the ANL program is to develop a useful conductor for high-temperature, high-field applications, with Tl-1223 being the most promising candidate at present. The rationale is that Tl-1223 has improved flux-pinning properties at 77 K when compared with Bi-2223 (Balachandran et al., 1994a), and the potential for improved intergranular coupling, first demonstrated by General Electric (GE) (DeLuca et al., 1992). Our progress has indicated that good phase purity and grain alignment are necessary, but not sufficient, to obtain the highest J_c in Tl-1223. It also is necessary to avoid significant intergranular weak links. Processing in the presence of a transient liquid phase seems to be a very effective way to accomplish this in bulk forms.

We continue to study synthesis and processing procedures that will overcome the intergranular weak-link problem in Tl-1223. Our approach is to concentrate on finding and using transient liquid phases at the crucial step in processing to assist in grain orientation and improved intergranular connectivity, while preserving reasonable phase purity. This program includes various PIT configurations, thick (20–50 μm) coatings, and thin films; much of it involves research agreements with GE, Intermagnetics General Corporation (IGC), State University of New York at Buffalo (SUNY–Buffalo), and the Thallium Working Group.

2.2.1 Ag-Clad Tl–1223 Tapes and Wires

Composition Studies

Bismuth and Pb substitution in Tl-1223 superconductors has been used extensively to increase T_c (Paranthaman and Hermann, 1994; Ren and Wang, 1993; Ren et al., 1995) and flux pinning, and stabilize the superconductor phase (Ren et al., 1995). The goals of this work were to find the role of Bi substitution in Tl-1223 in phase development of Ag-clad tapes and to determine how Bi substitution influences the melting behavior of Tl-1223. Liquids with excess Bi are common in other superconductor compounds (Schartman, 1993), and Bi oxides are less volatile than Tl oxides (Holstein, 1994).

Differential thermal analysis was used to determine the effect of Bi substitution on melting temperature (Fig. 34).

A single melting event was observed for x = 0 and x = 0.22, and was ascribed to the incongruent melting of Tl-1223. The melting point increased with Bi substitution until the solubility limit of Tl-1223 was exceeded. A low-temperature endotherm was observed for Bi substitutions >x = 0.22. The second endotherm correlates with the presence of $BaBiO_3$ from XRD data and suggests the possibility of a eutectic melt between impurity phases. The size of this endotherm increases with increasing Bi substitution.

SEM photomicrographs of calcined powder revealed that the particle size was significantly larger for high Bi content (Fig. 35).

Significant grain growth in Tl-based superconductors has been attributed to the presence of a liquid phase (Morgan et al., 1990). Results from EDX confirmed that the observed large platelike particles were Tl-1223.

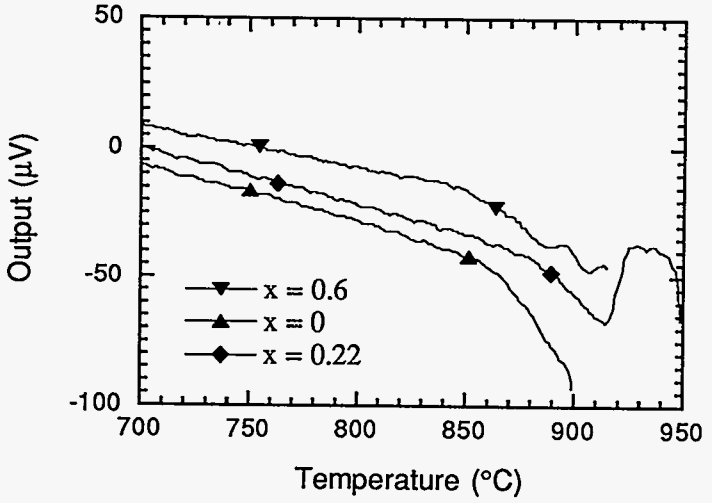

Fig. 34.
DTA data from calcined powders of $Tl_{1.1-x}Bi_xBa_{0.4}Sr_{1.6}Ca_2Cu_3O_x$.

Fig. 35.
SEM photomicrograph of calcined Tl-1223 powder: (a) Bi = 0.22 and (b) Bi = 0.8.

The effects of Bi substitution, O_2 partial pressure, and Ag addition on the Tl-1223 melt temperature are summarized in Table 2.

Table 2. Summary of melting behavior of $Tl_{1.1-x}Bi_xBa_{0.4}Sr_{1.6}Ca_2Cu_3O_x$

Bi content x =	pO_2 (%)	Ag (wt. %)	1st endotherm (°C)	2nd endotherm (°C)
0	8	0	855	-
0.22	8	0	860	-
0.4	8	0	890	860
0.6	8	0	895	850
0.8	8	0	893	857
0.22	100	0	944	-
0.22	21	0	880	-
0.22	8	30	860	-
0.22	21	30	875	-
0.22	100	30	912	-
0.4	8	30	850	-

The melting temperature is depressed 5-10°C when Ag powder is mixed with superconductor powder. Oxygen partial pressure (pO_2) significantly affects the melting temperature. As can be seen in Table 1, the melting point decreases 86°C when pO_2 is changed from 100 to 1%. The onset temperature of the first endotherm increases in proportion to the Bi content; however, a lower melting endotherm appears for a Bi substitution of x = 0.4.

Alternative approaches to creating a transient liquid phase will be explored in the future. Using the solubility of Pb in Bi-based superconductors as an analogy, Majewski et al. (1994) recently revealed a potential mechanism for a transient liquid phase. The solubility of Pb is lower in Bi-2212 than in Bi-2223, which provides an ideal scenario for a transient liquid phase that is based on a Pb-rich liquid (Dorris et al., 1994a). Future work will determine if there is a subtle difference between the Bi substitution limit of different phases in an assemblage that produces a nominal Tl-1223 composition. Such work may provide a reaction path in which a Bi-rich liquid phase is transient and consumed by a superconductor phase in which the solubility of Bi is not exceeded.

Fabrication of Ag-Clad Tl-1223 Tapes

Two primary fabrication efforts were undertaken in this area during the past year. Working with researchers at SUNY-Buffalo, we fabricated tapes from powders of $Tl_{0.78}Bi_{0.22}Sr_{1.6}Ba_{0.4}Ca_2Cu_3O_x$. Previous work had achieved transport J_c values at 77 K of $\approx 2 \times 10^4$ A/cm^2 (Ren and Wang, 1993; Ren et al., 1994, 1995). Most recently, we introduced an intermediate pressing step to the fabrication sequence.

We found that J_c increased to 2.2×10^4 A/cm^2 and that the in-field J_c also improved (Ren et al., 1995). Flux pinning also showed significant enhancement. The improvements were attributed primarily to a denser, more uniform core.

We also worked with researchers at the University of Arkansas to fabricate tapes from $Tl_{0.78}V_{0.22}Sr_{1.6}Ba_{0.4}Ca_2Cu_3O_x$.. The irreversibility line of this composition relative to that of undoped Tl-1223 has been improved (Li et al., 1994). Although a powder with good phase purity and platelike grains was synthesized, transport J_c values of the resultant Ag-clad tapes were rather low (<5 x 10^3 A/cm^2 at 77 K). The grains were found to be crushed during mechanical working and the resultant core microstructure was rather porous and exhibited no favorable texture (Li et al., 1995). Work with this alloy of Tl-1223 has been discontinued.

2.2.2 Tl-based Coatings and Films

Applied research on Tl-based coatings and films focused on a search for improved processing methods, whereas basic research focused on understanding fundamental mechanisms. As a consequence, both thick and thin films have been examined.

Tl-1223 Deposited Coatings

The program to improve transport properties of Tl-1223 thick films continued in several areas. In collaboration with IGC, we used the two-zone furnace to thallinate 0223 precursor tapes supplied by IGC. We then characterized these 100-μm-thick films (≈50 μm of coating on each side of an Ag substrate) and obtained I_c values at 77 K of 18 A (5.5 A/mm) in zero field, and 1.9 A at 1 T. The deposit morphology consisted of regions of c-axis-oriented platelike grains separated by regions of off-axis grains. We are investigating methods to limit the growth of the off-axis grains.

To ascertain whether precursor density plays a role in determining the transport properties of thick films, we began a study to measure the density of various films prior to thallination. Investigators at GE measured their spray-pyrolyzed films and determined an initial 0223 density of 4.6 g/cm^3, ≈90% of theoretical density. We measured our screened thick films and found a density of ≈2 g/cm^3 before and ≈3.5 g/cm^3 after pressing at 1 GPa. Thus, even after pressing, we achieved only 67% of theoretical density, significantly less than the density obtained with spray-pyrolyzed films.

We will concentrate on methods to promote biaxial texturing in thick films by promoting growth from a propagating front. To understand more fully the importance of density in precursors, we will hot press precursor bars to various densities. Using the two-zone furnace, we will thallinate these bars and conduct studies to determine the deepth at which the Tl reaction occurs, and the relationship between microstructure and transport properties and density.

Phase Development of (Tl,Bi)-1223 Thin Films

The microstructures of (Tl,Bi)-1223 films, prepared in collaboration with SUNY-Buffalo, were examined with the goal of understanding phase formation. This information will be used to help develop an optimized phase assemblage that may be incorporated into fabrication schemes for conductors of various geometries. The results indicate that, under conditions for best film quality, the Tl-1212 phase forms first, followed by growth of the Tl-1223 phase, suggesting a potential analogy with the two-powder process developed by Dorris et al. (1993) for Bi-2223. It was also found that Ag played an important role in film growth, both in enhancing Tl-1223 phase formation and in leading to texture (epitaxy).

The films that we studied were grown on $LaAlO_3$ and were typically ≈1 μm thick, although films as thick as 3 μm have been prepared by the same techniques. The films were prepared by first depositing, by laser ablation, a near-stoichiometric precursor film, containing both Tl and Bi in addition to the other elements. Subsequently, the films were annealed by wrapping them in Ag foil, together with a bulk pellet of the (Tl,Bi)-1223 composition. The J_c at 77 K in zero field was ≈2 x 10^6 A/cm^2 for the 1-μm-thick films.

Epitaxial films that were phase pure by XRD were produced for annealing times of 45–60 min. To follow phase development during the process, we studied samples that had been quenched after 10, 20, and 30 min. Figure 36 shows XRD θ-2θ patterns for each of these samples and one from an as-deposited precursor. As indicated by the XRD spectra, and confirmed by transmission electron microscopy (TEM), the as-deposited films are amorphous. The sequence of phase development is clearly indicated by the XRD patterns for samples annealed 10, 20, and 30 min. After 10 min, only (00*l*) reflections from the Tl-1212 phase are visible (together with some unindexed reflections due to alkaline-earth cuprates). After 20 min, the intensities of the Tl-1212 peak are higher, suggesting continued growth of the Tl-1212 phase. In addition, strong (00*l*) reflections from the Tl-1223 phase are also visible, suggesting competitive growth between the Tl-1212 and Tl-1223 phases. After 30 min, the (00*l*) reflections from the Tl-1223 phase become the dominant feature as the Tl-1212 reflections lose intensity, suggesting reversion or conversion of the Tl-1212 phase.

To further understand these phase transformations, we also studied these samples by SEM and TEM. The SEM results were somewhat ambiguous, partly because of the size scale of the features and partly because of the high degree of texture and epitaxy in these films. As a consequence, it was difficult to distinguish between the various phases. However, the broader view provided by SEM was important to confirm that the TEM results were representative. In essence, the SEM results suggest that although structure varies across a given sample, it appears that all parts of the sample undergo the transformation sequence, albeit possibly at slightly different times (<10 min).

Figure 37 shows TEM cross-sectional views of samples annealed 10, 20, and 30 min. As seen in Fig. 37a, the sample annealed for 10 min consists primarily of very small, randomly oriented grains. The specific identity of each of these phases is being studied further. The strong Tl-1212 (00*l*) reflections visible in the XRD spectrum (Fig. 36) arise from a thin epitaxial layer of Tl-1212, which ranges in thickness. The difference in structure suggested by XRD and observed by TEM illustrates the importance of using various techniques to complement one another in evaluating the microstructure of these samples. A representative view of the microstructure of a sample annealed 20 min is shown in Fig. 37b. At this point, the sample consists of an underlying layer of Tl-1212, a top layer of Tl-1223, and mixed alkaline-earth cuprates. These observations are consistent with the X-ray diffraction data, which indicated that the epitaxial Tl-1212 continues to grow at the same time that epitaxially oriented Tl-1223 begins to grow. The microstructure of a sample annealed for 30 min is shown in Fig. 37c. At this point, the sample is almost completely converted to Tl-1223, including the layer near the substrate. The specific mechanism of conversion is not yet clear and is a subject of further studies.

EDX was performed on each of these samples, in both scanning and transmission electron microscopes. The results indicate that Ag is present in the films, although the films were prepared without Ag. It was concluded that some Ag is incorporated into the

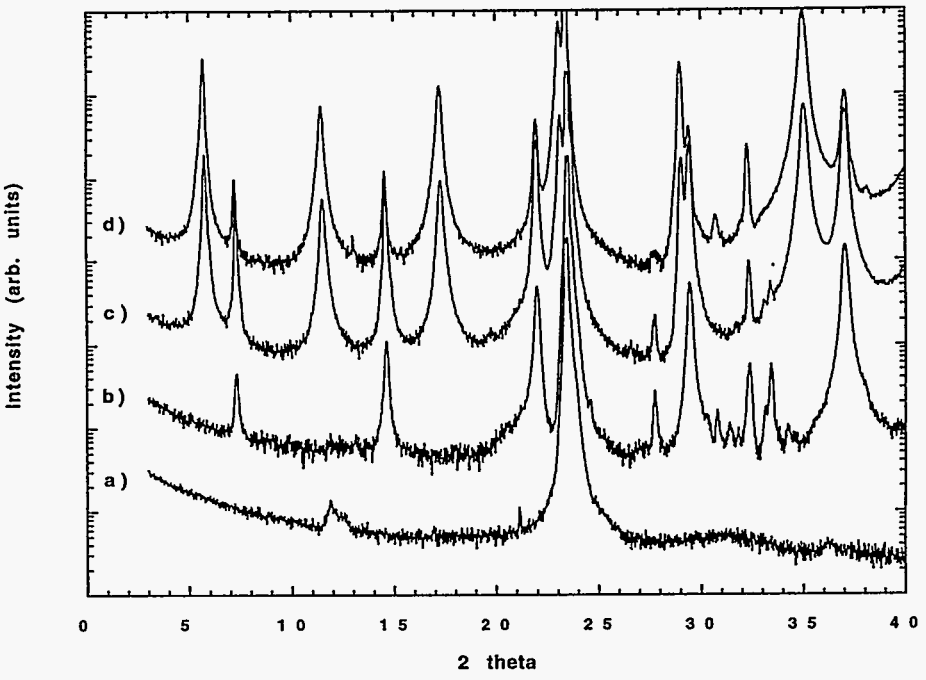

Fig. 36. XRD spectra of (Tl,Bi)-1223 films annealed for (a) zero time, (b) 10, (c) 20, and (d) 30 min.

films during the postdeposition annealing step, presumably from the Ag foil that was used as a wrap. To establish the role of Ag in phase development in these films, an additional sample was annealed for 30 min with Au wrap to remove any potential source of Ag. Figure 38 shows XRD θ-2θ patterns, which indicate a significant difference between films annealed with and without Ag. For the same annealing time, films annealed without Ag show broader, less intense Tl-1223 (00*l*) reflections when compared with films annealed in the presence of Ag. Figure 39 shows a representative TEM cross-sectional view of the film annealed in the Au wrap. This film shows an epitaxial layer of Tl-1212 near the substrate. In sharp contrast to a companion film annealed in an Ag wrap (Fig. 37c), the top layer of this film consists of randomly oriented grains of alkaline-earth cuprates and Tl-1223. The Tl-1223 grains were occasionally observed to grow directly from the substrate, but were almost never observed to be epitaxially oriented.

Future efforts will concentrate on further establishing the specific role that Ag plays in enhancing Tl-1223 phase formation and promoting texture. Transport measurements of these and similar films are also being carried out to establish the irreversibility line for the (Tl,Bi)-1223 and (Tl,Pb)-1223 phases.

Identification of Grain-Boundary and Flux-Creep Dissipation in Superconductors

Every large magnetic field application of Type-II superconductors requires strong pinning of vortices. Because of the short coherence lengths and large anisotropies in high-T_c superconductors, pinning energies are quite small. In addition, high-temperature Because of this, it is very important to investigate materials that contain nearly ideal pinning centers. In the case of highly anisotropic superconductors (Tl- and Bi-based compounds), for which vortices become nearly two-dimensional, an ideal pinning center

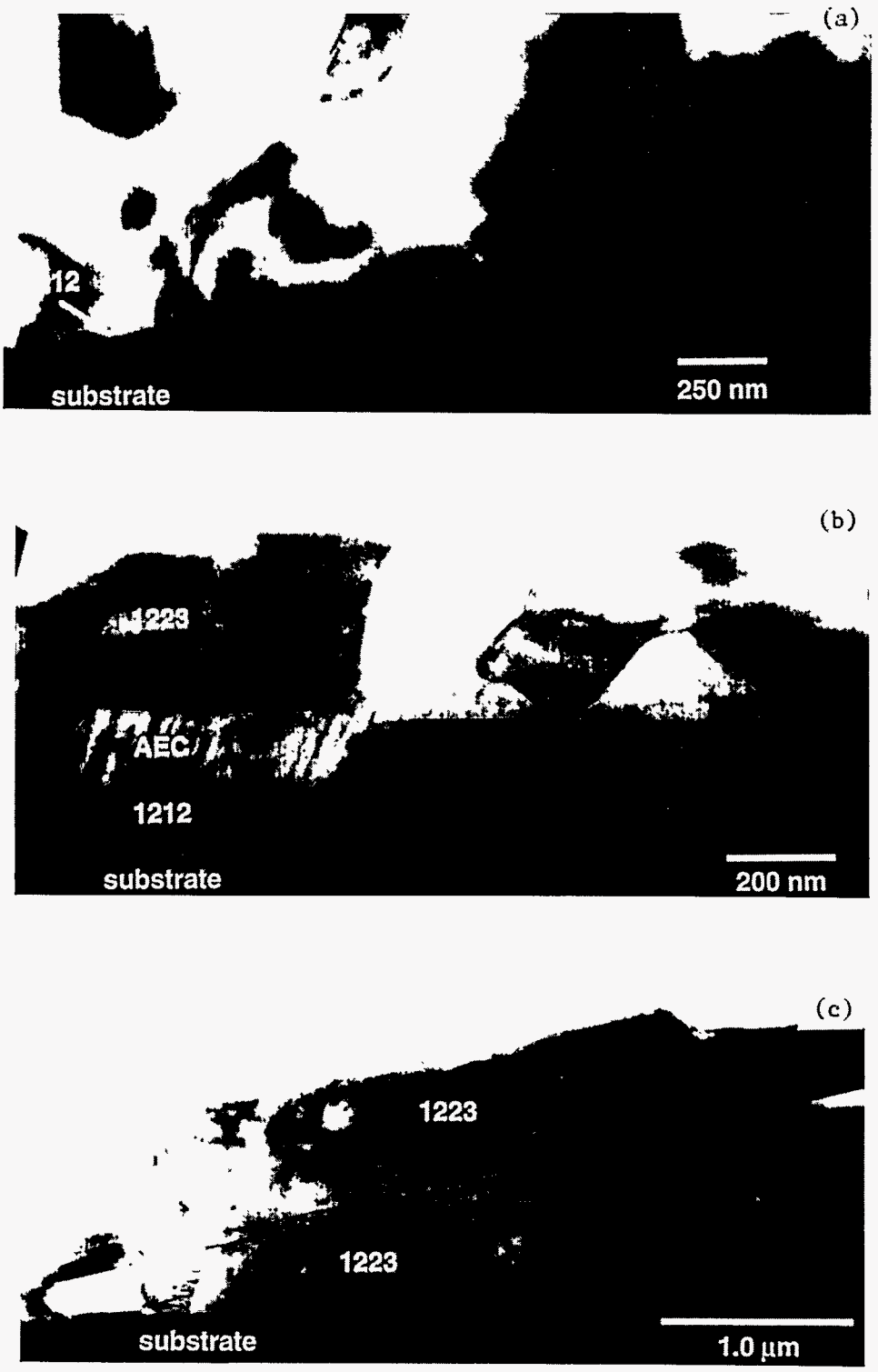

Fig. 37. Cross-sectional TEM photomicrographs of (Tl,Bi)-1223 films annealed in Ag foil for (a) 10, (b) 20, and (c) 30 min.

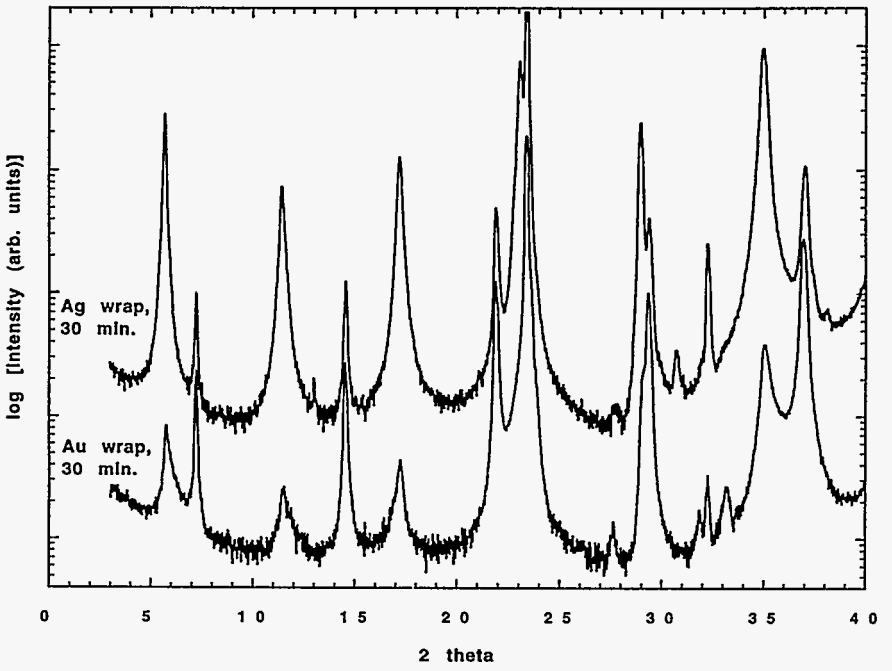

Fig. 38. XRD spectra for (Tl,Bi)-1223 films annealed for 30 min and wrapped in either Ag or Au foil.

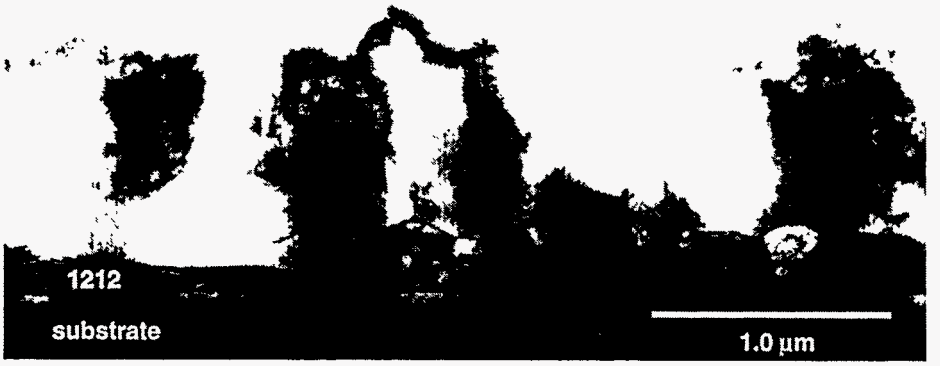

Fig. 39. Cross-sectional TEM photomicrograph of (Tl,Bi)-1223 films annealed in Au foil for 30 min.

introduces a pinning site in each and every superconducting layer. A columnar defect provides such a pinning center. In addition, a convenient way to distinguish between dissipation at grain boundaries and dissipation due to flux creep has been discovered through studies of columnar defects. Inasmuch as ion-track pinning greatly increases pinning strength, it can expose the fingerprint of grain boundaries because ion tracks significantly shift the I(V) characteristic (and therefore J_c) in weak-link free single crystals and epitaxial films, but they have almost no effect on grain boundaries that are in series with transport current.

Grain-boundary-free samples. We have measured I_c as a function of temperature, magnetic field, and defect density in 700 MeV Xe^{+42} ion-irradiated $Tl_2Ba_2CaCu_2O_8$ films (from Superconductor Technologies, Inc.). In these samples, which are relatively free of grain boundaries, flux motion limits the current-carrying capacity. We found that, at high temperatures when the vortex density is smaller than the areal density of columnar defects, the improvements in critical current with irradiation were substantial and relatively independent of defect density. However, at fields for which the vortices outnumbered the defects, the improvements were significantly smaller.

The situation changed at lower temperatures, where the effect of the defects was important in magnetic fields for which the vortex density was much larger than the areal density of defects. This finding emphasizes the importance of vortex/vortex interactions in determining the critical currents at low temperatures. These points are demonstrated graphically in Fig. 40.

Samples with grain boundaries. Samples with grain boundaries typically have smaller low-field J_c and have I(V) characteristics that are qualitatively similar to those of a Josephson junction. Figure 41 is a plot of electric field E versus current density J or the E(J) of a polycrystalline material (from GE) and epitaxial samples of Tl-1223 (made by GE and ANL) measured at 77 K and 2 T. The nearly identical responses at low current densities suggest that, at this magnetic field and temperature, vortex motion dominated the dissipation. However, as the current was increased, there was a clear departure of the dissipation in the polycrystalline material from that measured in the epitaxial sample. This departure was attributed to phase slip at grain boundaries.

To further validate our interpretation of Fig. 41, we introduced columnar defects through ion irradiation. These defects should only modify the dissipation that results from vortex motion. Any changes in dissipation due to phase slip processes at grain boundaries will be minimally affected through a loss in cross-sectional area available for transport current. Therefore, comparisons of the transport properties of polycrystalline materials before and after ion irradiation provide a way to separate the role of grain boundaries in the resulting dissipation. We have measured thick polycrystalline Tl-1224 films from GE, before and after irradiation. In Fig. 42, we plot the I(V) characteristic in both cases at 77 K and 2 T. Clearly, the voltage measured at small currents, previously thought to be due to flux motion, was suppressed, whereas dissipation at high currents was relatively unchanged.

The described procedure provides the first definitive method to distinguish between grain boundary and flux creep dissipation. In the future, we plan to use the procedure to make such identifications in various practical conductors, including PIT and thick-deposit specimens.

Effective Vortex Dimensionality and Pinning Force in Ion-Irradiated Samples

The effects of linear, ion-track pinning centers on dissipation and J_c were investigated in highly anisotropic Tl-cuprate superconductors. For unirradiated and irradiated samples at all fields, the dissipation accurately follows two-dimensional scaling. At intermediate fields, which rigorously follow such two-dimensional scaling without irradiation, the irradiated samples showed a dip in dissipation for fields parallel to the ion tracks. This seemingly contradictory behavior was explained as a balance between pinning and

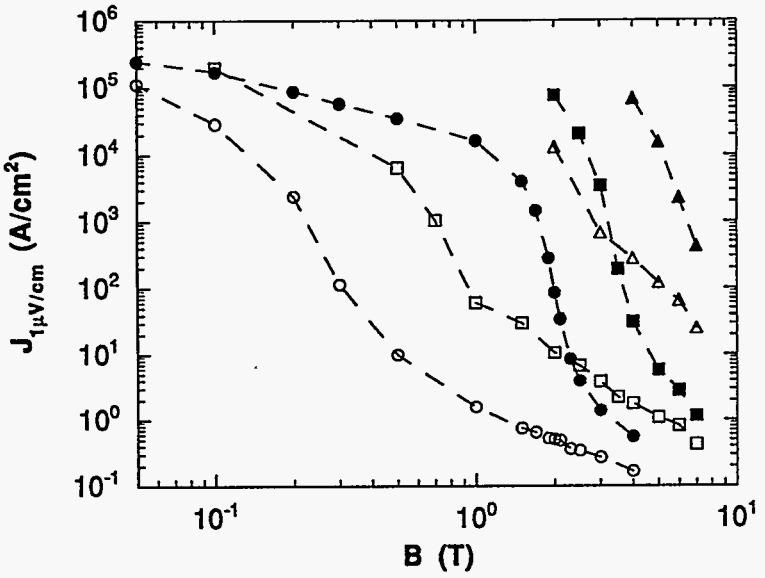

Fig. 40.
J_c vs. magnetic field B at various temperatures, before (open symbols) and after (solid symbols) ion irradiation: 40 K (triangles), 60 K (squares), and 77 K (circles).

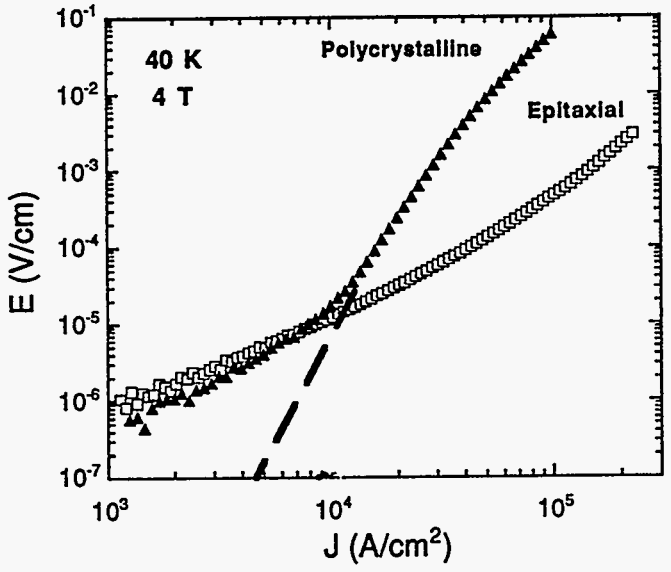

Fig. 41.
Electric field vs. current density of polycrystalline (open symbols) and epitaxial (solid symbols) materials: ε = voltage V/sample length, J = current I/cross-sectional area.

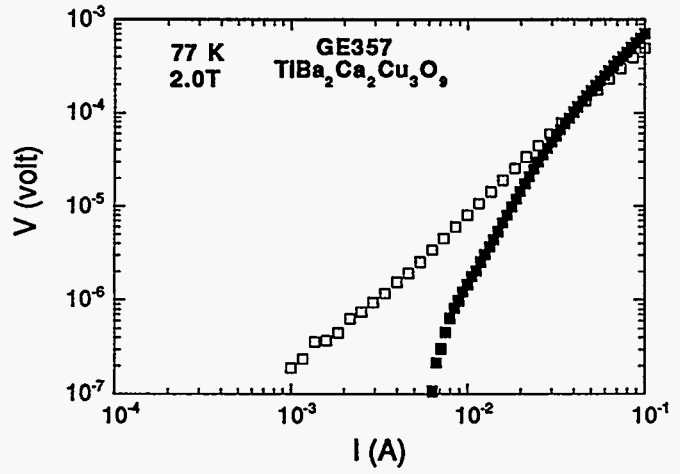

Fig. 42.
Voltage vs. current for the samples in Fig. 41 before (open symbols) and after (solid symbols) irradiation. Sharp reduction in dissipation at small currents in irradiated sample suggests that dissipation in the region is dominated by motion of magnetic flux.

Josephson interlayer coupling energies. In addition, the effective pinning field of the defects, for both dissipation and J_c, was clearly shown to be temperature dependent: it vanished at T_c and rose to roughly three to four times the effective ion-dose field at $\approx 0.4\ T_c$.

In conclusion, we have demonstrated the importance of vortex/vortex interactions at low temperatures by taking advantage of available pinning centers.

2.3 Y–Ba–Cu–O Superconductors

2.3.1 Melt–Processed Y–123

Bulk Y-123 superconductors show promise in applications such as low–friction superconductor/permanent magnet bearings and flywheel-energy-storage devices (Balachandran et al., 1994a). Melt-processing of Y-123 is a well-established technique to produce large-domain materials for levitation applications (Goretta et al., 1995a). Seeding with higher melting Re123 (Re: Sm, Nd) single crystals and use of well-defined temperature gradients are normally utilized to produce large single-domain levitators (Todt et al., 1995a). Alternatively, cube-shaped $Nd_{1+x}Ba_{2-x}Cu_3O_y$ seeds have been used to produce five-domain levitators (Todt et al., 1995b-d). Microstructural investigation of the five-domain materials revealed that these levitators are composed of five domains that are rotated 90° around a common [100]/[010] axis, relative to their neighboring domains. The levitation forces of the five-domain materials can be comparable to those of single-domain materials, but they show a much wider fluctuation of levitation force than single-domain materials.

To understand the high levitation forces, as well as the large fluctuations, detailed investigations of the microstructure have been carried out. Transmission electron microscopy revealed the existence of several special kinds of 90° grain boundaries. Pure symmetrical-tilt boundaries have been observed, as well as tilt boundaries parallel to the ab plane of one of the neighboring domains. Pure 90° twist grain boundaries have also been observed (Fig. 43). Reports indicate that this type of grain boundary can carry very high J_c values in thin films (Eom et al., 1991). Preliminary measurements on our bulk materials support this result.

Extensive cracking of many samples may be responsible for large fluctuations in levitation force. Thermal cycling experiments with single- and five-domain levitators showed a decreasing levitation force with an increasing number of thermal cycles for the five-domain levitator, whereas this dependence was much weaker for the single-domain levitators (Todt et al., 1995c). This finding indicates that thermal cycling damages the already cracked five-domain samples even more, thereby decreasing the well-connected areas in the sample. Single-domain samples exhibit cracking in the ab planes only, and the cracks do not propagate with cycling; therefore, no decrease in levitation force occurs.

2.3.2 Grain-Boundary Transport and Microstructure

To better quantify conduction across weak-link grain boundaries in superconductors, we have measured microstructure and transport on 24° [001]-tilt bicrystal grain boundaries in Y-123.

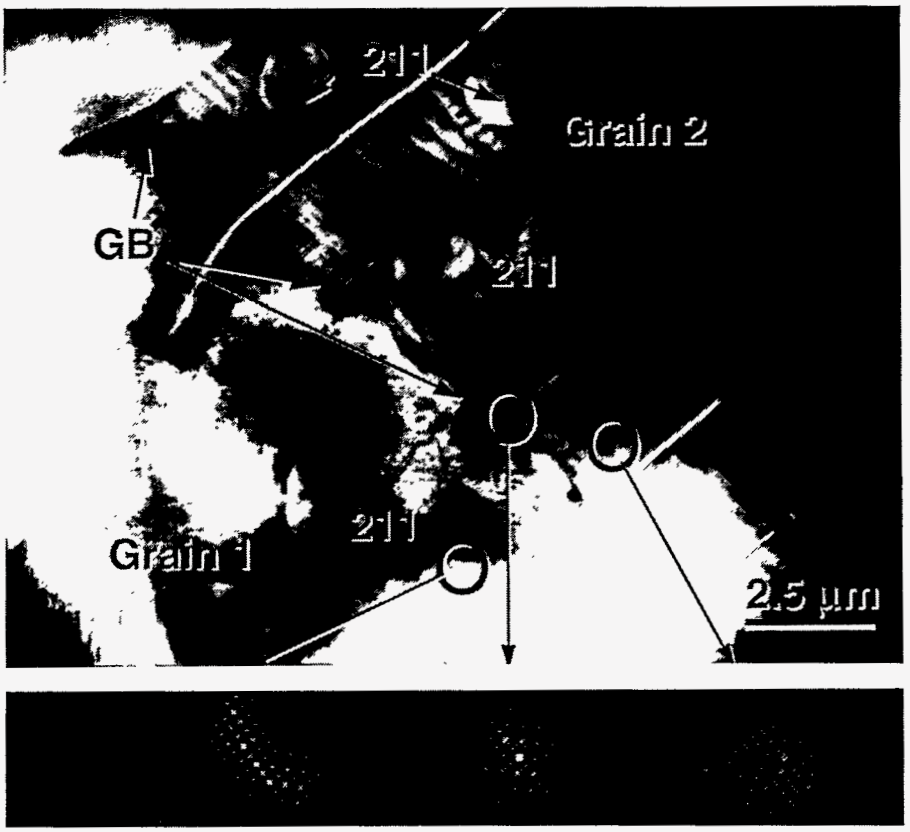

Fig. 43. TEM photomicrograph of 90° twist boundary in melt-processed Y-123.

Single grain boundaries were prepared by epitaxial growth of Y-123 onto bicrystalline $SrTiO_3$ substrates. Microstructural characterization by TEM showed that these artificially induced grain boundaries were periodically decorated by impurity phases. In addition, the boundaries were not always straight, but instead, frequently meandered away from the path of the underlying boundary in the substrate. The various facets produced by the meandering showed varying degrees of tilt and twists. Atomic-force microscopy studies suggested that this meandering behavior is related to the nucleation and growth mechanisms of the film, and based on this, we were able to vary the magnitude of the meandering by changing the growth conditions.

In addition, we measured the zero-field electrical transport properties and found them to be in excellent agreement with the Ambegaokar-Halperin model over an extended range of currents and voltages. This model gives a firm basis for characterizing and comparing boundaries, and provides two independent measures of the grain boundary critical current: these are found to differ significantly from each other. The difference provided new evidence that the boundary is not uniform, but composed of a number of small junctions in parallel. The implied junction size is consistent with gross defects found in TEM photomicrographs of such boundaries.

2.4 Properties of Bulk High–T_c Superconductors

2.4.1 Characterization Methods

Ceramic superconductor samples produced in ANL projects are characterized to help improve chemical formulations and forming and processing procedures. High-T_c products fabricated for devices also are characterized to evaluate product performance. The property of primary interest is DC transport critical current of the sample, measured as a function of intensity of an applied magnetic field. Power loss due to AC transport, as a function of frequency, current, temperature, and ambient magnetic field, is of interest for AC applications also. Selected samples are tested to find critical temperature, structural defects, strength of the diamagnetic response, remanent-field strength, and mechanical properties (Balachandran et al., 1994a). Thermal conductivity of sinter-forged Bi-2223 current leads through the 4–77 K temperature range are also obtained.

2.4.2 Electrical Characterization of Superconductors

DC Characterization

Critical current tests have continued at an average rate of 103 samples per month. Substantial differences among batches of bulk material or formed products required continual screening. The standard four-point resistance method was used with a 1 μV/cm criterion. Sample types consisted primarily of Ag-clad Bi-2223 tapes that were under development for magnetic coil applications and Y-123/Ag or Bi-2223 bars that were being developed for use in current leads. Results are discussed below and elsewhere in this report.

Tests of high-performance superconductors at high currents during this reporting period were supported by our pulsed-current facility, now upgraded to provide 1600-A pulses. Tapes were tested at 77 K individually in a low range, typically 10-40 A, and in parallel assemblies at currents to 1500 A. Individual Bi-2223 sinter-forged bars with 0.5-0.6 cm^2 cross-sectional areas and critical currents to 710 A were tested at 77 K through and beyond their critical values. Applied magnetic fields typical of current lead applications (50–100 G) decreased critical current negligibly.

AC Power-Loss Study

A small resistance to AC flow is displayed by high-T_c superconductors, even at currents well below the DC critical current. This resistance is associated with the magnetic hysteresis of the material. However, appropriate design can limit the power loss to a value sufficiently small for advantageous use of the material in applications such as AC downlinks operated at power-line frequencies (Balachandran et al., 1995a). AC losses in superconductor bars and tapes that are potentially useful in AC devices are being evaluated in support of design efforts. Typical results from sinter-forged Bi-2223 bars were shown in the previous report (Balachandran et al., 1994a). Studies of the effects of sample shape, ambient AC magnetic field, and current distribution in arrays of parallel samples continue.

Figures 44 and 45 show newly constructed apparatuses that support the AC power-loss studies. A multicontact fixture (Fig. 44) enables differential AC voltage measurements at several sites along both broad and edge surfaces of a rectangular bar specimen during a

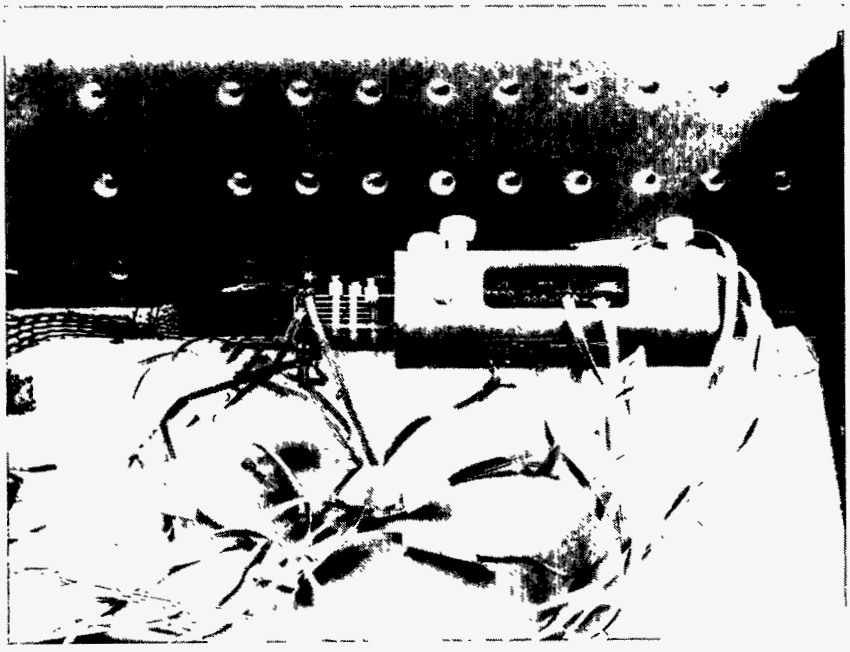

Fig. 44. Multicontact fixture for differential AC voltage measurements at several sites on superconductor bar; inductive pickup loops are incorporated to monitor local current flow.

single session of cryogenic testing. Inductive pickup loops are incorporated to measure local current flow. The fixture can be used on a specimen tested singly or as part of an array. The parallel-bar fixture (Fig. 45), which accepts up to eight samples and can be adjusted over a large range of sample lengths, provides a current-metering facility for each sample. The fixtures are used with a variable-frequency AC source capable of delivering up to 2150 A RMS sine waves to test an assembly being developed for power utility service at 2000 A RMS.

Contact Resistivity

Low-resistance contacts (Maroni 1991, 1992) are needed for DC and AC applications. Resistance to 50-Hz AC flow through Ag contacts sintered to high-T_c superconductors was measured with samples at 77 K and was compared with the resistance to DC flow. The AC resistance of such contacts at 4.2 K also was measured. A lap-joint sample configuration was used for all measurements of contact resistance. Sample lap area was 0.64 cm^2 for Y-123/Ag bars and 1.17 cm^2 for Bi-2223 bars. AC resistance was corrected for the relatively small contributions from the bulk high-T_c material included in the monitored length of each joint. The tests were done to aid interpretation of results from downlink heat-leak studies in which the question of large differences between AC and DC resistance, even in the current range <10% I_c, had been raised.

Half-joint resistivities in 77-K tests were 0.1 mW-cm^2 and 0.2 mW-cm^2 for Y-123/Ag and Bi-2223, respectively. Values with AC were nearly the same as with DC. The values include contributions from the Ag/ceramic interface, the Ag metal thickness, and a

Fig. 45. Array of high-temperature superconductor bars prepared for AC power-loss tests at 77 K: measurements are made of loss in a selected bar under influence of varying magnetic fields produced by AC current in adjacent bars; sinusoidal AC as great as 3200 A (peak) at selected frequencies in the 30-500 Hz range can be supplied.

minimal amount of Sn-Pb solder used to join the bars. At 4.2 K, the Bi-2223 AC value found was too small (19 nW-cm^2) to contribute substantially to heat-leak totals in the downlink studies. Tests of high-T_c/low-T_c joints at 4.2 K are being prepared.

Electrical-Cycling Tests

Long-term electrical-cycling tests of high-T_c bar samples produced by ANL were conducted jointly with ERIEZ Magnetics Technical Center of Erie, PA (ERIEZ). A set of five Y-123/Ag bars with critical current values from 99 to 129 A in 77-K tests were treated with spray wax, retested, and sent to ERIEZ for electrical cycling at 77 K, similar to that expected in possible application as downlinks in a magnetic separator. Three bars were energized to 23–24 A DC for 30 s once every 60 s until 104,000 such cycles had been applied, while two bars served as nonenergized controls in the same environment. The critical current values were monitored by ERIEZ during this treatment and by ANL afterwards. The finding of both laboratories was the same; no detrimental effect on the critical currents occurred from the electrical cycling or from any other cause in either test bars or controls during the year between ANL tests, during which the ERIEZ electrical treatments were applied. The absence of any effect of atmospheric exposure and time was likely due to isolation by the thin wax coating. Also, the wax and its carrier were shown to exert no detrimental effect. In contrast, during storage in plastic bags for several months before selection for use in this test, nonwaxed bars lost 10-28 % of their original critical current values.

Cooperative work was continued with the test of a Bi-2223 bar that was sinter forged at ANL and cycled electrically at 77 K at ERIEZ. The 565-A critical current (J_c = 1200 A/cm^2) was not significantly changed by 80,000 pulses at 50 A on a 30-s-on, 30-s-off schedule. The bar was coated with Krylon "anti-rust" spray wax before the cycling treatment. Again, there was no detrimental effect of waxing or elapsed time between tests (3 months). Also, the bar performance had not deteriorated in 4 months of storage before waxing, during which time the bar was protected by forged-on Ag foil that was removed for the subject test.

Material from a longitudinally sectioned, sinter-forged bar was pulse-tested at a series of temperatures below 77 K and in applied magnetic fields up to 1 T. A small slope change in J_c vs. T at 30–35 K when applied magnetic fields were present may indicate improved flux pinning below that temperature range. At zero applied field, the ratio of critical currents at 4 and 77 K was ≈6.

Pulsed DC tests were performed to evaluate candidate conductors for use as current downlinks in an SMES application. Superconductor bars made by ASC had been formed by aligning Bi-2223/Ag-Au tapes and sintering them together to make downlink elements rated at 1100 A in a 60-4 K temperature gradient with <0.4 W of heat leak per 50-cm-long bar. After tests showed that these criteria had been met, the bars were sectioned for further study. Nearly 1500 A DC were needed to reach the critical values of some of the segments.

2.4.3 Thermal Conductivity Measurements

Sinter-forged Bi-2223 bars are being applied in current leads that connect electric current through a 77–4 K temperature gradient to devices operating in liquid He. The relatively low thermal conductivity of the ceramic and its electrical superconductivity

produce a substantial advantage in thermal efficiency when compared with Cu downleads. Thermal conductivity is an important quantity in downlink design.

Literature values for thermal conductivity at 60–80 K for polycrystalline Bi-2223 made by static sintering differ by a factor of two, and the single-crystal values reported are much higher than those of polycrystalline samples (Uher, 1990). An improvement in J_c produced by sinter forging suggested that thermal conductivity may have increased as well.

Thermal conductivity tests were conducted by Uher (1990) on sections of a Bi-2223 bar sinter forged at ANL. The results are shown in Fig. 46. The thermal conductivity values approached those of single-crystal material and were rather uniform with varying position across the bar.

The unwanted increase in thermal conductivity tends to be counterbalanced by the higher J_c that was produced by sinter forging. Improvement in mechanical strength is an additional advantage of the process (Martin et al., 1993; Goretta et al., 1995a).

2.4.4 Mechanical Properties

Mechanical-property research has continued at cryogenic, room, and elevated temperatures. The low-temperature data are of direct interest to applications (Wu et al., 1994; Goretta et al., 1995b). The high-temperature data are of interest because they relate to processing conditions (Jimenez-Melendo et al., 1995).

Fracture Properties

Good strength and flexibility are required in most bulk applications. Various composite systems have been developed to improve both strength and toughness of high-temperature superconductors. In addition to use of Ag particles and flakes (Singh et al., 1993, 1994; Joo et al., 1994; Poeppel et al., 1993), several other additives have been shown to be effective. For best mechanical properties, very pure superconductor powders are generally required (Balachandran et al., 1992; Singh et al., 1995).

Ceramic additives, such as coated ZrO_2 and SnO_2, can approximately double fracture toughness (Goretta and Kullberg, 1993; Balachandran, 1995). Novel heat treatments that feature a partial solid-state decomposition step can increase strength by ≈50% (Singh et al., 1995). It is also possible to increase in-service failure loads by applying strong coatings directly on conductors (Wu et al., 1995).

To date, Y-123, Bi-2212, and Bi-2223 wires have been studied and improved. Much work with Tl-based superconductors is still required; relatively low phase purity has hampered previous efforts.

Elastic Properties

Studies of elastic moduli continued in collaboration with the University of Bath, United Kingdom. For Y-123, elastic properties, especially those at low temperature, were found to be strong functions of O content (Wang et al., 1995). For the Bi-based superconductors, dense and highly textured Bi-2212 bars are easiest to study (Fanggao et al., 1993). Current work is focused on effects of materials composition on moduli.

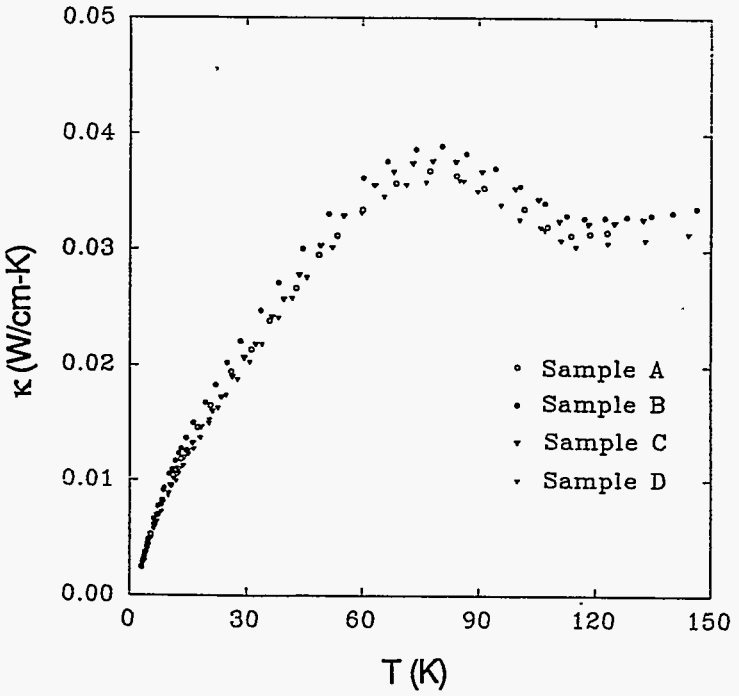

Fig. 46. Thermal conductivity of Bi-2223.

High–Temperature Deformation

Previous work focused on high-temperature plastic deformation of superconductors. Current efforts are focused on examining the properties of Ag sheaths at elevated temperature. Highly pure, commercial-purity, and precipitation-hardened alloys will be studied in FY 1996. The information gathered is expected to shed light on blistering and sagging phenomena that can occur during heat treatment of clad tapes.

2.4.5 Nondestructive Evaluation

Ultrasonic Examination of Tapes

The ultrasonic velocity-of-sound technique (Lanagan et al., 1995), developed for monitoring phase development within bulk superconductors, was applied to Ag-clad Bi-2223 and Tl-1223 PIT tapes. Melting and densification responses were monitored.

This technique has been demonstrated to our industrial partners and they have expressed substantial interest. A U.S. patent application on the technology is scheduled early in FY 1996.

On-line Examination of Bi-2223 Tapes

The goal of this project is to develop an on-line, efficient, nondestructive testing device that will provide information about defects during production of PIT wires and tapes. Recent efforts concentrated on investigating the feasibility of scanning acoustic microscopy and microfocus X-rays as tools for defect detection.

In the process of producing thin, clad tapes, the internal powder core can develop thickness variations (sausaging) that degrade performance. An on-line nondestructive testing device to provide information on sausaging and other defects in as-produced tapes is very much needed. Two nondestructive methods that are potentially capable of monitoring the production of defect-free superconducting tapes have been examined. Ag-clad Bi-2223 tapes ≈250 μm thick were used.

Acoustic microscopy. The nondestructive characterization of the tapes was conducted at Sonoscan Inc., Bensenville, IL. The work was performed under a CRADA. Acoustic microscopy may offer an excellent way of imaging the powder within the tube. The samples are relatively thin and can be immersed in an acoustic coupling medium such as water. A simplified block diagram of the setup is shown in Fig. 47. Because the samples are thin (core ≈75 μm), the focus is essentially though the entire thickness of the sample. Acoustic pulses travel forward and back through the tape, and are detected by the sending transducer, which is operated in a pulse-echo mode. Results are displayed as a gray-scale image, in which the shade of gray can be related to features in the tape. The image can also be displayed in color. Work is continuing in collaboration with Sonoscan.

Microfocus X-rays. Ag-clad Bi-2223 tapes were also studied with ANL's microfocus X-ray system (Fig. 48). This system consists of an X-ray source and a detector comprising a 14-bit CCD camera and an image intensifier. The X-ray source is a microfocus system, with a spot size of ≈10 μm, a tungsten target, and a maximum energy level of 160 kVp at 0.15 mA. The system is controlled by a computer, which also stores the raw image data.

Bi-2223 tapes were mounted in air to prevent any masking effects of solid mounting material. The tapes were aligned in front of the intensifier, and the image was projected onto the intensifier screen. The image was captured live through a digital CCD camera (filmless radiography).

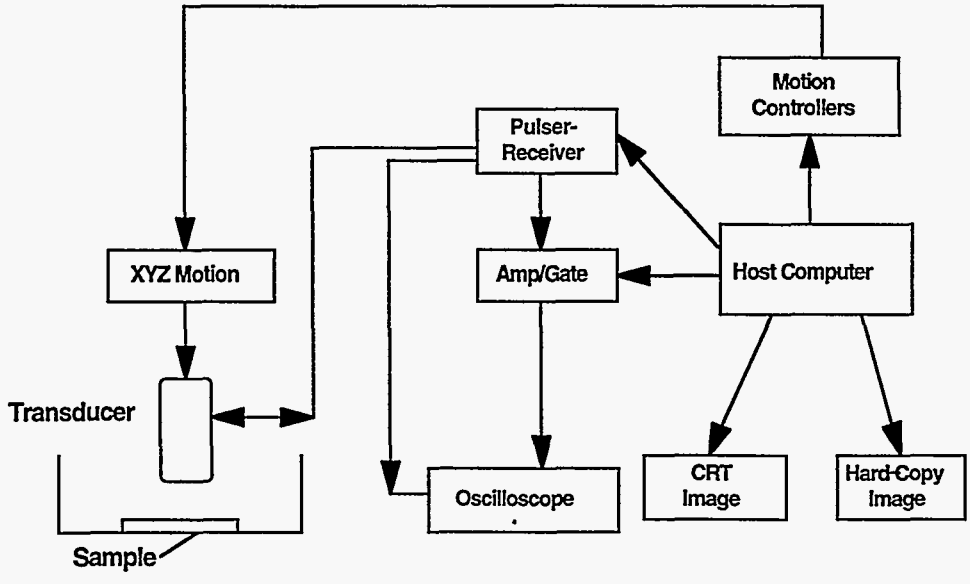

Fig. 47. Block diagram of acoustic microscopy setup for nondestructive characterization of Bi-2223 tapes.

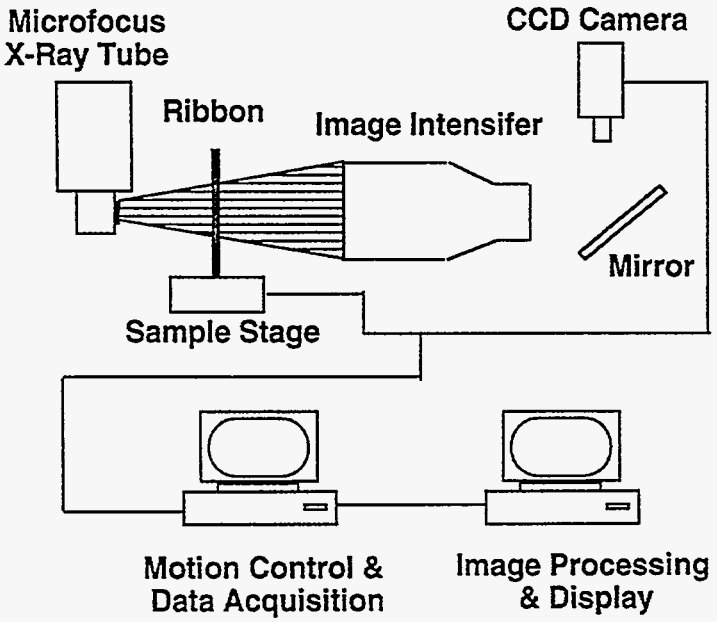

Fig. 48.
Schematic diagram of ANL microfocus X-ray system.

Preliminary results indicate that acoustic microscopy is feasible for examining superconducting tapes. Figure 49 shows the acoustic microscopy images of four tapes. The outside white region is the Ag tubing. The superconducting core is shown as the darker gray inner region of the image. Lighter regions represent low acoustic attenuation regions, and the dark regions indicate high attenuation. The dark and bright striations on the image represent density variations in the packed powder. The image clearly shows that the powder is not uniformly distributed inside the tape, which is known to be one of the causes of poor properties.

X-ray images of the same tapes are shown in Fig. 50. The scale factors of the acoustic pictures, and the X-ray pictures are different, which makes point-by-point comparison difficult. However, there is general agreement between the images on the nonuniformity of powder density. On the X-ray images, the dark gray regions represent low X-ray attenuation, and the white region corresponds to high attenuation. The outer darker region on the images represents Ag tubing, and the inner core shows dark and bright shades, depending on the local attenuation. Once again, these images confirm the nonuniform density of the powder in the Ag tube.

In future work, a second set of controlled sample tapes with different rolling reductions will be examined. We expect to obtain better correlation for the new set of controlled samples, when compared with the preliminary samples used in the present study. An additional set of controlled samples with various degrees of mechanical strain is now being prepared. In particular, we are interested in the formation of voids as a result of mechanical strain. All of the new samples will also be investigated by optical and SEM and the observations will be correlated with the results from the nondestructive imaging methods.

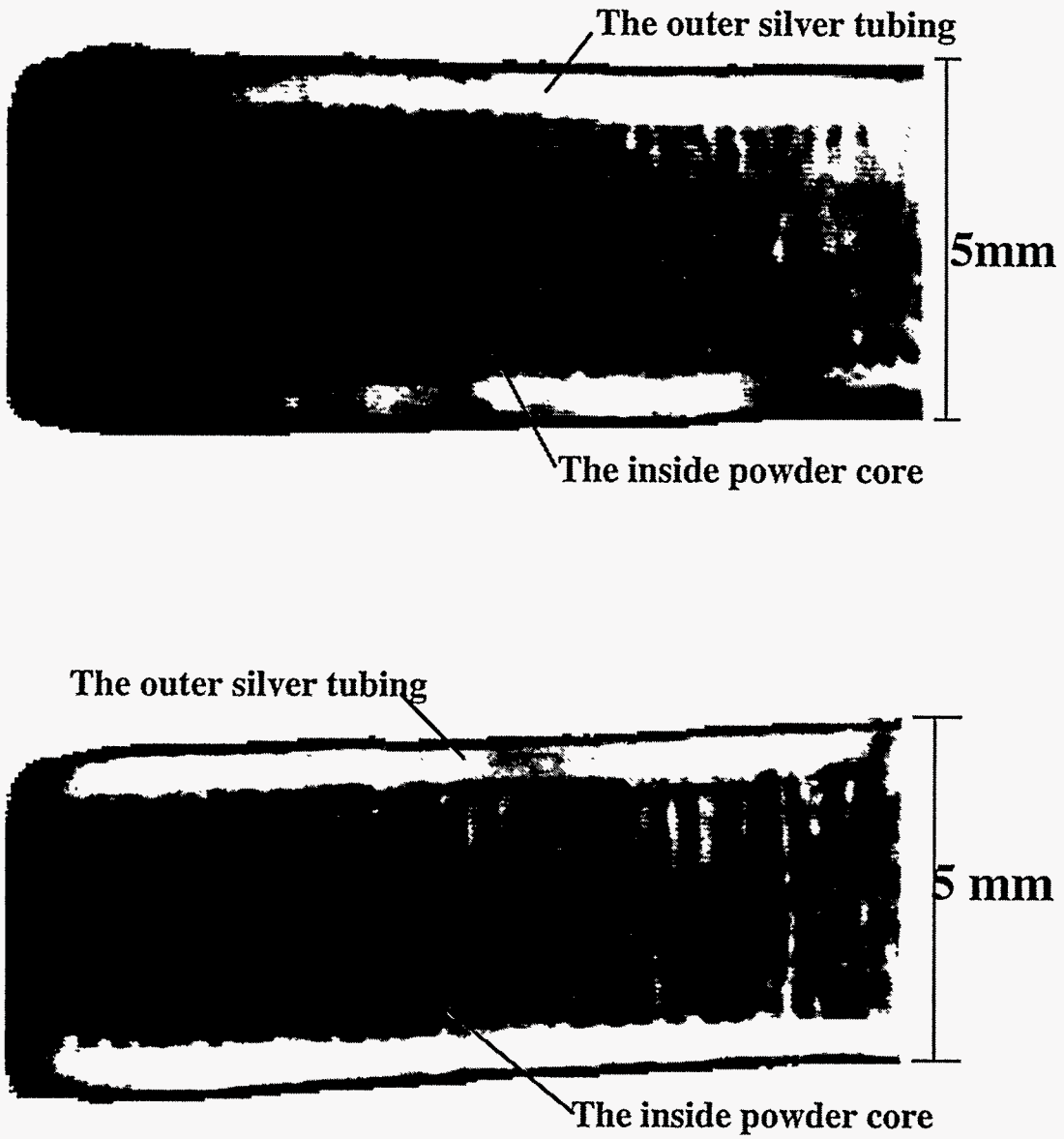

Fig. 49. Acoustic microscopy images of Bi-2223 tapes.

Magneto-optical imaging

Ag-clad Bi-2223 tapes have been provided to the staff of ANL's Materials Science Division for use in magneto-optical imaging studies, which have led to direct imaging of high- and low-current paths in the Bi-2223 core. These observations have been correlated with detailed electron microscopy (Welp et al., 1994, 1995) and are now being used to guide improvements in tape processing.

2.5 Applications and Devices

Application research and development are focused on production and testing of components, analysis of performance (Cha et al., 1994b; Hull et al., 1995), and design of new systems. Primary emphasis has been on current leads and magnetic bearings.

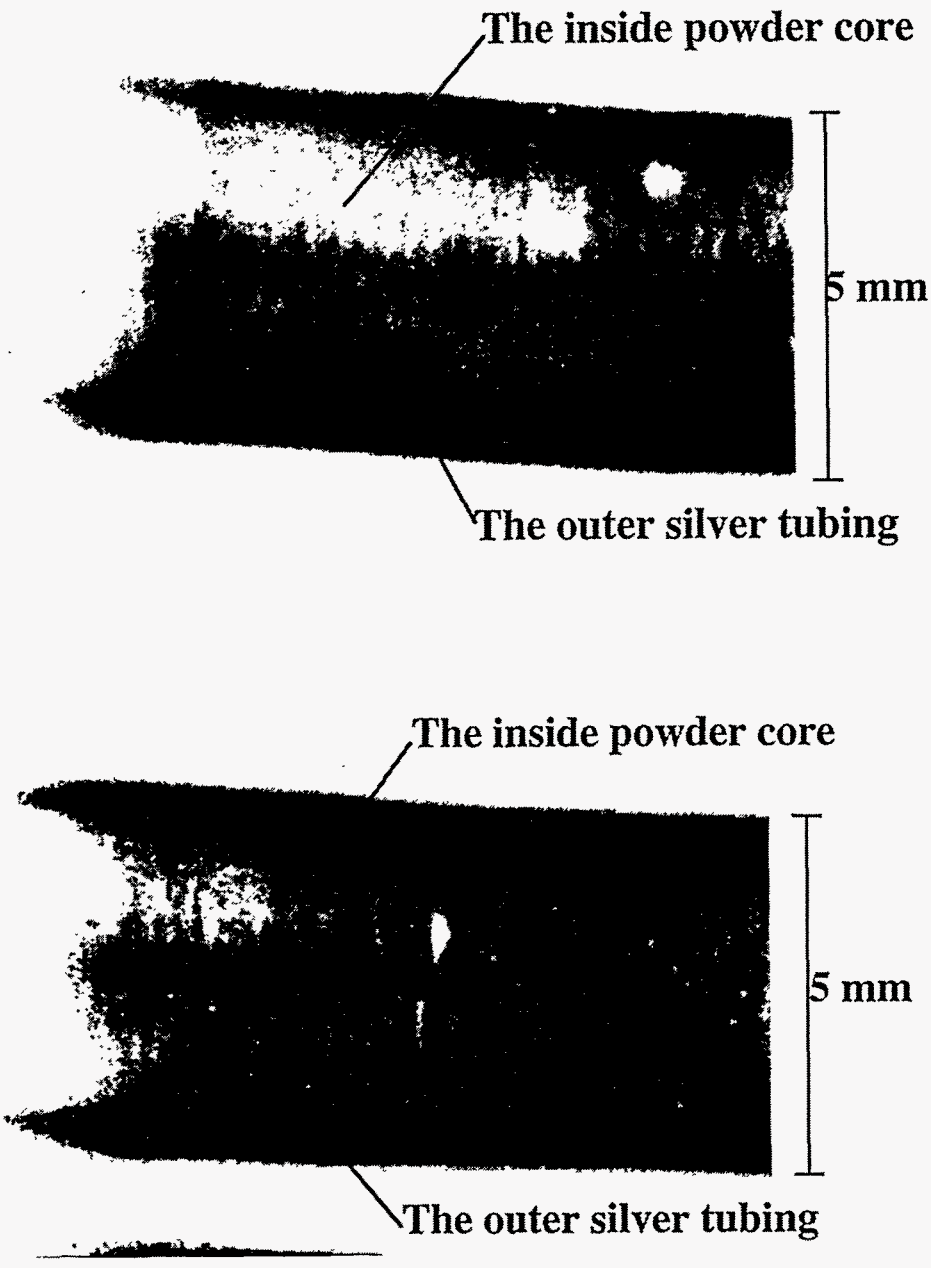

Fig. 50. Microfocus X-ray images of Bi-2223 tapes.

2.5.1 Current–Lead Projects

Current leads are a near-term application of high-T_c superconductors (Niemann et al., 1994a and b, 1995d). All of our high-T_c superconductor current lead activities involve an industrial partner. As this application has matured, involvement has been limited to (1) encouraging designs that promote the state-of-the-art of high-T_c superconductor, (2) assisting small companies that have active programs to commercialize high-T_c superconductor leads but do not have the resources to maintain comprehensive capabilities in high-T_c superconductor materials, and (3) using unique facilities to characterize lead

performance so that these facilities need not be duplicated by companies with limited resources (Cha et al., 1995a,b). In all of the collaborations, the preference is to construct leads with commercially available high-T_c superconductor materials.

Superconductivity, Inc., Leads

An ongoing superconductor current lead project is a collaboration with Superconductivity, Inc., to develop a 1500-A high-T_c superconductor lead (Fig. 51) for use in a power-quality control SMES system. Staff from the company have participated in all stages of the project. Technical progress in FY 1995 has consisted of evaluating the performance of components and leads. A key component in the project has been the development of a heat intercept at the warm end of a high-T_c superconductor that has a very high electrical resistivity (electrical isolation) but a low thermal resistivity (heat transfer). Such intercepts are necessary features for high-T_c superconductor leads if their performance is to be substantially better than conventional, vapor-cooled Cu leads (Niemann et al., 1995e).

The leads, constructed in FY 1994, have been installed in a performance-evaluation cryostat and instrumented. The leads have been cooled to operating temperature and have been operated to 1150 A during measurement system checkout (Niemann et al., 1995a and b). Joint technology development efforts with Superconductivity, Inc., include current lead design methodologies, which include performance, safety, reliability, and cost; intermediate-temperature heat intercepts with low heat transfer and high voltage isolation; and demountable screw-type electrical connections.

A follow-on program has been initiated for the purpose of designing second-generation 1500-A high-T_c superconductor current leads and performing associated conductor burnout evaluations. Conceptual lead design is underway and burnout analysis has been initiated. Figure 52 indicates the predicted burnout; i.e., burnout time for a 0.5-cm-diameter x 15-cm-long Bi-2212 rod with initial cold and warm end temperatures of 4 K and 77 K, respectively, when T_{max} = 300 K.. At 77 K, the J_c below which the conductor is in perfect superconducting state, is 1747 A/cm^2. Therefore, if the operating current density is less than the J_c, there is no heat generation. For a 400-A operating current, the current density becomes 2037 A/cm^2, which is greater than the J_c and there will be generation of flux-flow resistivity heat. The temperature change is concentrated near the warm end. Initially, the temperature rise is very slow because the low flux-flow resistivity is low. However, when the maximum temperature reaches the critical temperature (T_{crit} = 90 K), the portion of the rod where the temperature is greater than the critical temperature becomes normal. The normal-state resistivity is much greater than the flux-flow resistivity. The maximum temperature of the rod reaches burnout temperature, i.e., 300 K, very quickly after the maximum temperature reaches critical temperature. By numerical calculation, the burnout time is 2.9 s. Burnout test apparatus to verify the performance predictions is under construction. We plan to evaluate the burnout characteristics of both bulk and PIT conductors.

Babcock & Wilcox Leads

In a collaborative project with Babcock & Wilcox, a 16-kA high-T_c superconductor lead for use in an 0.5 MWh SMES device is being developed. Features of the design include a conduction-cooled high-T_c superconductor stage and use of multiple elements of PIT Bi-2223 with an Ag/3% Au sheath embedded in a stainless steel safety lead (Niemann et al.,

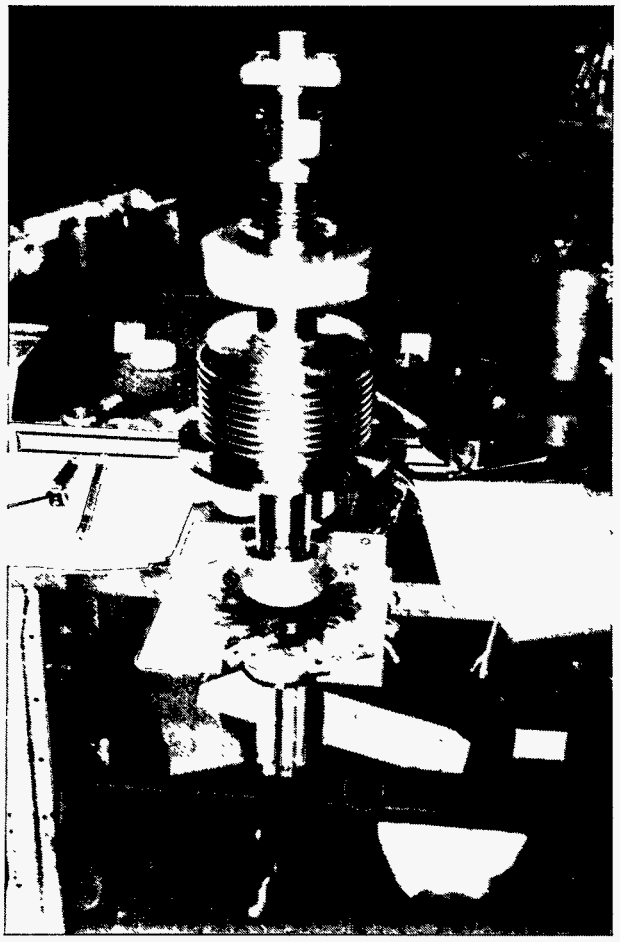

Fig. 51.
Superconductivity, Inc., current lead prior to installation in performance-evaluation cryostat; six parallel YBCO w/15% Ag high-T_c superconductor rods and a thermally effective, electrically isolating heat intercept assembly are incorporated.

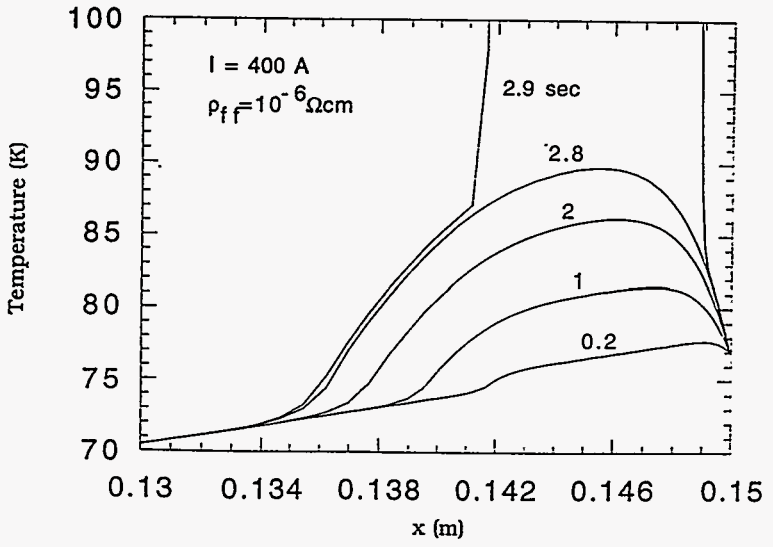

Fig. 52. Burnout time prediction for Bi-2212 rod.

1995a,1995c). Work included design of the lead, evaluation of vendor-supplied high-T_c superconductor elements, construction of a prototype lead, and initiation of construction of a lead assembly. Staff from the company are involved in all stages of the development, including construction of the lead.

The high-T_c superconductor element consists of a composite sintered stack of clad tapes (Fig. 53). Eighteen conductor elements are mounted in parallel in a safety lead assembly (Fig. 54). A prototype lead assembly was built to develop manufacturing methods, quality verification, and assembly procedures. The prototype safety lead is shown in Fig. 55.

Two preproduction samples of conductor elements intended for use in the current lead assembly have been evaluated under anticipated use conditions. The conductor elements were manufactured by ASC. Critical current at 77 K in self field with a 1-mV/cm criterion was measured at ASC in a DC mode and at ANL in a pulsed-current mode. The critical current values measured in the DC mode were somewhat lower than those measured in the pulsed-current mode, most likely because of resistive heating of normal metal contacts. Critical current at 60 K and B//b and B//c was measured in a pulsed-current mode. Typical results for one of the samples are shown in Fig. 56. One sample conductor element was subjected to 50 295-K Æ 77-K Æ 295-K thermal cycles with no significant change in critical current. One sample conductor element was subjected to 600 electrical ramp cycles, corresponding to those predicted for the SMES current lead application, with no significant change in critical current.

Specific resistivities of metallic contacts to the superconductive cores of tape samples, comparable to those used in the composite bars, were measured. Half-joint resistivities at 77 K ranged from 0.031 to 0.037 $\mu\Omega$-cm^2. Lap-joint resistivity tests were performed with specially formed Ag metal connectors sintered to the tapes. The average resistivity of the half joints at 77 K, including the contribution from the Ag connector and its sintered interface to the tapes, was $\approx$1 $\mu\Omega$-cm^2. The irreversible strain limit of both sample conductor elements was 0.2%, and retained critical current was >90% (Fig. 57). The sample conductor elements displayed a high degree of structural and electrical integrity with no noticeable performance degradation despite being handled many times by various individuals.

In FY 1996, a test of a single high-T_c superconductor lead assembly under the anticipated operating conditions of the SMES magnet will be conducted at the National High Field Magnet Laboratory. Current lead performance evaluations include conventional upper-stage heat leak, mass flow and temperature optimization, integrated assembly ramp to 17,600 A when B = 0.2 T, optimization of mass flow and temperature at 16,000 A when B = 0.2 T, and determination of heat leak. Reliability evaluations include thermal cycles, electrical cycles, and safety lead function.

Joint technology development with Babcock & Wilcox included design methodologies that include performance, safety, reliability, and cost; demountable screw-type electrical connections; design and fabrication of PIT tape composite conductors with ASC to give a conductor with specified performance along with structural integrity and the dimensional precision required for straightforward construction of multielement current lead assemblies.

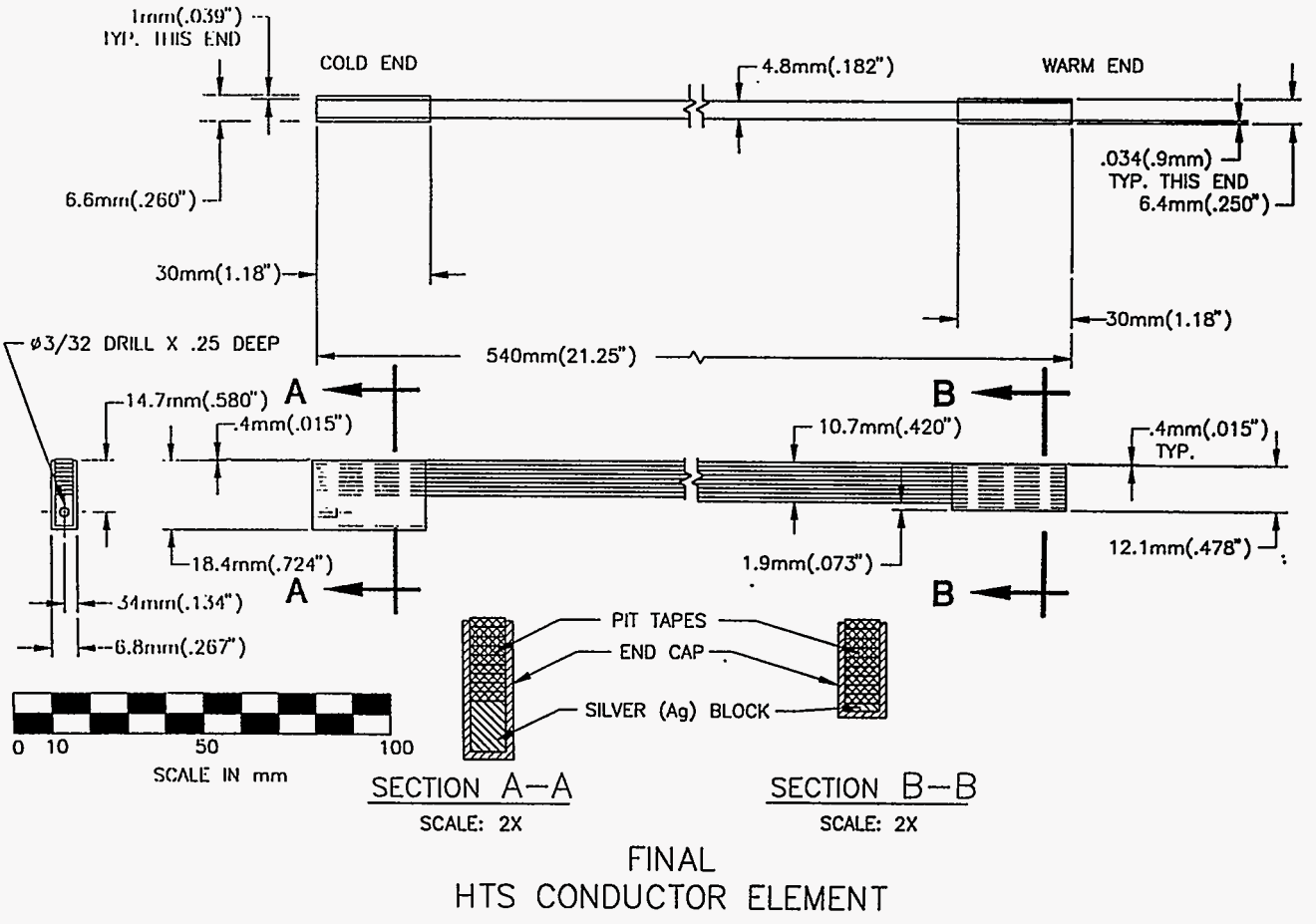

Fig. 53. Babcock & Wilcox high-T_c superconductor: geometry of elements.

American Superconductor Corporation Leads

High-current composite conductor elements from ASC will be electrically characterized at 60 K. The characterization will provide a correlation with performance at 77 K, which is readily measured by ASC. This correlation will be an important factor in the design of future high-current high-T_c superconductor leads.

Critical current will be measured in the ANL facility that consists of a variable-temperature He cryostat, a superconducting magnet, and a current pulser. The variable-temperature cryostat is configured to contain two samples and will be rotated in the magnet to provide B//b and B//c applied-field orientations. The magnet provides a high-homogeneity, large-volume field, with magnitudes to 2.5 T. The superconducting magnet and variable-temperature cryostat are shown in Fig. 58.

ZerRes Corporation Leads

As part of a collaborative agreement with ZerRes Corporation (ZerRes), ANL has conducted experiments to measure the critical currents of a high-T_c superconductor current lead supplied by ZerRes under various thermal and magnetic field conditions. The composite leads are manufactured by a proprietary process developed by ZerRes (Zimmerman et al., 1993).

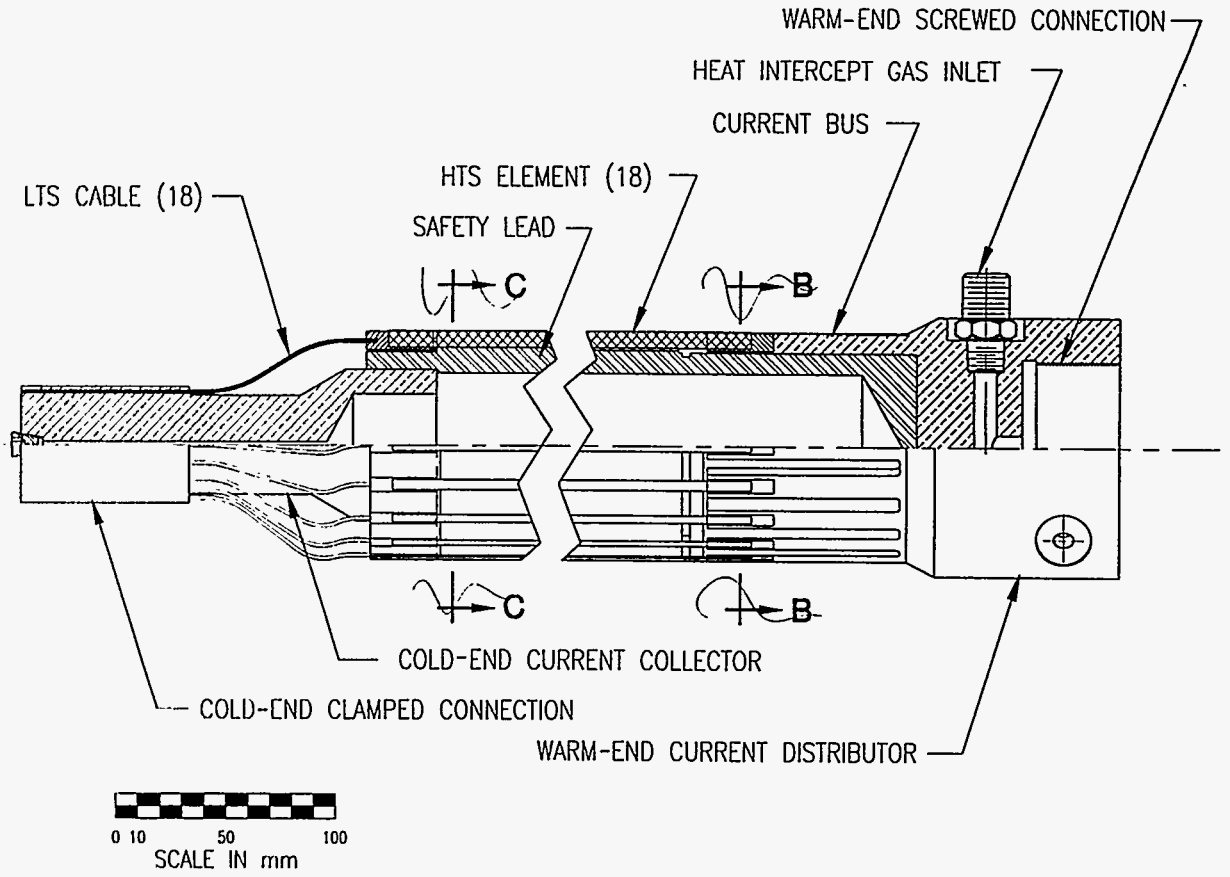

Fig. 54. Babcock & Wilcox middle-stage (60-K Æ 5-K) current lead assembly. Eighteen conductor elements in parallel carry a current of 16,000 A. A stainless steel safety lead provides an alternate current path and thermal stabilization for the high-T_c superconductor elements.

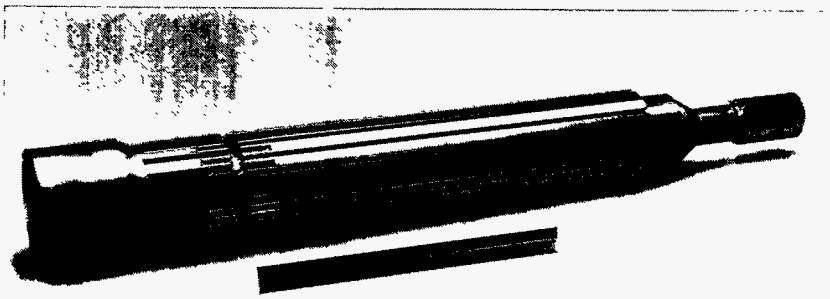

Fig. 55. Babcock & Wilcox prototype safety lead assembly.

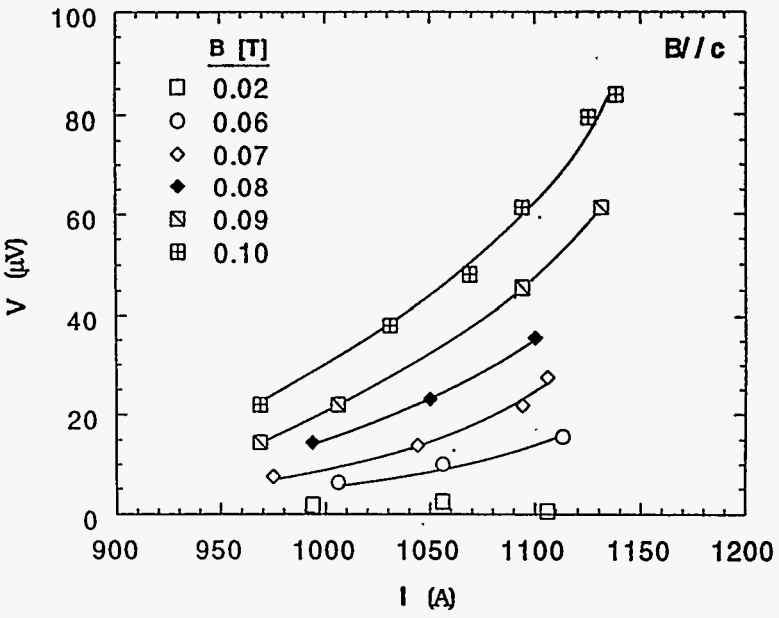

Fig. 56.
Voltage drop vs. current at 60 K and B//c (250-mm electrode gap) of a Babcock & Wilcox conductor element.

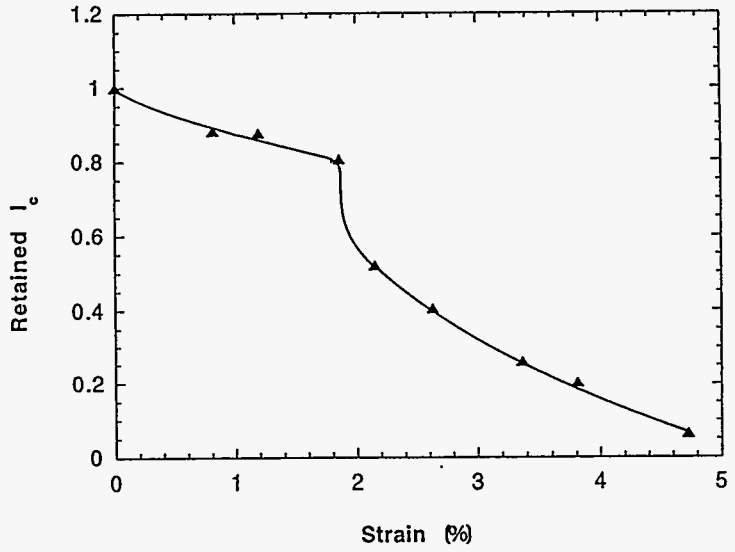

Fig. 57.
Variation of retained I_c fraction with axial strain of Babcock & Wilcox element.

The experimental apparatus includes an R & A magnet, a measurement cryostat, an insert, and the instrumentation systems. The insert includes primarily the current lead, the temperature sensors, the voltage taps, and three resistive heaters. The lead is housed in an epoxy/fiberglass composite tube with brass caps on both ends. Two silicon diodes were installed on the brass caps to measure the temperature at the upper and lower ends of the current lead. Two voltage taps were soldered to the Cu wires on both ends of the lead to measure the voltage drop across the lead. Two heaters were mounted on the brass caps of the lead for temperature control. A third heater was installed near the bottom of the cryostat in case more boiloff was needed for temperature control. The entire insert assembly also included a liquid-He-level sensor and a current return path (a Cu wire) for the lead. By adjusting the current through the heaters and the liquid He level in the cryostat, the desired temperatures and temperature gradients were obtained.

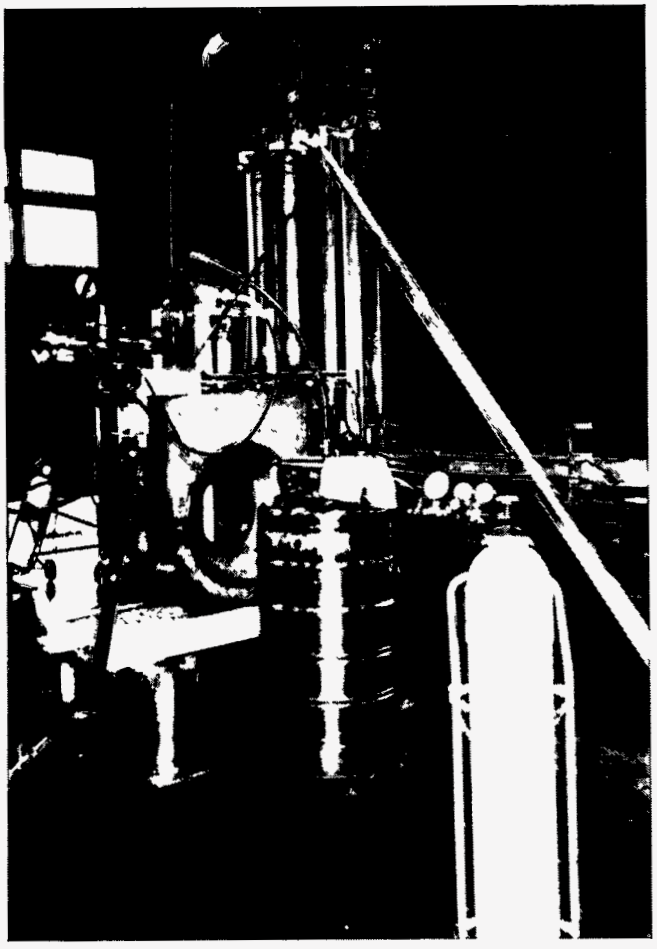

Fig. 58.
Superconducting magnet and variable-temperature cryostat in ANL facility for measuring I_c.

Critical current was tested by pulsing a constant current through the lead and observing the corresponding voltage drop across the lead. The battery-powered current supply was driven by a ground-isolated wave function generator. The desired current was obtained by adjusting the amplitude of the generator output. Current-pulse duration was fixed at 200 ms for all tests reported here. The shape and magnitude of the current pulse were monitored and stored on a ground-isolated oscilloscope. Output from the voltage taps was fed into a differential preamplifier and displayed and stored on another oscilloscope.

Two types of tests, isothermal and thermal gradient, were performed. Isothermal tests were carried out at 5.4, 21, and 59 K. Two temperature gradient tests, 20-60 K and 5-70 K, were conducted. For each test, the lead was subjected to a constant applied field of 0, 260, 520, and 1040 G. Each test is begun by adjusting the currents through the two heaters and the liquid He level in the cryostat. Once the specified temperature or temperature gradient is reached, voltage-vs.-current measurement commences. Current is gradually increased until either the voltage drop becomes too large or the thermal runaway condition is reached. Thermal runaway is the effect of internal heating in the lead as a result of dissipation in the superconductor. More information on dissipation and thermal runaway can be found in Askew et al. (1993). In addition, tests at liquid N_2 temperature were conducted with a different setup. The applied fields for the liquid N_2 tests were 0 and 55 G.

Figures 59–61 show the voltage-vs.-current (V/I) characteristics of the ZerRes lead at various temperatures and applied fields. The effect of the applied magnetic field on the critical current of the lead is evident from these figures. Figure 62 shows the V/I characteristics at different temperatures with zero applied field. As expected, critical current decreases with increasing temperature. In general, the lowest critical current for a given applied field is associated with the 5–70 K gradient test, followed by the isothermal test at 60 K. The only exception is that at zero applied field, the critical currents for the 20–60 K and the 5–70 K gradient tests are smaller than that at 77 K. This abnormal behavior is probably not real and can likely be attributed to the fact that the temperature in the lead has not reached the steady-state conditions under zero applied field. The two temperature gradient tests at zero applied field begin immediately after the temperature at both ends of the lead reached specified values. Because the thermal conductivity of the high-T_c superconductor lead is relatively poor, the temperatures along the lead are not likely to have reached steady state in such a short period of time. Subsequent tests at nonzero applied field did not show this abnormal behavior because these tests were always conducted after the zero field tests and there was sufficient time for the lead to reach steady state.

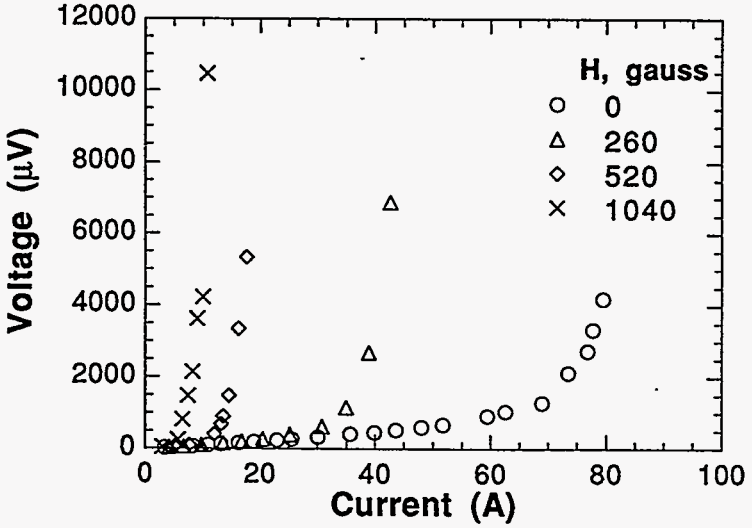

Fig. 59. Voltage-vs.-current characteristics of ZerRes lead at various applied fields for T = 21 K.

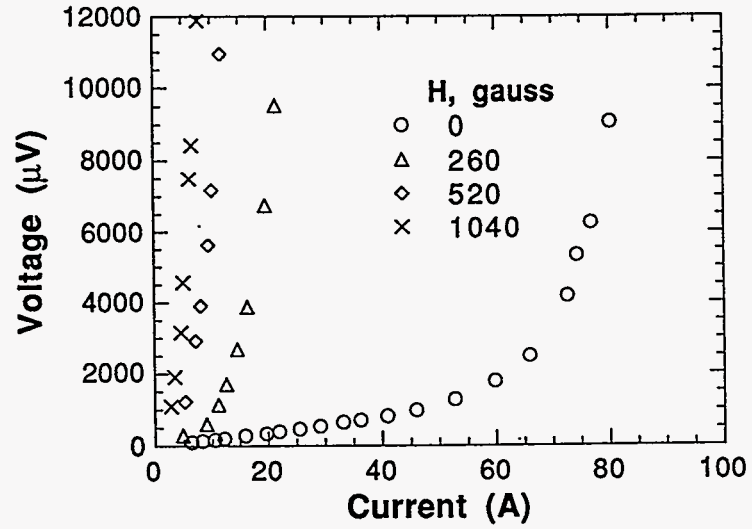

Fig. 60. Voltage-vs.-current characteristics of ZerRes lead at various applied fields for T = 59 K.

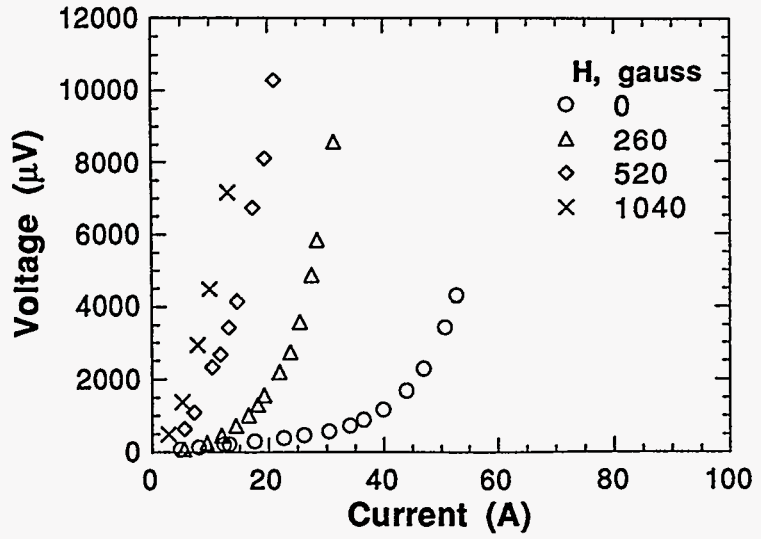

Fig. 61. Voltage-vs.-current characteristics at various applied fields for a temperature gradient of 20-60 K across the lead.

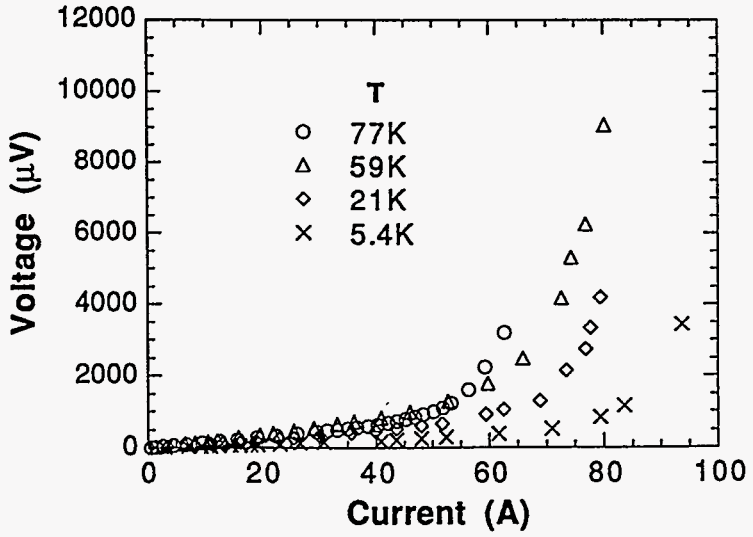

Fig. 62. Voltage-vs.-current characteristics of ZerRes lead at various temperatures for zero applied field.

2.5.2 Superconducting Magnetic Bearings

The effort to develop superconducting magnetic bearings for flywheel-energy-storage (FES) applications continued as a major collaborative program with Commonwealth Research Corporation (CRC). Electrical energy storage on a utility scale is currently not practical for most utilities because of the requirements for special geography and the inefficiencies of existing storage systems. A potential solution to this problem is FES with very low rotational losses (Abboud et al., 1994, Hull, 1994, 1995; Hull et al., 1995; Rossing and Hull, 1995).

The project objective is to establish a technology base for improved FES systems through efficiency enhancements made possible by incorporation of high-T_c superconductor magnetic bearings. A critical issue is to demonstrate that low-loss high-T_c superconductor bearings can be scaled up to sizes of interest for utility FES applications (Hull et al., 1994a). The FES Test Apparatus (FTA) at ANL was developed specifically for this purpose, as described in Balachandran et al. (1994a). High-speed flywheels,

that incorporate high-T_c superconductor bearings with inertial rims made from high-strength composite materials, combined with new-technology motor/generators (M/Gs), offer the potential for very high (>90%) diurnal storage efficiencies.

Significant advances were made during FY 1995 in the development of materials and components for very-low-friction high-T_c superconductor magnetic bearings, and in establishment of a design data base through laboratory scaleup and spindown tests in the large FTA vacuum test chamber (Fig. 63). Some major FY 1995 accomplishments include continued development of improved high-T_c superconductor materials and innovative high-T_c superconductor bearing concepts; fabrication/testing of a new rotor (Rotor B) in the 10-kg category that incorporates a high-T_c superconductor bearing and a graphite composite rim, and demonstration of an order-of-magnitude reduction in the coefficient of friction for FES rotors in the 10-kg class; modification of the FTA for high-speed tests with remote operation; and investigation of improved M/G designs and their integration with flywheel rotors.

The superconducting magnetic bearing project task elements for this year included

(1) Development of high-T_c superconductor materials with improved levitation characteristics, and processing of large quantities of YBCO stator elements for magnetic bearing experiments.

(2) Fabrication and testing of Rotor B, a second-generation flywheel rotor in the 10-kg class.

(3) Installation of the FTA in a safety pit, with system modifications for high-speed rotor tests.

(4) Conceptual design of Rotor C in the 100-kg category.

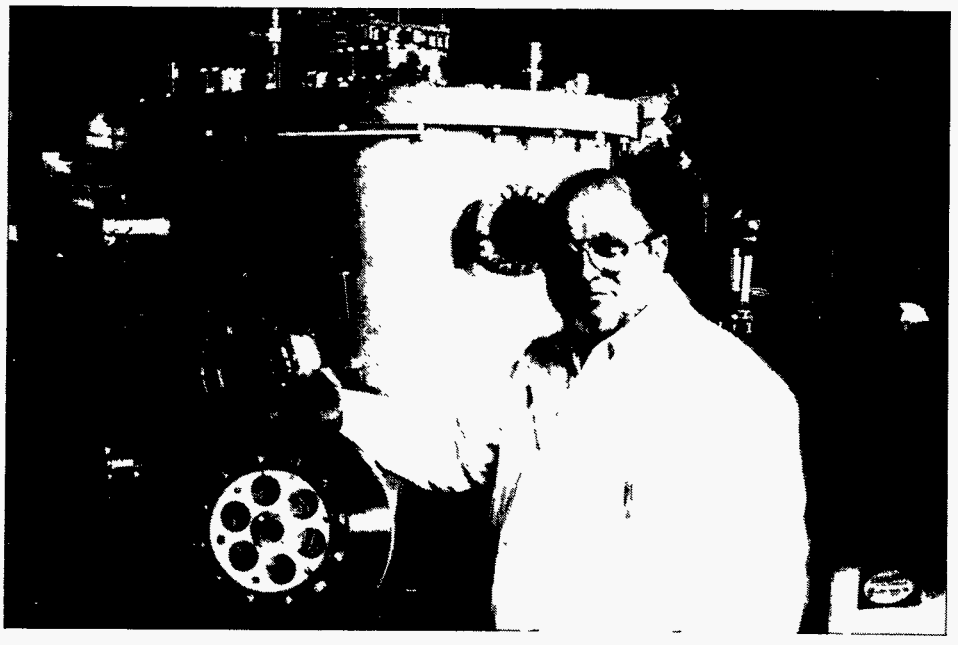

Fig. 63. Rotor A and FTA vacuum test chamber.

(5) Upgrade of the FTA M/G system to operate at up to 30,000 r/min, and continuing development of advanced M/G units based on Halbach array concepts.

(6) Modification of an existing thick-walled spin chamber for use in spin-to-failure tests of small flywheel rotors levitated by high-T_c superconductor magnetic bearings.

(7) Continuation of high-T_c superconductor magnetic bearing bell-jar experiments to investigate new design concepts on a small scale.

As reported earlier in this report, the levitation characteristics of bulk Y-123 superconductor elements continued to improve through the use of seeding for improved structure, enhanced melt-processing techniques, and other innovations. Many Y-123 tile elements were melt processed at ANL for the high-T_c superconductor magnetic-bearing development efforts. The best Y-123 levitators were selected to construct the second-generation high-T_c superconductor magnetic-bearing stator array. In December 1994, the new array was installed in the FTA liquid N_2 cryochamber, replacing the original high-T_c superconductor stator array. Outside dimensions that exceeded 20 cm were required for both high-T_c superconductor stator arrays for effective levitation of Rotors A and B, with their associated 20-cm outer-diam ring magnets.

The technology for fabricating bulk high-T_c superconductor materials has progressed to the stage where it is now being transferred to commercial manufacturers (Todt et al., 1994; Todt et al., 1995a-c). Bulk Y-123 tile elements are currently being fabricated by Superconductive Components, Inc. (Columbus, OH), and will be used in the third-generation stator assembly that is to be installed in the FTA. The levitation characteristics of each puck or tile are determined at ANL by force measurements with a standard reference magnet and well-defined procedures.

The collaborative efforts with UGIMAG (Valparaiso, IN) continued in the development of high-strength permanent-magnet (PM) rotors. The impact of azimuthal inhomogeneities and other characteristics of rare-earth PMs on rotor performance has continued to be of interest. Spindown tests and characterization of the 20-cm outer-diam, double-ring, PM for Rotor B were completed. The azimuthal magnetic field homogeneity of the Rotor B magnet was significantly better than the previous Rotor A magnet of the same size. Figure 64 shows the coefficient of friction measured in low-speed FTA spin tests for the Rotor B permanent magnet alone, without composite banding, as a function of rim velocity for three levitation gap heights between the bottom of the magnet and the top of the high-T_c superconductor array (Mulcahy et al., 1995).

Design of a 39-cm outer-diam graphite fiber/epoxy composite rim for Rotor B was completed as a collaborative effort that involved ANL, CRC, and Pennsylvania State University (PSU). The composite rim was then fabricated by PSU. Rotor B is designed for higher rotational speeds than was the case for Rotor A. Following assembly of the rim, hub, and PM rings, spin tests of Rotor B were conducted in the FTA with the second-generation high-T_c superconductor stator array (Mulcahy et al., 1995). Coefficients of friction of $\approx 1 \times 10^{-5}$ were achieved with Rotor B during low-speed tests. Higher speed tests are scheduled for early FY 1996.

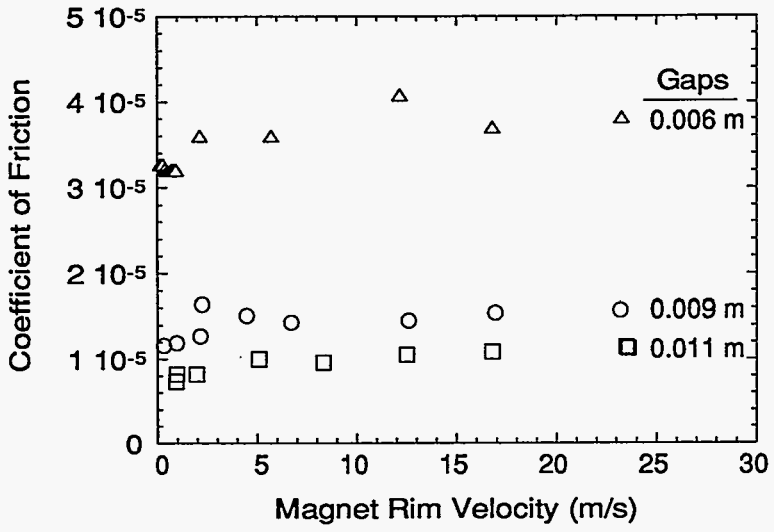

Fig. 64.
Friction coefficient for Rotor B permanent magnet as a function of levitation gap height.

A 1/4-hp M/G with an eddy current clutch was installed in the FTA during FY 1995, replacing the air jet previously used for rotor spinup. The eddy current clutch drive interacts with an Al plate mounted on the rotor hub to provide spinup torque. The M/G and clutch drive are retractable and can be re-engaged at will. In generator mode, energy is extracted from the flywheel rotor as it is slowed. In November 1994, the FTA was used with Rotor A to demonstrate power output from an FES system, based on high-T_c superconductor magnetic bearing technology, and a light bulb was successfully lit.

Several other enhancements were made to the FTA. A motorized positioning platform was installed to field cool the magnetic bearing rotors at any desired elevation above the high-T_c superconductor stator elements. Another drive system was installed to raise and lower the 1/4-hp M/G unit and its associated clutch drive. The FTA has been instrumented with capacitance position sensor probes to measure both vertical and radial motion due to vibrations and other displacements. The FTA vacuum chamber was relocated into a concrete pit as a safety precaution for higher speed tests (beyond 10,000 r/min) of Rotor B. Development for a 5-hp M/G unit is near completion, and will increase the FTA spinup capability to 30,000 r/min. Three camcorders have been installed in the pit for remote monitoring of the FTA and for viewing rotor dynamics inside the vacuum test chamber. The test pit will be covered by three large (5900 kg each) reinforced concrete blocks during high-speed testing. A ballistic nylon blanket will be spread over the blocks as an additional precaution. All FTA instruments and operating equipment have been modified for remote operation (Lorimer et al., 1995; Yang et al., 1995).

A Halbach magnet array M/G has been assembled and bench tests are in progress. Halbach M/G units show definite potential for FES applications, and we plan to incorporate them into future FTA tests.

High-T_c superconductor bearing bell-jar experiments were continued to further delineate potential loss mechanisms. Investigations have been carried out on means to improve the magnetic bearing characteristics of both PM rotor rings and high-T_c superconductor stator arrays. A new concept for high-T_c superconductor bearing design, a mixed-mu system, was bench tested and produced a coefficient of friction of 10^{-9}.

References

R. Abboud, J. Hull, K. Uherka, and T. Mulcahy, in Proc. Am. Power Conf., Vol. 56-II (1994) p. 1356.

T. R. Askew, J. G. Nestell, R. B. Flippen, D. M. Groski, and N. McN. Alford, IEEE Trans. Appl. Supercond. **3**, 1398 (1993).

U. Balachandran, R. B. Poeppel, J. E. Emerson, and S. A. Johnson, U.S. Patent 5,086,034 (Feb. 4, 1992).

U. Balachandran, et al., Practical Superconductor Development for Electrical Power Applications: Annual Report for FY 1994, Argonne National Laboratory Report ANL-94/39 (1994a).

U. Balachandran, A. N. Iyer, C. A. Youngdahl, L. R. Motowidlo, and P. Haldar, Adv. Cryo. Eng. **40 A**, 289 (1994b).

U. Balachandran, U.S. Patent 5,409,887 (April 25, 1995).

U. Balachandran et al., in Advances in Superconductivity VII, Proc. 7th Intl. Symp. on Supercond. (ISS-94), Vol. 2 (Springer-Verlag, Tokyo, 1995a) p. 1243.

U. Balachandran, C. A. Youngdahl, M. T. Lanagan, S. E. Dorris, J. J. Picciolo, J. Cluff, T. Brent, M. Marinelli, B. Fisher, P. Winandy, J. Wenzlaff, T. Askew, R. C. Niemann, and R. B. Poeppel, Appl. Supercond., in press (1995b).

Y. S. Cha, M. T. Lanagan, K. E. Gray, V. Z. Jankus, and Y. Fang, Appl. Supercond. **2**, 47 (1994a).

Y. S. Cha, R. C. Niemann, and J. R. Hull, Cryogenics **34**, 99 (1994b).

Y. S. Cha, W. J. Minkowycz, and S. Y. Seol, Int. Comm. Heat Mass Trans. **22**, 461 (1995a).

Y. S. Cha, R. C. Niemann, and J. R. Hull, in Thermal Engineering 1995, Vol. 1, eds. L. S. Fletcher and T. Aihara (ASME, New York, 1995b) p. 115.

N. Chen, A. C. Biondo, S. E. Dorris, K. C. Goretta, M. T. Lanagan, C. A. Youngdahl, and R. B. Poeppel, Supercond. Sci. Technol. **6**, 674 (1993).

J. A. DeLuca, P. L. Karas, J. E. Tkaczyk, C. L. Briant, M. F. Garbauskas, and P. J. Bednarczyk, Mater. Res. Soc. Symp. Proc. **275**, 669 (1992).

L. P. De Rochemont, V. A. Maroni, M. Klugerman, R. J. Andrews, and W. C. Kelliher, Appl. Supercond. **2**, 281 (1994).

S. E. Dorris, B. C. Prorok, M. T. Lanagan, S. Sinha, and R. B. Poeppel, Physica C **212**, 66 (1993).

S. E. Dorris, B. C. Prorok, M. T. Lanagan, N. M. Browning, M. R. Hagen, J. A. Parrell, Y. Feng, A. Umezawa, and D. C. Larbalestier, Physica C **223**, 163 (1994a).

S. E. Dorris, B. C. Prorok, M. T. Lanagan, V. A. Maroni, and R. B. Poeppel, U.S. Patent 5,354,535 (October 11, 1994b).

S. X. Dou, Y. C. Guo, J. Yan, and H. K. Liu, Supercond. Sci. Technol. **6**, 195 (1993).

J. W. Ekin, D. K. Finnemore, Q. Li, J. Tenbrink, and W. Carter, Appl. Phys. Lett. **61**, 858 (1992).

C. B. Eom, A. F. Marshall, Y. Suzuki, B. Boyer, R. F. W. Pease, and T. H. Geballe, Nature **353**, 544 (1991).

Y. Fang, S. Danyluk, M. T. Lanagan, C. A. Youngdahl, X. Xu, and K. Nomata, Physica C, in press (1995).

C. Fanggao, P. J. Ford, G. A. Saunders, L. Jiaquing, D. P. Almond, B. Chapman, M. Cankurtaran, R. B. Poeppel, and K. C. Goretta, Supercond. Sci. Technol. **6**, 484 (1993).

K. C. Goretta and M. L. Kullberg, U.S. Patent 5,202,306 (April 13, 1993).

K. C. Goretta, M. T. Lanagan, T. J. Brent, S. E. Dorris, J. Joo, R. A. Shearer, J. P. Singh, S. Wasylenko, P. M. Winandy, X. W. Wang, C. A. Youngdahl, R. B. Poeppel, D. J. Miller, T. Holesinger, P. Kostic, and N. Chen, Appl. Supercond. **2**, 411 (1994).

K. C. Goreta, B. P. Brandel, M. T. Lanagan, J. Hu, D. J. Miller, S. Sengupta, J. C. Parker, M. N. Ali, and N. Chen, IEEE Trans. Appl. Supercond. **5**, 1309 (1995a).

K. C. Goretta, J. A. Cluff, J. Joo, M. T. Lanagan, J. P. Singh, N. Vasanthamohan, Y. Xin, and K. W. Wong, in Proc. 4th World Congress on Superconductivity, NASA Conference Publication 3290, ed. K. Krishen and C. Burnham (NASA, Washington, 1995b) p. 633.

J.-C. Grivel, A. Jeremie, B. Hensel, and R. Flükiger, ICMAS-93, Superconducting Materials (1993) p. 359.

J. Guo, J. A. Lewis, and K. C. Goretta, IEEE Trans. Appl. Supercond. **5**, 1860 (1995a).

J. Guo, J. A. Lewis, K. C. Goretta, and J. Schwartz, J. Appl. Phys. **78**, 4596 (1995b).

P. Haldar, J. G. Hoehn Jr., L. R. Motowidlo, U. Balachandran, and Y. Iwasa, Adv. Cryo. Eng. **40 A**, 313 (1994).

W. L. Holstein, Appl. Supercond. **2**, 345 (1994).

J. R. Hull, J. L. Passmore, T. M. Mulcahy, and T. D. Rossing, J. Appl. Phys. **76**, 577 (1994).

J. R. Hull, in 1995 Int. Workshop on Superconductivity Co-Sponsored by ISTEC and MRS (ISTEC, Tokyo, 1995) p. 129.

J. R. Hull, T. M. Mulcahy, K. L. Uherka, and R. G. Abboud, IEEE Trans. Appl. Supercond. **5**, 626 (1995).

A. Jeremie, K. Alami-Yadri, J.-C. Grivel, and R. Flükiger, Supercond. Sci. Technol. **6**, 730 (1993).

J. Jimenez-Melendo, A. R. De Arellano-López, A. Dominguez-Rodriguez, K. C. Goretta, and J. L. Routbort, Acta Metall. Mater. **43**, 2429 (1995).

J. Joo, J. P. Singh, T. Warzynski, A. Grow, and R. B. Poeppel, Appl. Supercond. **2**, 401 (1994).

P. Krishnaraj, M. Lelovic, N. G. Eror, and U. Balachandran, Physica C **215**, 305 (1993).

M. T. Lanagan, D. S. Kupperman, G. A. Yaconi, S. H. Kilgore, and A. Saigal, IEEE Trans. Appl. Supercond. **5**, 1475 (1995).

D. C. Larbalestier, X. Y. Cai, Y. Feng, H. Edelman, A. Umezawa, G. N. Riley, and W. L. Carter, Physica C **221**, 299 (1994).

M. Lelovic, P. Krishnaraj, N. G. Eror, and U. Balachandran, Physica C **242**, 246 (1995a).

M. Lelovic, P. Krishnaraj, N. G. Eror, and U. Balachandran, Supercond. Sci. Technol. **8**, 336 (1995b).

Y. F. Li, Z. Z. Sheng, S. Sengupta, K. C. Goretta, and P. E. D. Morgan, Physica C **232**, 184 (1994).

Y. F. Li, Z. Z. Sheng, Z. F. Ren, J. H. Wang, and K. C. Goretta, Supercond. Sci. Technol. **8**, 174 (1995).

W. L. Lorimer, D. K. Lieu, J. R. Hull, T. M. Mulcahy, and T. D. Rossing, IEEE Trans. Magn. **30**, 3004 (1994).

J. S. Luo, S. E. Dorris, M. T. Lanagan, and V. A. Maroni, Proc. Microscop. Soc. Am. **52**, 798 (1994a).

J. S. Luo, N. Merchant, E. J. Escorcia-Aparicio, V. A. Maroni, B. S. Tani, W. L. Carter, and G. N. Riley Jr., J. Mater. Res. **9**, 3059 (1994b).

P. Majewski, B. Hettich, K. Schulze, and G. Petzow, Adv. Mater. **3**, 488 (1991).

P. Majewski, S. Kaesche, H.–L. Su, and F. Aldinger, Physica C **221**, 295 (1994).

V. A. Maroni, U.S. Patent 5,010,053 (April 23, 1991).

V. A. Maroni, U.S. Patent 5,079,233 (January 7, 1992).

L. J. Martin, K. C. Goretta, J. Joo, J. P. Singh, S. R. Olson, S. Wasylenko, R. B. Poeppel, and N. Chen, Mater. Lett. **17**, 232 (1993).

N. Merchant, J. S. Luo, V. A. Maroni, G. N. Riley Jr., and W. L. Carter, Appl. Phys. Lett. **65**, 1039 (1994a).

N. Merchant, J. S. Luo, V. A. Maroni, S. N. Sinha, G. N. Riley Jr., and W. L. Carter, Appl. Supercond. **2**, 217 (1994b).

T. A. Miller, J. E. Ostenson, Q. Li, L. A. Schwartzkopf, D. K. Finnemore, J. Righi, R. A. Gleixner, and D. Zeigler, Appl. Phys. Lett. **58**, 2159 (1991).

P. E. D. Morgan, M. Okada, T. Matsumoto, and A. Soeta, in Adv. Supercond. II; Proc. 2nd Int. Symp. on Superconductivity (ISS'89) eds. T. Ishiguro and K. Kajimura (Springer-Verlag, Berlin, 1990) p. 435.

T. M. Mulcahy, J. R. Hull, K. L. Uherka, R. G. Abboud, J. H. Wise, C. W. Gabrys, and C. E. Bakis, IEEE Trans. Magn., in press (1995).

R. C. Niemann, Y. S. Cha, J. R. Hull, W. E. Buckles, and M. A. Daugherty, Adv. Cryo. Eng. **39**, 1153 (1994a).

R. C. Niemann, J. D. Gonczy, and T. H. Nicol, Adv. Cryo. Eng. **39**, 1665 (1994b).

R. C. Niemann, W. E. Buckles, Y. S. Cha, K. D. Dixon, J. R. Hull, C. M. Rey, and B. R. Weber, in Proc. 30th Intersociety Energy Conv. Eng. Conf., Vol. 3 (ASME, New York, 1995a) p. 293.

R. C. Niemann, Y. S. Cha, J. R. Hull, W. E. Buckles, B. R. Weber, and S. T. Yang, IEEE Trans. Appl. Supercond. **5**, 793 (1995b).

R. C. Niemann, Y. S. Cha, J. R. Hull, C. M. Rey, and K.D. Dixon, IEEE Trans. Appl. Supercond. **5**, 789 (1995c).

R. C. Niemann, J. D. Gonczy, and T. H. Nicol, in Thermal Engineering 1995, Vol. 1, ed. L. S. Fletcher and T. Aihara (ASME, New York, 1995d) p. 43.

R. C. Niemann, J. D. Gonczy, and T. H. Nicol, U.S. Patent 5,356,870 (Feb. 7, 1995e).

S. Nomura, H. Fuke, H. Yoshino, and K. Ando, Supercond. Sci. Technol. **6**, 858 (1993).

A. Otto, L. J. Masur, J. Gannon, E. Podtburg, D. Daly, G. J. Yurek, and A. P. Malozemoff, IEEE Trans. Appl. Supercond. **3**, 915 (1993).

M. Paranthaman and A. M. Hermann, in Organic Conductors: Fundamentals and Applications, ed. J. P. Farges (Marcel Dekker, New York, 1994) p. 735.

A. E. Pashitski, A. Polyanskii, A. Gurevich, J. A. Parrell, and D. C. Larbalestier, Physica C **246**, 133 (1995).

R.B. Poeppel et al., Practical Superconductor Development for Electrical Power Applications: Annual Report for FY 1993, Argonne National Laboratory Report ANL-93/33 (1993).

R. B. Poeppel, K. C. Goretta, M. T. Lanagan, S. Danyluk, M. McNallan, and R. Troendly, U.S. Patent application 08/317,353 (1994).

J. Polonka, M. Xu, A. Goldman, and D. K. Finnemore, J. Appl. Phys., **4**, 7397 (1993).

Z. F. Ren and J. H. Wang, Physica C **216**, 199 (1993).

Z. F. Ren, J. H. Wang, D. J. Miller, and K. C. Goretta, Physica C **229**, 137 (1994).

Z. F. Ren, C. A. Wang, J. H. Wang, D. J. Miller, and K. C. Goretta, Physica C **247**, 163 (1995).

T. D. Rossing and J. R. Hull, Quantum **5**(4), 22 (1995).

R. R. Schartman, R. Sakidja, and E. E. Hellstrom, J. Am. Ceram. Soc. **76**, 724 (1993).

J. P. Singh, J. Joo, D. Singh, T. Warzynski, and R. B. Poeppel, J. Mater. Res. **8**, 1226 (1993).

J. P. Singh, D. Singh, D. S. Kupperman, and S. Majumdar, in High Performance Composites: Commonality of Phenomena, eds. K. K. Chawla, P. K. Liaw, and S. G. Fishman (TMS, Warrendale, 1994) p. 143.

J. P. Singh, R. B. Poeppel, K. C. Goretta, and N. Chen, U.S. Patent 5,401,712 (March 28, 1995).

M. Suenaga, Y. Fukumoto, and P. Haldar, unpublished information (1995).

M. Tetenbaum, M. C. Hash, B. S. Tani, J. S. Luo, and V. A. Maroni, Physica C **235-240**, 321 (1994).

M. Tetenbaum, M. C. Hash, B. S. Tani, J. S. Luo, and V. A. Maroni, Physica C **249**, 396 (1995).

V. R. Todt, S. Sengupta, D. Shi, P. R. Sahm, P. J. McGinn, R. Poeppel, and J. R. Hull, J. Electron. Mater. **23**, 1127 (1994).

V. R. Todt, D. J. Miller, and S. Sengupta, in 1995 Int. Workshop on Superconductivity Co-Sponsored by ISTEC and MRS (ISTEC, Tokyo, 1995a) p. 355.

V. R. Todt, S. Sengupta and D. J. Miller, Appl. Supercond. **3**, 175 (1995b).

V. R. Todt, S. Sengupta, D. J. Miller, Y. Chen, U. Balachandran, K. C. Goretta, and J. Guo, IEEE Trans. Appl. Supercond. **5**, 1623 (1995c).

V. R. Todt, S. Sengupta, and D. Shi, U.S. Patent Applications 08/372,042 and 08/372,067; V. R. Todt, S. Sengupta, D. J. Miller, and D. Shi, U.S. Patent Application 08/372,142 (1995d).

C. Uher, J. Supercond. **3**, 337 (1990).

Q. Wang, G. A. Saunders, M. Cankurtaran, D. P. Almond, and K. C. Goretta, Phys. Rev. B **52**, 3711 (1995).

U. Welp, D. O. Gunter, G. W. Crabtree, J. S. Luo, V. A. Maroni, P. Haldar, R. S. Sokolowski, V. K. Vlasko-Vlasov, and I. Nikitenko, Appl. Phys. Lett. **66**, 1270 (1994).

U. Welp, D. O. Gunter, G. W. Crabtree, W. Zhong, U. Balachandran, W. L. Carter, V. K. Vlasko-Vlasov, and I. Nikitenko, Nature **376**, 44 (1995).

W. Wu, M. T. Lanagan, B. Wang, R. B. Poeppel, and S. Danyluk, Appl. Supercond. **2**, 387 (1994).

W. Wu, C.-Y. Chu, K. C. Goretta, and J. L. Routbort, U.S. Patent 5,411,938 (May 2, 1995).

M. Xu, D. K. Finnemore, U. Balachandran, and P. Haldar, Appl. Phys. Lett. **66**, 3359 (1995a).

M. Xu, D. K. Finnemore, U. Balachandran, and P. Haldar, J. Appl. Phys. **78**, 360 (1995b).

Z. J. Yang, J. R. Hull, T. M. Mulcahy, and T. D. Rossing, J. Appl. Phys. **78**, 2097 (1995).

J. Yau and N. Savvides, Appl. Phys. Lett. **65**, 1454 (1994).

G. O. Zimmerman, Y. Z. Negm, M. Z. Tahar, R. E. Powers, and R. McConeghy, Physica C **209**, 291 (1993).

Distribution for ANL-95/42

Internal:

T. Askew
U. Balachandran (25)
I. D. Bloom
Y. S. Cha
G. Crabtree
D. R. Diercks
S. E. Dorris
H. Drucker
B. Dunlap
J. T. Dusek
W. A. Ellingson
J. E. Emerson
B. L. Fisher
F. Y. Fradin
R. Giese
K. C. Goretta
K. E. Gray
D. Gruen
M. Hanley
J. R. Hull
J. Jorgensen
R. T. Kampwirth
M. Kirk
D. S. Kupperman
S. Lake
M. T. Lanagan
C. A. Malefyt
M. Marinelli
V. A. Maroni
R. L. McDaniel
D. J. Miller
T. Mulcahy
R. C. Niemann
J. J. Picciolo
R. B. Poeppel
A. C. Raptis
J. L. Routbort
W. J. Shack
W. W. Schertz
J. P. Singh
C. E. Till
K. L. Uherka
A. Wagh
A. Wantroba
R. W. Weeks
A. M. Wolsky
C. A. Youngdahl
TIS Files

External:

DOE-OSTI, for distribution per UC-1394 (154)
ANL Libraries
ANL-E
ANL-W

Chicago Field Office, DOE:
Manager
F. Herbaty

U.S. Department of Energy, Washington:

Office of Advanced Utility Concepts, Conservation and Renewable Energy:
J. Daley
R. Eaton III
C. Kang
C. Platt
Basic Energy Sciences-Materials Science, Energy Research:
I. L. Thomas

Energy Technology Division Review Committee:
H. K. Birnbaum, University of Illinois, Urbana
R. C. Buchanan, University of Cincinnati, Cincinnati, OH
S.-N. Liu, Fremont, CA
H. S. Rosenbaum, Fremont, CA

R. K. Shah, University of Kentucky, Lexington
S. Smialowska, Ohio State University, Columbus
R. E. Smith, Altran Corp., Huntersville, NC

Other – Industry – University
R. G. Abboud, Commonwealth Edison Co., Zion, IL
J. Badin, Energetics, Inc., Columbia, MD
A. L. Bement, Jr., Midwest Superconductivity Consortium, Purdue University
T. Bickel, Sandia National Laboratories
K. Blohowiak, Boeing Corporation, Seattle, WA
R. W. Boom, University of Wisconsin – Madison
J. Bray, General Electric Company, Schenectady, NY
W. Buckles, Superconductivity, Inc., Madison, WI
D. Burlone, BASF Corp., Enka, NC
L. Capuano, Conductus, Sunnyvale, CA
R. Cass, HiTc Superconco, Inc., Lambertville, NJ
J. Clem, Ames Laboratory
B. Currie, Pacific Northwest Laboratory
S. Danyluk, Georgia Institute of Technology
M. DeGuire, Case Western Reserve University
L. P. de Rochemont, Radiation Monitoring Devices, Inc., Watertown, MA
D. Divecha, Naval Surface Warfare Center, Silver Spring, MD
B. Dorothy, DuPont, Wilmington, DE
D. Driscoll, Reliance Electric, Cleveland
M. Eddy, Superconductor Technologies, Inc., Santa Barbara, CA
N. Eror, University of Pittsburgh
D. K. Finnemore, Ames Laboratory
M. Fluss, Lawrence Livermore National Laboratory
S. Foner, Francis Bitter National Magnet Lab., Massachusetts Institute of Technology
J. R. Gaines, Jr., Superconductive Components, Inc., Columbus, OH
C. Gallo, Superconix, St. Paul, MN
T. Grudkowski, United Technologies Research Center, East Hartford, CT
D. Gubser, Naval Research Laboratory
P. Haldar, Intermagnetics General Corp., Latham, NY
S. D. Harkness, Westinghouse, Pittsburgh
R. A. Hawsey, Oak Ridge National Laboratory
J. Hodge, Illinois Superconductor Corp., Mt. Prospect, IL
D. L. Johnson, Northwestern University
J. B. Ketterson, Northwestern University
J. L. Kirtley, Jr., Massachusetts Institute of Technology
M. Klein, University of Illinois, Urbana
S. F. Kral, Babcock & Wilcox, Lynchburg, VA
D. K. Kroeger, Oak Ridge National Laboratory
H. Kroger, Microelectronics and Computer Technology Corporation, Austin, TX
D. C. Larbalestier, University of Wisconsin – Madison
A. Lauder, DuPont, Wilmington, DE
E. Leung, Lockheed Martin, San Diego, CA
M. Levy, University of Wisconsin – Milwaukee
J. Lewis, University of Illinois, Urbana
D. H. Liebenberg, Office of Naval Research, Arlington, VA

P. Lindhorst, MagneTek, St. Louis
R. Loehman, Sandia National Laboratories
J. Loncoski, Virginia Power, Glen Allen, VA
H. Madler, J. C. Petlau, Inc., Wheeling, IL
D. Madura, General Dynamics, San Diego, CA
A. Malozemoff, American Superconductor Corp., Westborough, MA
K. Marken, Oxford Instruments, Inc., Carteret, NJ
C. Martin, SSC, Inc., Woodinville, WA
A. Marwick, IBM, Yorktown Heights, NY
T. Mason, Northwestern University
R. Mathisen, Foster-Miller, Inc., Waltham, MA
B. McConnell, National Renewable Energy Laboratory
P. J. McGinn, University of Notre Dame
D. Moon, Westinghouse, Pittsburgh
M. W. Morgan, Ability Engineering Technology, Inc., South Holland, IL
L. Motowidlo, IGC Advanced Superconductors, Inc., Waterbury, CT
W. Nellis, Lawrence Livermore National Laboratory
C. A. Parker, AlliedSignal, Inc., Des Plaines, IL
D. Peterson, Los Alamos National Laboratory
N. Phillips, Lawrence Berkeley National Laboratory
T. Pillai, Department of Physics, University of Wisconsin, LaCrosse
R. Raman, Ceracon, Sacramento, CA
R. F. Ranellone, Newport News Shipbuilding, Newport News, VA
R. A. Roehl, Commonwealth Edison Co., Chicago
C. H. Rosner, Intermagnetics General Corp., Latham, NY
J. Schwartz, Florida State University
D. K. Sharma, Electric Power Research Institute, Palo Alto, CA
S. Sinha, University of Illinois, Chicago
G. Smith, SSC, Inc., Woodinville, WA
O. Smith, Illinois Superconductor Corp., Mt. Prospect, IL
D. M. Smyth, Lehigh University
M. Suenaga, Brookhaven National Laboratory
P. T. Tsivitse, Reliance Electric, Cleveland
R. Weber, Containerless Research, Inc., Evanston, IL
B. Weinberger, United Technologies Research Center, East Hartford, CT
D. O. Welch, Brookhaven National Laboratory
R. E. Williams, Ocean and Atmospheric Science, Inc., Dobbs Ferry, NY
J. Worth, Oxford Instruments, Inc., Carteret, NJ
J. Wu, Westinghouse Electric Corporation, Science and Technology Center, Pittsburgh
G. J. Yurek, American Superconductor Corporation, Westborough, MA
C. Zahopoulos, Northeastern University
G. O. Zimmerman, ZerRes Corp., Boston